

This dissertation has been 65-5615  
microfilmed exactly as received

BARRON, Randall Franklin, 1936-  
HEAT AND MASS TRANSFER TO A  
CRYOSURFACE IN FREE CONVECTION.

The Ohio State University, Ph.D., 1964  
Engineering, mechanical

University Microfilms, Inc., Ann Arbor, Michigan

HEAT AND MASS TRANSFER TO A CRYOSURFACE  
IN FREE CONVECTION

DISSERTATION

Presented in Partial Fulfillment of the Requirements for  
the Degree Doctor of Philosophy in the Graduate  
School of The Ohio State University

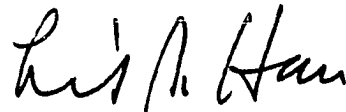
By

Randall Franklin Barron, B.S.M.E., M.Sc.

\* \* \* \*

The Ohio State University  
1964

Approved by:

A handwritten signature in cursive script, appearing to read "L. A. Han", written over a horizontal line.

Adviser  
Department of Mechanical Engineering

## ACKNOWLEDGMENTS

I wish to express my sincere appreciation to Dr. L. S. Han, Professor of Mechanical Engineering at the Ohio State University, for his assistance and guidance during the course of the investigation taken up in this dissertation. I also wish to acknowledge the assistance given by the people at CryoVac, Inc., Columbus, Ohio, who constructed the apparatus used in the experimental portion of the investigation. Finally, I wish to express my deepest thanks to my wife, Shirley, for her help and encouragement during my doctoral studies.

## VITA

May 16, 1936 . . . . . Born in Many, Louisiana

August 1958 . . . . . B.S.M.E., Louisiana Polytechnic Institute,  
Ruston, Louisiana

1958 - 1964 . . . . . Instructor, Mechanical Engineering Department,  
The Ohio State University, Columbus, Ohio

June 1961 . . . . . M. Sc., The Ohio State University, Columbus,  
Ohio

1962 - 1964 . . . . . Consultant, CryoVac, Inc., Columbus, Ohio

## PUBLICATIONS

1. Low-Temperature Properties of Engineering Materials, Machine Design, Vol. 32, No. 6, pp. 189-195, March 1960.
2. Superinsulations, Machine Design, Vol. 33, No. 5, pp. 116-120, March 1961.
3. Superconductivity, Machine Design, Vol. 34, Nos. 4 and 5, pp. 24-28, February 1962.
4. C. B. Hood, Jr., W. W. Vogelhuber, and R. F. Barron, "Theoretical Study of Large Capacity Refrigeration Systems for 38°K and 20°K Loads," AEDC Tech. Doc. Rept. 63-71, March 1963.
5. C. B. Hood, Jr., W. W. Vogelhuber, C. B. Barnes, and R. F. Barron, "Research Study of Thermodynamic Systems for Temperature Control of Heat Sinks in Space Simulation Chambers," AEDC Tech. Doc. Rept. 64-121, June 1964.

## CONTENTS

	Page
ACKNOWLEDGEMENTS . . . . .	ii
VITA . . . . .	iii
ILLUSTRATIONS . . . . .	vi
TABLES . . . . .	vii
SYMBOLS . . . . .	viii
CHAPTERS	
I. INTRODUCTION . . . . .	1
II. SURVEY OF PREVIOUS LITERATURE ON FROST FORMATION . . .	3
Frost formation in forced convection . . . . .	3
Frost formation in free convection . . . . .	8
III. ANALYTICAL CONSIDERATIONS . . . . .	11
Basic boundary layer equations . . . . .	11
Equations for coupled heat and mass transfer . . . .	21
Solution for laminar flow . . . . .	26
Solution for turbulent flow . . . . .	43
Transition Grashof number . . . . .	53
IV. EXPERIMENTAL APPARATUS AND PROCEDURE . . . . .	55
Description of experimental apparatus . . . . .	55
Experimental procedure . . . . .	63
V. DISCUSSION OF RESULTS . . . . .	73
Effect of thermal diffusion . . . . .	73

	Page
Effect of mass transfer on heat transfer . . . . .	76
Experimentally measured heat transfer rates . . . . .	82
Mass transfer results . . . . .	87
Frost thermal conductivity . . . . .	99
Application of the results . . . . .	105
VI. SUMMARY AND CONCLUSIONS . . . . .	106
APPENDIX	
A. PROPERTIES OF AIR AT LOW TEMPERATURES . . . . .	113
B. DETERMINATION OF THE THERMAL DIFFUSION CONSTANT FOR WATER VAPOR AND AIR . . . . .	121
C. DETERMINATION OF GUARD SHIELD TEMPERATURE RISE . .	130
D. TIME RESPONSE FOR FREE CONVECTION . . . . .	139
E. APPLICATION OF RESULTS . . . . .	145
F. EXPERIMENTAL DATA . . . . .	151
BIBLIOGRAPHY . . . . .	163

## ILLUSTRATIONS

Figure	Page
1. Volume element used in derivation of continuity, momentum, and energy equations . . . . .	13
2. Volume element used in development of the diffusion equation . . . . .	19
3. Physical system and system of coordinates . . . . .	30
4. Schematic of test apparatus . . . . .	56
5. Frost thickness and temperature measurement probe . . .	62
6. Variation of $\overline{Nu}/(Gr_L Pr)^{1/4}$ with $w_{1\infty}$ for laminar flow .	80
7. Variation of $\overline{Nu}/(Gr_L Pr)^{2/5}$ with $w_{1\infty}$ for turbulent flow	81
8. Heat transfer measurements . . . . .	83
9. Experimental heat transfer correlation . . . . .	85
10. Experimentally measured mass flux . . . . .	88
11. Experimental mass transfer correlation . . . . .	90
12. Frost thickness vs. time . . . . .	98
13. Frost thermal conductivity vs. time . . . . .	101
14. Frost thermal conductivity vs. mean frost temperature .	102
15. Frost thermal conductivity vs. frost density . . . . .	104
16. Variation of thermal diffusion ratio with $w_1$ . . . . .	127
17. Variation of thermal diffusion constant with $w_1$ . . . .	128
18. Model and coordinate system for analysis of guard shield temperature distribution . . . . .	131

## TABLES

Table	Page
1. Properties of Dry Air at 14.7 psia . . . . .	116
2. Thermal and Dynamic Properties of Dry Air at 14.7 psia .	118
3. Heat of Sublimation and Saturation Mass Fraction of Water	120
4. Solution to Example Problem . . . . .	149
5. Experimental Data for Run No. 1 . . . . .	152
6. Calculated Data for Run No. 1 . . . . .	153
7. Experimental Data for Run No. 2 . . . . .	155
8. Calculated Data for Run No. 2 . . . . .	156
9. Experimental Data for Run No. 3 . . . . .	158
10. Calculated Data for Run No. 3 . . . . .	159
11. Experimental Data for Run No. 4 . . . . .	160
12. Calculated Data for Run No. 4 . . . . .	161



## SYMBOLS

$a$	thermal diffusion constant, $k_T/w_1 w_2 = k_T/w (1 - w_1)$ , dimensionless.
$a_i$	accomodation coefficient, dimensionless.
$A$	heat transfer area, $\text{ft}^2$ .
$B_1$	thermal diffusion parameter (see Eq. 3-53), dimensionless.
$B_2$	thermal diffusion parameter (see Eq. 3-54), dimensionless.
$B_3$	dimensionless parameter (see Eq. 3-84)
$B_4$	dimensionless parameter (see Eq. 3-143).
$c_p$	specific heat at constant pressure, $\text{Btu/lb}_m\text{-}^\circ\text{R}$ .
$C_1$	constant (see Eqs. 3-74 and 3-133).
$C_2$	constant (see Eqs. 3-75 and 3-134).
$d_1$	diameter of the water vapor molecule, $\text{cm}$ .
$d_2$	diameter of the air "molecule", $\text{cm}$ .
$d_3$	diameter of the frost particle, $\text{cm}$ .
$D$	cylinder diameter, $\text{ft}$ .
$D_{12}$	diffusion coefficient, $\text{ft}^2/\text{hr}$ .
$D_T$	thermal diffusion coefficient, $\text{ft}^2/\text{hr}$ .
$e$	emissivity, dimensionless.
$E$	constant in Eq. (4-4).
$F_a$	accomodation coefficient factor (see Eq. 4-2); orifice diameter contraction factor (see Eq. 4-3), dimension- less.
$F_c$	orifice Reynolds number correction factor, $1 + (E/\text{Re}_o)$ , dimensionless.

$F_e$	emissivity factor (see Eq. C-16), dimensionless.
$F_m$	orifice meter factor (see Eq. 4-3), $(\text{lb}_m\text{-ft}^3/\text{hr}^2\text{-in. WG})^{1/2}$ .
$ Fo$	Fourier number, $\alpha\tau/L^2$ , dimensionless.
$g$	local acceleration due to gravity, ft/hr.
$g_C$	conversion factor in Newton's Second Law of Motion, $4.18 \times 10^8 \text{ lb}_m\text{-ft}/\text{lb}_f\text{-hr}^2 = 32.174 \text{ lb}_m\text{-ft}/\text{lb}_f\text{-sec}^2.$
$Gr_x$	Grashof number based on the distance from the leading edge of the plate (see Eq. 3-89), dimensionless.
$Gr_L$	Grashof number based on the length of the plate, dimensionless.
$h_c$	local convective heat transfer coefficient, Btu/hr-ft <sup>2</sup> -°F.
$\bar{h}_c$	average convective heat transfer coefficient, Btu/hr-ft <sup>2</sup> -°F.
$\bar{h}_i$	average enthalpy transport coefficient (see Eq. 3-104), ft/hr.
$h_m$	local mass transfer coefficient (see Eq. 3-96), ft/hr.
$i$	enthalpy, Btu/lb <sub>m</sub> .
$i_{fg}$	heat of vaporization, Btu/lb <sub>m</sub> .
$i_{sg}$	heat of sublimation, Btu/lb <sub>m</sub> .
$j_q$	local conductive heat flux, Btu/hr-ft <sup>2</sup> .
$j_1$	local diffusive mass flux of component 1 (water vapor), $\text{lb}_m/\text{hr-ft}^2$ .
$j_2$	local diffusive mass flux of component 2 (air), $\text{lb}_m/\text{hr-ft}^2$ .
$k$	thermal conductivity, Btu/hr-ft-°F.
$k_b$	Boltzmann constant, $1.3804 \times 10^{-16} \text{ erg/}^\circ\text{K}$ .
$k_f$	frost thermal conductivity, Btu/hr-ft-°F.
$k_s$	thermal conductivity of guard shield, Btu/hr-ft-°F.
$k_T$	thermal diffusion ratio, $D_T/D_{12}$ , dimensionless.

$L_{ij}$	linear coefficients (see Eqs. 3-9, 3-10, and 3-11); $L_{11}$ , $L_{12}$ , $L_{21}$ , $L_{22}$ ( $\text{lb}_m\text{-hr/ft}^3$ ); $L_{13}$ , $L_{23}$ , $L_{31}$ , $L_{32}$ ( $\text{lb}_m\text{/ft-hr}$ ); $L_{33}$ ( $\text{Btu/hr-ft}$ ).
$L$	length of vertical plate, ft.
$m_1$	mass flux of component 1 (water vapor), $\text{lb}_m\text{/hr-ft}^2$ .
$m_2$	mass flux of component 2 (air), $\text{lb}_m\text{/hr-ft}^2$ .
$\dot{m}_b$	boil-off mass flow rate, $\text{lb}_m\text{/hr}$ .
$m_r$	reduced mass, gm.
$M_1$	molecular weight of mixture, $\text{lb}_m\text{/mole}$ .
$M_2$	molecular weight of component 1 (water vapor = 18), $\text{lb}_m\text{/mole}$ .
$M$	molecular weight of component 2 (air = 28.96), $\text{lb}_m\text{/mole}$ .
$n$	number of molecules per unit volume, $\text{cm}^{-3}$ .
$n_i$	mole fraction of $i$ th component, dimensionless.
$\bar{N}_i$	enthalpy number, $\bar{h}_i L/\alpha$ , dimensionless.
$Nu_x$	local Nusselt number, $h_c x/k$ , dimensionless.
$\bar{Nu}$	average Nusselt number, $\bar{h}_c L/k$ , dimensionless.
$p_1$	pressure, psia.
$p$	pressure upstream of orifice (see Eq. 4-5), psia.
$p_b$	barometric pressure, psia.
$\Delta p$	pressure drop across orifice, in. WG.
$Pr$	Prandtl number, $\mu c_p/k = \nu/\alpha$ , dimensionless.
$q_c$	convective heat flux, $\text{Btu/hr-ft}^2$ .
$q_m$	latent heat transport flux, $m_1 i_{sg}$ , $\text{Btu/hr-ft}^2$ .
$q_r$	radiant heat flux, $\text{Btu/hr-ft}^2$ .
$q_{\text{total}}$	total heat flux, $q_c + q_m + q_r$ , $\text{Btu/hr-ft}^2$ .

$q_x$	local convective heat flux, Btu/hr-ft <sup>2</sup> .
$r$	radial coordinate, ft.
$R$	gas constant, Btu/lb <sub>m</sub> -°R or ft-lb <sub>f</sub> /lb <sub>m</sub> -°R.
$\bar{R}$	universal gas constant, Btu/mole-°R or ft-lb <sub>f</sub> /mole-°R.
$Re_o$	Reynolds number based on the orifice diameter, dimensionless.
$s$	rate of reduction of frost thickness due to melting and diffusion (see Eq. 2-1), hr <sup>-1</sup> .
$Sc$	Schmidt number, $\nu/D_{12}$ , dimensionless.
$Sh_x$	local Sherwood number, $h_m x/D_{12}$ , dimensionless.
$\bar{Sh}$	average Sherwood number, $\bar{h}_m L/D_{12}$ , dimensionless.
$t$	thickness of guard shield, ft.
$t_f$	thickness of frost layer, ft.
$T$	temperature, °F or °R.
$T_a$	temperature of vacuum jacket, °R.
$T_o$	temperature of fluid in guard vessel, °F.
$T_{max}$	maximum temperature of the guard shield, °F.
$T_s$	temperature of plate, °F.
$T_w$	temperature of the frost-air interface, °F.
$T_\infty$	ambient air temperature, °F.
$u$	velocity in the x-direction, ft/hr.
$u_m$	velocity proportional to maximum velocity in the boundary layer (see Eq. 3-59 and 3-115), ft/hr.
$v$	velocity in the y-direction, ft/hr.
$v_w$	velocity normal to the plate at the frost-air interface, ft/hr.

$w_1$	mass fraction of component 1 (water vapor), dimensionless.
$w_{1w}$	mass fraction of water vapor at the frost-air interface, dimensionless.
$w_{1\infty}$	mass fraction of water vapor in ambient air, dimensionless.
$w_2$	mass fraction of component 2 (air), $w_2 = 1 - w_1$ , dimensionless.
$W$	specific humidity, $W = w / (1 - w)$ , $\text{lb}_m \text{H}_2\text{O} / \text{lb}_m \text{dry air}$ .
$x$	coordinate tangential to the plate surface, ft.
$\underline{X}_j$	driving force for heat and mass transfer (see Eqs. 3-20, 3-21, and 3-22), $\underline{X}_1$ and $\underline{X}_2$ ( $\text{ft/hr}^2$ ); $\underline{X}_3$ ( $\text{ft}^{-1}$ ).
$y$	coordinate normal to the plate surface, ft.

#### Greek letters

$\alpha$	thermal diffusivity, $k/\rho c_p$ , $\text{ft}^2/\text{hr}$ .
$\beta_m$	concentration coefficient of expansion (see Eq. 3-48), dimensionless.
$\beta_t$	coefficient of thermal expansion (see Eq. 3-47), $^{\circ}\text{R}^{-1}$ .
$\gamma$	ratio of specific heats, $c_p/c_v$ , dimensionless.
$\delta$	thermal and hydrodynamic boundary layer thickness, ft.
$\delta_m$	concentration or diffusion boundary layer thickness, ft.
$\theta$	temperature function $(T - T_{\infty})/(T_w - T_{\infty})$ , dimensionless.
$\mu$	viscosity, $\text{lb}_m/\text{ft-hr}$ .
$\bar{\mu}_i$	molar chemical potential, Btu/mole.
$\nu$	momentum diffusivity or kinematic viscosity, $\text{ft}^2/\text{hr}$ .

$\xi$	ratio of diffusion boundary layer thickness to thermal boundary layer thickness, $(\delta_m/\delta)$ , dimensionless.
$\rho$	density, $\text{lb}_m/\text{ft}^3$ .
$\rho_f$	frost density, $\text{lb}_m/\text{ft}^3$ .
$\rho_1$	gas density upstream of orifice (see Eq. 4-3), $\text{lb}_m/\text{ft}^3$ .
$\sigma$	Stefan-Boltzmann constant, $0.173 \times 10^{-8} \text{ Btu/hr-ft}^2\text{-}^\circ\text{R}^4$ .
$\tau$	time, hr.
$\tau_{ss}$	time to reach steady-state, hr.
$\tau_w$	interfacial shear stress between fluid and the frost-air interface, $\text{lb}_f/\text{ft}^2$ .
$\phi$	mass fraction function, $(w_1 - w_{1\infty})$ , dimensionless.
$\psi$	Prandtl number function defined by Eq. (3-91) for laminar flow and by Eq. (3-147) for turbulent flow, dimensionless.
$\nabla$	nabla or gradient operator, $\text{ft}^{-1}$ . For cartesian coordinates, $\nabla = \underline{e}_1 \frac{\partial}{\partial x} + \underline{e}_2 \frac{\partial}{\partial y} + \underline{e}_3 \frac{\partial}{\partial z}$ , where $\underline{e}_1$ , $\underline{e}_2$ , and $\underline{e}_3$ are the unit vectors for cartesian coordinates.

### Subscripts

a	vacuum jacket wall.
c	convection heat transfer.
f	frost
m	mass transfer or associated with mass transfer.
r	radiation
s	surface of cryoplate.

ss	steady-state.
w	frost-air interface.
$\infty$	ambient conditions.
none	refers to mixture of water vapor and air.
1	component 1 or water vapor
2	component 2 or air.
x	local or point value.
sat.	saturation conditions.
trans.	transition.

#### Special symbols

- (1) A bar placed over a symbol denotes the average value integrated over the plate surface, such as  $\bar{h}_c$ , which is defined by:

$$\bar{h}_c = (1/L) \int_0^L h_c dx$$

- (2) A bar placed under a symbol denotes a vector quantity, such as

$$\underline{j}_1.$$

## CHAPTER I

### INTRODUCTION

In recent years the increased use of cryogenic fluids in space technology, applied and basic research, medicine, and many other areas, has resulted in an increased interest in heat transfer in low-temperature equipment. In such applications as rapid transfer of liquid oxygen on space vehicles and in vaporizers and pressurization coils for cryogenic fluid storage vessels, the heat transfer process takes place between ambient air and a metallic surface at cryogenic temperatures. Under these conditions, the heat transfer process is accompanied by the simultaneous transfer of mass from ambient air. These two processes are coupled together and directly affect each other.

When a cryogenically cooled surface (or a cryosurface) is initially exposed to ambient air, frost begins to form at the surface, since the temperature of the cryosurface is much below the dew point of ambient air. As the mass transfer process proceeds, the layer of frost begins to affect the convective heat transfer rate, because the frost layer introduces an additional resistance to heat transfer and the frost surface temperature is higher than the temperature of the cryosurface. The mass transfer affects the total energy transport in another way -- latent heat is transferred to the frost surface as water vapor is condensed. This energy transmission rate is directly proportional to the water vapor mass transfer rate.



In summary, the heat and mass transfer phenomenon at the surface of a body at cryogenic temperatures is complicated by several factors: (a) the entire process is transient in nature, (b) the temperature difference across the frost layer depends strongly on the mass transfer taking place, (c) the properties of the insulating frost layer are not constant with time and are not functions of temperature only, but also are functions of the mass transfer rate, type of mass transfer process (whether free or forced convection), and temperature, and (d) mechanical failure of the frost layer results in patches of frost falling from the surface.

The purpose of this investigation was to determine analytical expressions for the convective heat transfer and mass transfer to a vertical flat plate cooled to cryogenic temperatures and to check these analytical expressions by experimentation. The heat and mass transfer processes were carried out under free convection conditions. Experimental runs were made for different mass fractions of water vapor in ambient air and for different plate sizes. All runs were made with the plate surface temperature above the condensation temperature of air, so that no condensation of air took place on the plate. In view of the large temperature gradients existing at the surface of the plate in the presence of simultaneous mass transfer, the effect of thermal diffusion and diffusion thermoeffect was also considered in developing the analytical expressions, although it was found that this effect was extremely small for the situation considered in this investigation.

## CHAPTER II

### SURVEY OF PREVIOUS LITERATURE ON FROST FORMATION

Because the formation of frost on a cold surface is of interest in the air-conditioning and refrigeration industry as well as in cryogenics, several experimental investigations have been carried out at temperatures in the vicinity of 32°F for both forced convection and free convection conditions. In many of these investigations, data was obtained on the gross effect of frost formation on the performance of a refrigeration process, rather than the investigation of the detailed mechanisms of heat and mass transfer under frosting conditions.

#### 2.1. Frost formation in forced convection

In the area of forced convection, Beatty et al. (1)<sup>1</sup> investigated the effects of air velocity, air conditions, and surface temperature on heat transfer under frosting conditions. The heat transfer surface used in this investigation was a cylinder with air flow parallel to the cylinder axis in an annular passage. A similar investigation was made by Kamei et al. (2) in which the Colburn analogy between mass and heat transfer was applied in correlating the experimental data. One important result of Kamei's work was the

---

<sup>1</sup> Numbers in parenthesis refer to similarly numbered references in the Bibliography.

data correlation for the frost density and frost thermal conductivity. The temperature range of these measurements was  $-22^{\circ}\text{F}$  to  $40^{\circ}\text{F}$ , which was far above the cryogenic temperature regime.

Chung and Algren (3) presented an extensive theoretical analysis of heat and mass transfer for laminar flow over a cylinder placed normal to the direction of flow of moist air. Analytical expressions were developed from solutions of the boundary layer equations for flow over a cylinder to describe the variation of heat and mass transfer rates with respect to time. The analytical study was followed by an experimental study in which the validity of the Colburn analogy between heat and mass transfer was demonstrated by the agreement between analytical and experimental studies. A similar experimental study was carried out by Andrichak (4) on formation of frost in cross flow over a cylinder. The results of this study confirmed that the effect of frost density variation had a pronounced effect on heat transfer to the cylinder. Neither frost density nor frost surface temperature was measured by Andrichak, so no correlation could be made between frost density and frost thermal conductivity from his work.

Sugawara et al. (5) studied the frost formation problem for a flat plate in forced convection, and again the validity of the Colburn heat-and-mass-transfer analogy was demonstrated to be valid from their studies. All of the previously mentioned investigations showed that the frost layer increased in thickness until a temperature of  $32^{\circ}\text{F}$  was attained at the frost surface, and after this point, a steady-state condition was reached, in which liquid water was

formed on the frost surface, and no further build-up of frost was observed.

An extensive experimental study of frost formation on a cylinder in cross flow of air was carried out by Richards et al. (6) at the National Bureau of Standards Cryogenic Engineering Laboratory. In this experimental work, the tube was cooled to approximately  $-320^{\circ}\text{F}$  (liquid nitrogen temperature) and the air velocity, humidity, and temperature were controlled in a wind tunnel within the following ranges: air velocity: 5 to 60 mph; air temperature:  $40^{\circ}\text{F}$  to  $100^{\circ}\text{F}$ ; and specific humidity: 16 to 325 grains/lb<sub>m</sub> dry air. In this study, it was found that the heat flux at low air velocities was smallest for the lower specific humidity values. At low humidities, a dry fluffy frost was formed; whereas, for higher humidities near the saturation specific humidity, a wet frost was formed. The dry frost was a better insulator than the wet frost; therefore, the heat flux was lower for the cases in which dry frost was formed. At wind velocities of 5 mph, the dry frost was mechanically strong enough to resist being torn away from the surface. At higher wind velocities (25 to 55 mph) the dry frost was blown from the surface, while the wet frost had sufficient strength to build up and remain on the test section. In the cases of high wind velocities, the situation was reversed, i.e., the heat flux was lower for the higher values of specific humidity than for the low humidity runs.

In the NBS-CEC experimental program on forced convection, a cyclic variation in the heat and mass transfer was noted at high values of specific humidity. The frost layer rapidly formed and became

twice as thick on the top and bottom of the tube than it did on the upstream and downstream sides. During this build-up process, the frost thickness increased until the frost surface reached 32°F, at which time water droplets formed. The water then soaked into the frost and caused a decrease in the frost thickness and an increase in frost thermal conductivity; therefore, the frost surface temperature decreased below 32°F, and more frost began to form. This cyclic process was repeated as many as three times before the final steady-state operation was achieved.

An analytical study of frost formation in cross-flow was made by Loper (7), in which the entire system from ambient air to the cold surface was considered. In this analysis, a constant frost density was assumed, and the analytical results were not in agreement with experimental data. This suggested that the assumption of constant frost density was not valid, and more details of the mechanism of frost formation and values of frost density and thermal conductivity were required. This conclusion was also supported by the work of Andrichak at temperatures near 32°F.

A more detailed analysis of the frosting phenomena on a tube at cryogenic temperatures in cross-flow was made by Smith et al. (8), in which the NBS-CEC experimental data of Richards et al. was utilized. A rough correlation was obtained between the ratio of heat flux at any time to heat flux at the point at which the frost surface reached 32°F and the ratio of time to the time required for the frost surface to reach 32°F. Another rough correlation was obtained between the time required for the frost surface to reach 32°F and

the parameter  $m_1 (T_\infty - T_w)$ , where  $m_1$  = mass flux to the surface,  $\text{lb}_m \text{ water/hr-ft}^2$ ,  $T_\infty$  = ambient temperature,  $^\circ\text{F}$ , and  $T_w$  = temperature of the frost surface,  $^\circ\text{F}$ . Large scatter in the experimental points around the correlating curve was attributed to mechanical failure of the frost layer at higher wind velocities.

One significant result of the investigation of Smith et al. was the observation that the frost thickness and frost thermal conductivity for low values of specific humidity was dependent upon diffusion of water vapor within the frost layer. For the specific ambient air conditions and plate surface temperature, the frost thermal conductivity could be expressed as follows:

$$k_f = k_{f,\text{lim}} (1 - e^{-s \tau}) \quad (2-1)$$

where  $k_{f,\text{lim}}$  = limiting or steady-state value of the frost thermal conductivity,  $s$  = rate of reduction in thickness per unit frost thickness due to melting and diffusion of water vapor toward the cryosurface, and  $\tau$  = time. From the experimental data, it was found that the parameter  $s$  could be expressed as follows:

$$s = \frac{q}{0.295 k_{f,\text{lim}} (T_w - T_s)} \quad (2-2)$$

and the limiting value of frost thermal conductivity was approximately related to the average mass flux by:

$$k_{f,\text{lim}} = 0.5 m_1 \quad (2-3)$$

where the British system of units ( $\text{ft-lb}_m\text{-hr-Btu}$ ) must be used in the preceding expressions. These equations were essentially

empirical expressions, and only gave a hint as to the happenings within the frost layer which affect heat and mass transfer in forced convection. There is as yet much room for basic research in this area for both forced and free convection situations.

Van Gundy and Uglum (9) conducted a series of tests on forced convection across a flat plate cooled to liquid hydrogen temperature ( $-423^{\circ}\text{F}$ ), although no correlations between the experimental data and a theoretical analysis was obtained. The problem of heat and mass transfer to a plate cooled by liquid hydrogen is more complicated than the case in which the plate temperature is above the condensation temperature of air, since liquid air or solid air will form on the plate for low air velocities. In fact, Van Gundy and Uglum observed that solid air "frost" always formed initially with a thin film of liquid air over the solid layer. When the layer of solid air became thick enough that liquid air no longer condensed, then water vapor frost began to accumulate. In cases in which the surface was rapidly covered (usually under conditions of high specific humidity), a mixture of solid air and liquid air was initially observed. The solid would eventually stick to the surface in random areas and spread to cover the surface.

## 2.2. Frost formation in free convection

Because of the interest in the insulating effect of frost on the outer surface of space vehicle liquid oxygen storage vessels, Ruccia and Mohr (10) investigated the heat and mass transfer process for an uninsulated liquid oxygen vessel exposed to various weather

environments. This study was one of the first investigations into the general problem of frost formation at cryogenic temperatures. Ruccia and Mohr did not control the ambient air conditions except to blow air over the surface for the forced convection runs. The experimental setup consisted of a cylinder 18 inches in diameter and 22 feet high filled with liquid oxygen (normal boiling point  $-298^{\circ}\text{F}$ ). Empirical correlations for heat transfer with no mass transfer and for mass transfer with no heat transfer were used in an attempt to correlate the data. The frost surface temperature was not measured; so no conclusions could be drawn as to the validity of the heat transfer correlation. On the other hand, the mass of frost formed on the surface was measured, and the predicted mass transfer (predicted by the empirical equation for zero heat transfer) differed from the measured mass transfer by as much as a factor of five. Ruccia and Mohr attributed this discrepancy to the fact that frost particles formed in the boundary layer in natural convection, and not all of the frost which was formed became attached to the cryosurface.

A more extensive experimental study on frost formation on an uninsulated liquid oxygen container under controlled ambient conditions was made by Holten (11), who used a spherical container having a diameter of 5.375 inches as the test surface. As in the case of the work of Ruccia and Mohr, the frost surface temperature was not measured and empirical equations were used in an attempt to correlate the experimental data. The empirical mass transfer equation



was found to over-predict the amount of frost deposited on the surface by approximately the same factor as found by Ruccia and Mohr for long vertical cylinders.

A detailed analytical and experimental study of frost formation in free convection on a vertical flat plate in laminar flow was made by Whitehurst (12) for plate surface temperatures around 0°F. In this investigation, dry bulb and wet bulb temperatures were measured within the boundary layer, and the frost surface temperature was determined experimentally. For plate surface temperatures near 32°F at which no frost formed in the boundary layer, good agreement was attained between the theoretical expressions and experimental measurements for both heat and mass transfer. For lower values of plate surface temperature, however, only the theoretical heat transfer expression was in agreement with the experimental measurements. In addition, turbulent flow was observed in some cases for the lower plate temperatures, so that the theoretical heat transfer expression derived for laminar flow could not be applied. No theoretical study of heat and mass transfer for turbulent flow was made in the work of Whitehurst.

## CHAPTER III

### ANALYTICAL CONSIDERATIONS

#### 3.1. Basic boundary layer equations

The problem presented in this study involved the combined heat and mass transfer process in free convection to a vertical plate held at cryogenic temperatures. The diffusing species was water vapor, and all quantities which refer to water vapor alone will be denoted by subscript 1. Subscript 2 will denote the second species, which was air in this case. Quantities with no numerical subscript refer to the mixture of air and water vapor. The subscript  $\infty$  refers to the free stream; the subscript w refers to the frost-air interface (the surface of the frost layer); and the subscript s denotes the solid plate surface.

The complete set of boundary-layer equations which govern the combined heat, mass, and momentum transport in general have been derived elsewhere (13). These equations are second order, non-linear, coupled partial differential equations. Rather than attempt a numerical solution of the partial differential equations, the von-Karman-Pohlhausen integral method was used in the present study. Since the resulting equations differed from the equations developed for heat transfer without the transfer of mass, the basic equations will be developed from fundamental principles first.

The following assumptions were used in the derivation of the basic equations:

- a. The flow is two-dimensional.
- b. The fluid properties are constant, except for a slight variation in density with temperature and mass fraction of water vapor.
- c. Expansion work and viscous energy dissipation effects are negligible.
- d. The flow is quasi-steady.
- e. The total pressure of the fluid remains constant over the surface of the plate.

With these assumptions in mind, the continuity equation, momentum equation, energy equation, and diffusion equation were developed as follows.

Consider a volume element in the boundary layer, as shown in Figure 1, having dimensions  $dx$  in the  $x$ -direction,  $\delta$  in the  $y$ -direction, and unity in the  $z$ -direction. The fluid velocity components are  $u$  in the  $x$ -direction,  $v$  in the  $y$ -direction, and zero in the  $z$ -direction (from assumption a), and the velocities are considered positive in the positive coordinate directions. In the free stream, the  $x$ -component of velocity is  $u_\infty = U$ , the  $y$ -component of velocity is  $v = v_\infty$ , the fluid temperature is  $T_\infty$ , and the mass fraction of water vapor in the air is  $w_{1\infty}$ . At any distance  $y$  from the frost surface within the boundary layer, the respective values of the previously mentioned quantities are  $u$ ,  $v$ ,  $T$ , and  $w_1$ . At the frost-air

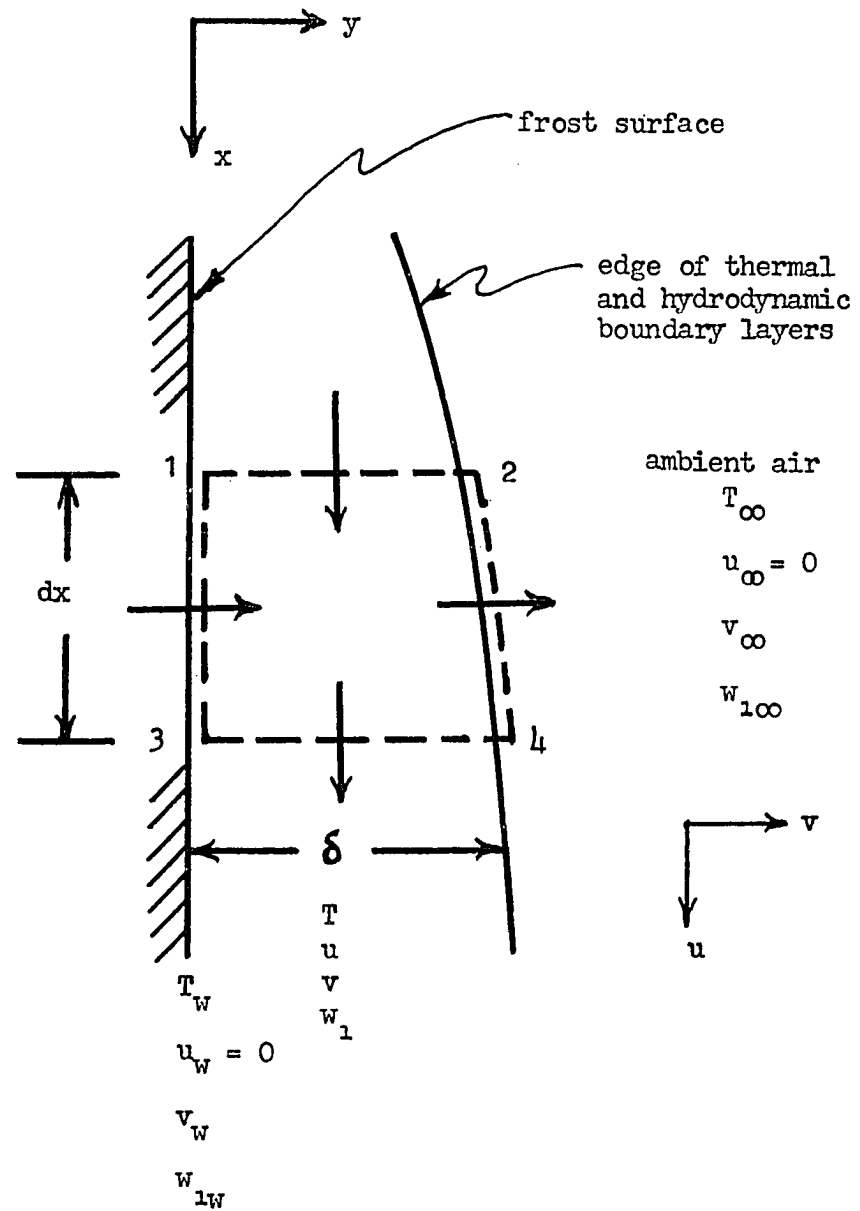


Figure 1. Volume element used in derivation of continuity, momentum, and energy equations.

interface, the state of the fluid is specified by  $u_w = 0$ ,  $v_w$ ,  $T_w$ , and  $w_{1w}$ .

### 3.1.1. Continuity equation

The continuity equation may be derived from the conservation of mass principle for the mixture applied to the small volume element shown in Figure 1. The mass flow through the area 1-2 is:

$$\int_0^\delta \rho u dy$$

Through the length  $dx$ , the mass flow in the  $x$ -direction changes by an amount

$$\frac{d}{dx} \left[ \int_0^\delta \rho u dy \right] dx$$

The mass flow through area 2-4 is

$$\rho_\infty v_\infty dx$$

and the mass flow through area 1-3 is

$$\rho_w v_w dx$$

The principle of conservation of mass states that in steady state the net flow into the volume element is equal to the net flow out of the volume element. Applying this principle to the volume element shown in Figure 1, there is obtained the following expression, which is the continuity equation for this problem.

$$\frac{d}{dx} \left[ \int_0^\delta \rho u dy \right] + \rho_\infty v_\infty = \rho_w v_w \quad (3-1)$$

### 3.1.2. Momentum equation

The momentum equation may be derived from the conservation of momentum principle applied to the volume element shown in Figure 1. The momentum transfer in the x-direction through area 2-4 is zero, since the x-component of velocity is zero at this point. The momentum transfer through area 1-3 in the x-direction is zero for the same reason. The momentum transfer through area 1-2 is

$$\int_0^{\delta} \rho u^2 dy$$

Through the length  $dx$ , the momentum transfer in the x-direction changes by an amount

$$\frac{d}{dx} \left[ \int_0^{\delta} \rho u^2 dy \right] dx$$

There are two forces which act on the element: (a) a frictional shear force acting at the wall, given by

$$- \tau_w dx$$

where  $\tau_w$  is the fluid shear stress at the wall, and (b) a buoyancy force, given by

$$\left[ \int_0^{\delta} (\rho - \rho_{\infty}) g dy \right] dx$$

where  $g$  is the local acceleration due to gravity.

The conservation of momentum principle states that in steady state the net momentum transfer is equal to the net force acting on the element. Applying this principle to the volume element shown in Figure 1, there is obtained the following expression, which is the momentum equation for this problem.

$$\frac{d}{dx} \left[ \int_0^\delta \rho u^2 dy \right] = -\tau_w + \int_0^\delta (\rho - \rho_\infty) g dy \quad (3-2)$$

### 3.1.3. Energy equation

The energy equation may be derived from the First Law of Thermodynamics applied to the volume element shown in Figure 1, assuming that the thermal boundary layer thickness is the same as the hydrodynamic boundary layer thickness. The enthalpy transport through area 2-4 is zero if the base for enthalpy is taken as the free stream condition. The enthalpy transport through area 1-3 is

$$\rho_w v_w c_p (T_w - T_\infty) dx$$

where the enthalpy base is taken as the free stream condition, and the fluid is considered to act as a calorically perfect gas (a valid assumption for all gases at low pressures relative to the critical pressure of the gas). The enthalpy transport for the fluid entering the element through area 1-2 is

$$\int_0^\delta \rho u c_p (T - T_\infty) dy$$

In a distance  $dx$ , the enthalpy of the fluid changes by an amount

$$\frac{d}{dx} \left[ \int_0^\delta \rho u c_p (T - T_\infty) dy \right] dx$$

Through area 1-3, there is a conductive heat flux, which is denoted by  $j_q$ , so the heat transferred through area 1-3 is

$$j_q dx$$

No heat is conducted through area 2-4 because the temperature and mass fraction gradients across this area are zero.

The First Law of Thermodynamics states that for steady state conditions the net heat transfer minus the net work transfer is equal to the net total enthalpy transport to the system. For free convection, the velocities are so small that the kinetic energy of the fluid is much smaller than the static enthalpy changes; therefore, the total enthalpy is practically equal to the static enthalpy. Applying this principle to the volume element shown in Figure 1, the energy equation is obtained.

$$\frac{d}{dx} \left[ \int_0^{\delta} \rho u c_p (T - T_{\infty}) dy \right] = j_q + \rho_w v_w c_p (T_w - T_{\infty}) \quad (3-3)$$

Both the continuity equation and the momentum equation are the same as the conventional boundary layer equations for heat transfer in free convection without mass transfer; however, the energy equation in this problem differs from the conventional boundary layer equations by the additional term  $\rho_w v_w c_p (T_w - T_{\infty})$ . This additional term represents a convective energy flux associated with mass transfer.

#### 3.1.4. Diffusion equation

The diffusion equation is essentially the result of applying the conservation of mass principle to the diffusing component of the gas mixture (water vapor in this case), which is denoted by subscript 1. In the previous developments, the momentum and temperature boundary layers were considered to have the same thickness; however, it



can be shown that the diffusion boundary layer will not have the same thickness as the temperature boundary layer, except in the special case in which  $Pr/Sc = 1$  for the gas. In order that this development not be limited by this condition, the diffusion boundary layer will be considered to have a thickness  $\delta_m$ , which can be different from the temperature boundary layer thickness  $\delta$ , as shown in Figure 2. The diffusion boundary layer is that region near the surface in which the mass fraction of water vapor deviates from the free stream value.

The mass transfer of component 1 through area 2-4 is

$$\rho_{\infty} v_{\infty} w_{1\infty} dx$$

The mass transfer of component 1 through area 1-3 consists of a diffusive portion  $j_{1w} dx$  and a convective portion  $\rho_w v_w w_{1w} dx$ . The mass transfer of component 1 through area 1-2 is

$$\int_0^{\delta_m} \rho u w_1 dy$$

Within a distance  $dx$ , the mass transfer changes by an amount

$$\frac{d}{dx} \left[ \int_0^{\delta_m} \rho u w_1 dy \right] dx$$

Applying the conservation of mass principle to the volume element shown in Figure 2 for component 1, there is obtained the following:

$$j_{1w} + \rho_w v_w w_{1w} = \frac{d}{dx} \left[ \int_0^{\delta_m} \rho u w_1 dy \right] + \rho_{\infty} v_{\infty} w_{1\infty} \quad (3-4)$$

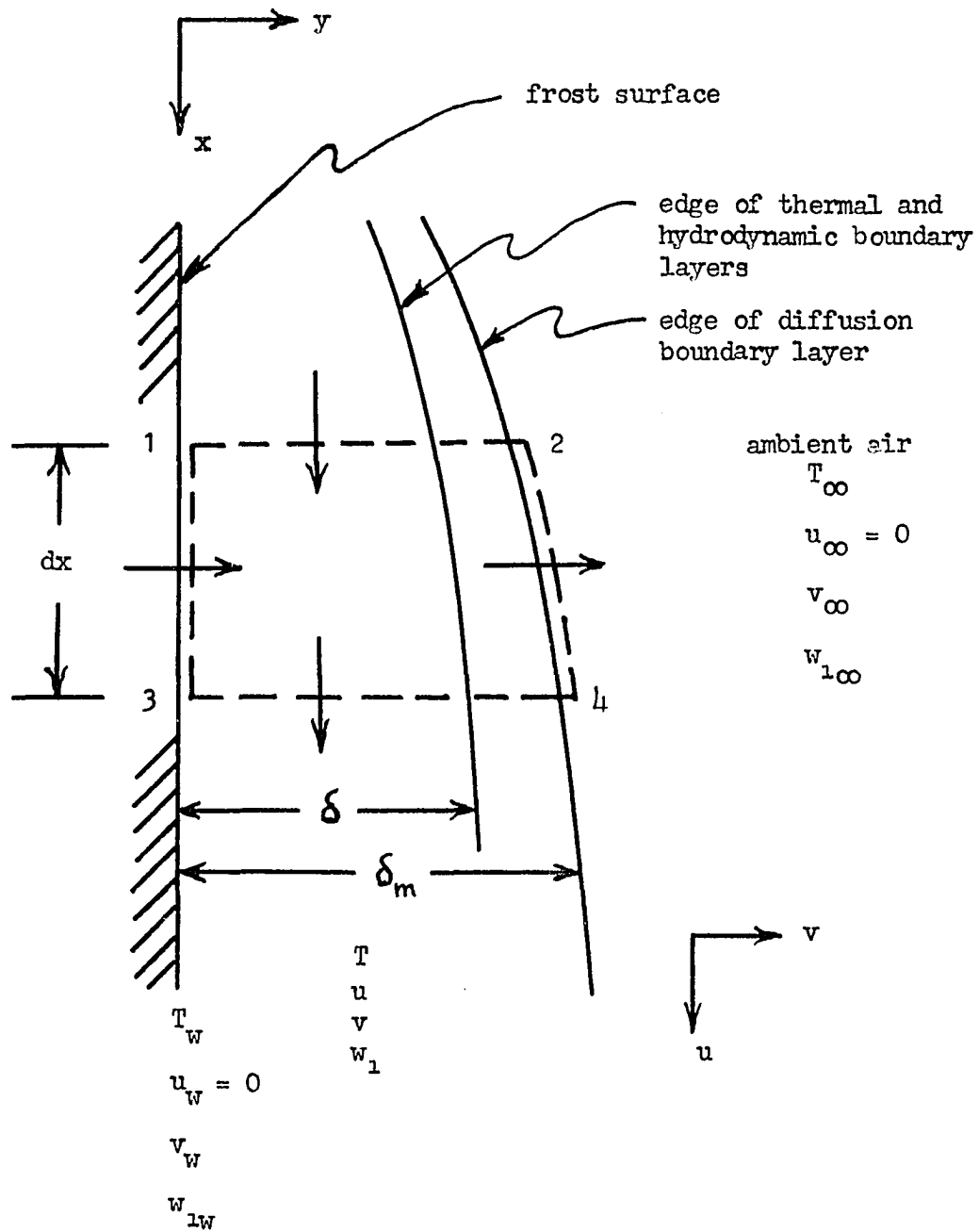


Figure 2. Volume element used in development of the diffusion equation.

The velocity  $v_\infty$  may be eliminated from Eq. (3-4) by solving for this quantity from the continuity equation, Eq. (3-1). Making this substitution, and noting that  $w_{1\infty}$  is a constant, the diffusion equation is obtained.

$$\frac{d}{dx} \left[ \int_0^{\delta_{mp}} u(w_1 - w_{1\infty}) dy \right] = j_{1w} + \rho_w v_w (w_{1w} - w_{1\infty}) \quad (3-5)$$

### 3.1.5. Normal velocity at the frost surface

In order to complete the set of equations necessary for solution of this problem, the velocity normal to the frost surface must be determined. The mass transfer of air to the frost surface is considered to be zero, and the application of this condition supplies the necessary expression for the normal velocity  $v_w$ . The mass flux of component 2 (air in this case) is made up of two parts: (a) a diffusive mass flux and (b) a convective mass flux, or

$$m_{2w} = j_{2w} + \rho_w w_{2w} v_w = 0 \quad (3-6)$$

For diffusion of two components of a gas mixture,  $j_1 = -j_2$ , and from the definition of mass fraction,  $w_2 = 1 - w_1$ . Making these substitutions into Eq. (3-6), the expression for the normal velocity is obtained.

$$v_w = \frac{j_{1w}}{\rho_w (1 - w_{1w})} \quad (3-7)$$

By substituting the expression for the normal velocity, Eq. (3-7), into the diffusion equation, Eq. (3-5), the modified diffusion equation is obtained.

$$\frac{d}{dx} \left[ \int_0^{\delta_m} \rho u (w_1 - w_{1\infty}) dy \right] = \left[ \frac{1 - w_{1\infty}}{1 - w_{1w}} \right] j_{1w} \quad (3-8)$$

### 3.2. Equations for coupled heat and mass transfer

The theory of coupled flows of heat and mass, heat and charge, etc., is a subject covered by the area of irreversible thermodynamics (14, 15). In accordance with this theory, as a first approximation, the vector equations for diffusional flow of component 1 and component 2 in a gas mixture and the energy conduction may be written as a set of linear vector equations, in which the fluxes of mass and energy are linear functions of properly defined driving forces.

$$\underline{j}_1 = L_{11} \underline{X}_1 + L_{12} \underline{X}_2 + L_{13} \underline{X}_3 \quad (3-9)$$

$$\underline{j}_2 = L_{21} \underline{X}_1 + L_{22} \underline{X}_2 + L_{23} \underline{X}_3 \quad (3-10)$$

$$\underline{j}_q = L_{31} \underline{X}_1 + L_{32} \underline{X}_2 + L_{33} \underline{X}_3 \quad (3-11)$$

Only three of the coefficients  $L_{ij}$  are independent, as is demonstrated in the following.

The diffusive mass flux terms for a binary gas mixture are defined such that  $j_1 = -j_2$ . If this condition is to be valid for any arbitrary values of the driving forces  $\underline{X}_j$ , then from Eqs. (3-9) and (3-10), the following relations are obtained.

$$L_{11} = -L_{21} \quad (3-12)$$

$$L_{12} = -L_{22} \quad (3-13)$$

$$L_{13} = -L_{23} \quad (3-14)$$

Additional relations are supplied by the Onsager Reciprocity Theorems.

$$L_{12} = L_{21} \quad (3-15)$$

$$L_{13} = L_{31} \quad (3-16)$$

$$L_{23} = L_{32} \quad (3-17)$$

With these relationships, Eqs. (3-9) through (3-11) may be written as:

$$\underline{j}_1 = -\underline{j}_2 = L_{11} (\underline{X}_1 - \underline{X}_2) + L_{13} \underline{X}_3 \quad (3-18)$$

$$\underline{j}_q = L_{13} (\underline{X}_1 - \underline{X}_2) + L_{33} \underline{X}_3 \quad (3-19)$$

The proper driving forces for heat and mass transfer are (16):

$$\underline{X}_1 = -T \underline{\nabla} (\bar{\mu}_1 / T) \quad (3-20)$$

$$\underline{X}_2 = -T \underline{\nabla} (\bar{\mu}_2 / T) \quad (3-21)$$

$$\underline{X}_3 = -\underline{\nabla} (\ln T) \quad (3-22)$$

where  $\bar{\mu}_i$  is the chemical potential and  $\underline{\nabla}$  is the nabla or gradient operator. For a perfect gas, the chemical potential is given by:

$$\bar{\mu}_i = \bar{\mu}^0 + \bar{R} T \ln n_i \quad (3-23)$$

where  $\bar{\mu}^0$  is a function of temperature alone,  $\bar{R}$  is the universal gas constant, and  $n_i$  is the mole fraction of component  $i$ . For a perfect gas mixture, the driving force may be written

$$(\underline{X}_1 - \underline{X}_2) = -\bar{R} T \left[ \left( 1/n_1 \right) \underline{\nabla} n_1 - \left( 1/n_2 \right) \underline{\nabla} n_2 \right] \quad (3-24)$$

Since for a binary mixture,  $n_1 + n_2 = 1$ , then

$$\underline{\nabla} n_1 = -\underline{\nabla} n_2$$

Making this substitution into Eq. (3-24), the driving force in molar units is obtained.

$$(\underline{X}_1 - \underline{X}_2) = -(\bar{R} T / n_1 n_2) \underline{\nabla} n_1 \quad (3-25)$$

Converting to mass units, the driving force for mass transfer may be written as follows:

$$(X_1 - X_2) = - \left[ \frac{M^2 R T}{M_1 M_2 w_1 w_2} \right] \nabla w_1 \quad (3-26)$$

where  $M$  = molecular weight of the mixture, and  $M_1$  and  $M_2$  are the molecular weights of components 1 and 2 respectively.

For isothermal mass transfer,  $\nabla (\ln T) = - \frac{X_3}{T} = 0$ ; therefore, Eq. (3-18) may be written as

$$(j_1)_{T=c} = - \left[ \frac{L_{11} M^2 R T}{M_1 M_2 w_1 w_2} \right] \nabla w_1 = - \rho D_{12} \nabla w_1 \quad (3-27)$$

where  $D_{12}$  is the conventional diffusion coefficient for mass transfer. From Eq. (3-27), the coefficient  $L_{11}$  is found to be:

$$L_{11} = \frac{M_1 M_2 w_1 w_2 \rho D_{12}}{M^2 R T} \quad (3-28)$$

The coupling coefficient  $L_{13}$  is directly related to the thermal diffusion coefficient by:

$$L_{13} = \rho D_T \quad (3-29)$$

With the substitutions given by Eqs. (3-20) through (3-29), the mass flux and heat flux equations, Eqs. (3-18) and (3-19), may be written as follows:

$$j_1 = - j_2 = - \rho D_{12} \nabla w_1 - (\rho D_T / T) \nabla T \quad (3-30)$$

$$j_q = - \left[ \frac{M^2 R T \rho D_T}{M_1 M_2 w_1 w_2} \right] \nabla w_1 - (L_{33} / T) \nabla T \quad (3-31)$$

The first term on the right side of Eq. (3-31) represents the diffusion thermo-effect, or the transfer of energy due to the presence of concentration gradients, and the second term on the right side of Eq. (3-30) represents the thermal diffusion effect, or the transfer of mass due to the presence of temperature gradients. The one remaining coefficient  $L_{33}$  may be related to the conventional thermal conductivity as follows.

For zero mass diffusion, the mass fraction gradient and temperature gradient are related by Eq. (3-30) for  $j_1 = 0$ .

$$(\underline{v}_w)_1 j_1=0 = - (D_T/D_{12}) (\underline{v}_T)_{j_1=0} \quad (3-32)$$

The ordinary thermal conductivity for a gas is measured under conditions of zero mass diffusion; therefore, by definition,

$$(\underline{j}_q)_{j_1=0} = -k (\underline{v}_T)_{j_1=0} = \left[ \frac{M^2 R \rho D_T^2}{M_1 M_2 w_1 w_2 D_{12}} - \frac{L_{33}}{T} \right] (\underline{v}_T)_{j_1=0} \quad (3-33)$$

From Eq. (3-33), the coefficient  $L_{33}$  is given by

$$L_{33} = k T + \frac{M^2 R T \rho D_T^2}{M_1 M_2 w_1 w_2 D_{12}} \quad (3-34)$$

It is often more convenient to use the property called the thermal diffusion ratio  $k_T$  instead of the thermal diffusion coefficient, where the thermal diffusion ratio is defined by

$$k_T = D_T/D_{12} \quad (3-35)$$

Using this property, Eqs. (3-30) and (3-31) may be written as follows:

$$\underline{j}_1 = -\underline{j}_2 = -\rho D_{12} \underline{\nabla w}_1 + (k_T/T) \underline{\nabla T} \quad (3-36)$$

$$\underline{j}_q = - \left[ \frac{M^2 R T \rho D_{12} k_T}{M_1 M_2 w_1 w_2} \right] \underline{\nabla w}_1 - \left[ k + \frac{M^2 R \rho k_T^2 D_{12}}{M_1 M_2 w_1 w_2} \right] \underline{\nabla T} \quad (3-37)$$

The heat flux equation may also be written as follows:

$$\underline{j}_q = -k \underline{\nabla T} + \left[ \frac{M^2 R T k_T}{M_1 M_2 w_1 w_2} \right] \underline{j}_1 \quad (3-38)$$

From Eq. (3-37) it is observed that the heat flux for  $w_1$  very small (approaching zero) would be very large even for small temperature gradients, if the thermal diffusion ratio  $k_T$  were treated as a constant. This behavior has never been observed experimentally, and one would intuitively believe that it would not happen; therefore, one is led to the conclusion that the thermal diffusion ratio is not constant, but is a strong function of the mass fraction  $w_1$ . From experimental work (17), the thermal diffusion ratio may be written to a first approximation as the following function of mass fractions:

$$k_T = a w_1 w_2 = a w_1 (1 - w_1) \quad (3-39)$$

where  $a$  is called the thermal diffusion constant. Using this expression, Eqs. (3-36) and (3-37) may be written as follows:

$$\underline{j}_1 = -\underline{j}_2 = -\rho D_{12} \left[ \underline{\nabla w}_1 + (a w_1 w_2 / T) \underline{\nabla T} \right] \quad (3-40)$$



$$\underline{j}_q = - \left[ \frac{M^2 R T \rho D_{12} a}{M_1 M_2} \right] \underline{v}_w - \left[ k + \frac{M^2 R \rho D_{12} a^2 w w}{M_1 M_2} \right] \underline{v}_T \quad (3-41)$$

$$\text{Or, } \underline{j}_q = -k \underline{v}_T + \left[ \frac{a M^2 R T}{M_1 M_2} \right] \underline{j}_1 \quad (3-42)$$

These equations may be applied to the present problem, in which gradients in the y-direction or direction normal to the plate surface are the only important gradients. In this case, the vector equations may be written as scalar equations by substituting the following:

$$\frac{\partial w_1}{\partial y} \quad \text{for} \quad \underline{v}_w \quad \text{and} \quad \frac{\partial T}{\partial y} \quad \text{for} \quad \underline{v}_T$$

### 3.3. Solution for laminar flow

In this section, the general equations of momentum, energy, and diffusion will be solved under the additional assumption that laminar flow exists in the boundary layer. In section 3.1 it was stated that properties would be assumed constant, except for the slight variation of density with temperature and mass fraction. This density variation may be expressed as follows.

For a perfect gas, the density is

$$\rho = p/RT = M p / \bar{R} T \quad (3-43)$$

where the molecular weight of a two-component gas mixture is

$$M = [ (w_1/M_1) + (w_2/M_2) ]^{-1} = \left[ w_1 \left( \frac{1}{M_1} - \frac{1}{M_2} \right) + \frac{1}{M_2} \right]^{-1} \quad (3-44)$$

Or,

$$M = \frac{M_2}{\frac{w_1 (M_2 - M_1)}{M_1} + 1} \quad (3-45)$$

Making this substitution for the molecular weight into Eq. (3-43), the following expression for density is obtained.

$$\rho = \frac{M_2 p}{\left[ \frac{w_1 (M_2 - M_1)}{M_1} + 1 \right] \bar{R} T} \quad (3-46)$$

The variation of density with temperature, holding pressure and mass fraction of component 1 constant is

$$\left( \frac{\partial \rho}{\partial T} \right)_{p, w_1} = - \frac{M_2 p}{\left[ \frac{w_1 (M_2 - M_1)}{M_1} + 1 \right] \bar{R} T^2}$$

By definition, the temperature coefficient of thermal expansion  $\beta_t$  is

$$\beta_t = - \frac{1}{\rho} \left( \frac{\partial \rho}{\partial T} \right)_{p, w_1} = \frac{1}{T} \quad (3-47)$$

Similarly, the variation of density with mass fraction of component 1, holding pressure and temperature constant is

$$\left( \frac{\partial \rho}{\partial w_1} \right)_{p,T} = - \frac{M_2 p}{\left[ \frac{w_1 (M_2 - M_1)}{M_1} + 1 \right]^2 \bar{R} T}$$

A concentration coefficient of expansion  $\beta_m$  may be defined as follows:

$$\beta_m = - \frac{1}{\rho} \left( \frac{\partial \rho}{\partial w_1} \right)_{p,T} = \frac{\left[ (M_2 - M_1) / M_1 \right]}{\left[ \frac{w_1 (M_2 - M_1)}{M_1} + 1 \right]} \quad (3-48)$$

The total change in density is then given by:

$$d\rho = \left( \frac{\partial \rho}{\partial T} \right)_{p,w_1} dT + \left( \frac{\partial \rho}{\partial w_1} \right)_{p,T} dw_1$$

$$\text{Or, } -d\rho = \rho \beta_t dT + \rho \beta_m dw_1 \quad (3-49)$$

For the density changes across the boundary layer, the differentials may be approximated by finite differences as follows:

$$- \frac{(\rho - \rho_\infty)}{\rho_\infty} = \beta_t (T - T_\infty) + \beta_m (w_1 - w_{1\infty}) \quad (3-50)$$

The physical system to be considered with the coordinates used for the problem is shown in Figure 3. At this point, the following defined quantities are introduced:

$$\theta = (T - T_{\infty}) / (T_w - T_{\infty}) \quad (3-51)$$

$$\phi = w_1 - w_{1\infty} \quad (3-52)$$

$$B_1 = \frac{a R M^2 T_w}{M_1 M_2 c_p (T_w - T_{\infty})} \quad (3-53)$$

$$B_2 = a w_{1w} (1 - w_{1w}) (T_w - T_{\infty}) / T_w \quad (3-54)$$

For laminar flow, the wall shear stress may be written as

$$\tau_w = \mu \left( \frac{du}{dy} \right)_w \quad (3-55)$$

Using the preceeding expressions and the assumptions of constant fluid properties, the momentum, energy, and diffusion equations for laminar flow may be written as follows.

(a) Momentum equation:

$$\begin{aligned} \frac{d}{dx} \left[ \int_0^{\delta} u^2 dy \right] &= g (T_{\infty} - T_w) \beta_t \int_0^{\delta} \theta dy - g \beta_m \int_0^{\delta} \phi dy - \\ &\quad - \mu \left( \frac{du}{dy} \right)_w \end{aligned} \quad (3-56)$$

(b) Energy equation:

$$\begin{aligned} \frac{d}{dx} \left[ \int_0^{\delta} \theta u dy \right] &= - \alpha \left( \frac{d\theta}{dy} \right)_w - B_1 D_{12} \left[ \left( \frac{d\phi}{dy} \right)_w + B_2 \left( \frac{d\theta}{dy} \right)_w \right] - \\ &\quad - \frac{D_{12}}{(1 - w_{1w})} \left[ \left( \frac{d\phi}{dy} \right)_w + B_2 \left( \frac{d\theta}{dy} \right)_w \right] \end{aligned} \quad (3-57)$$

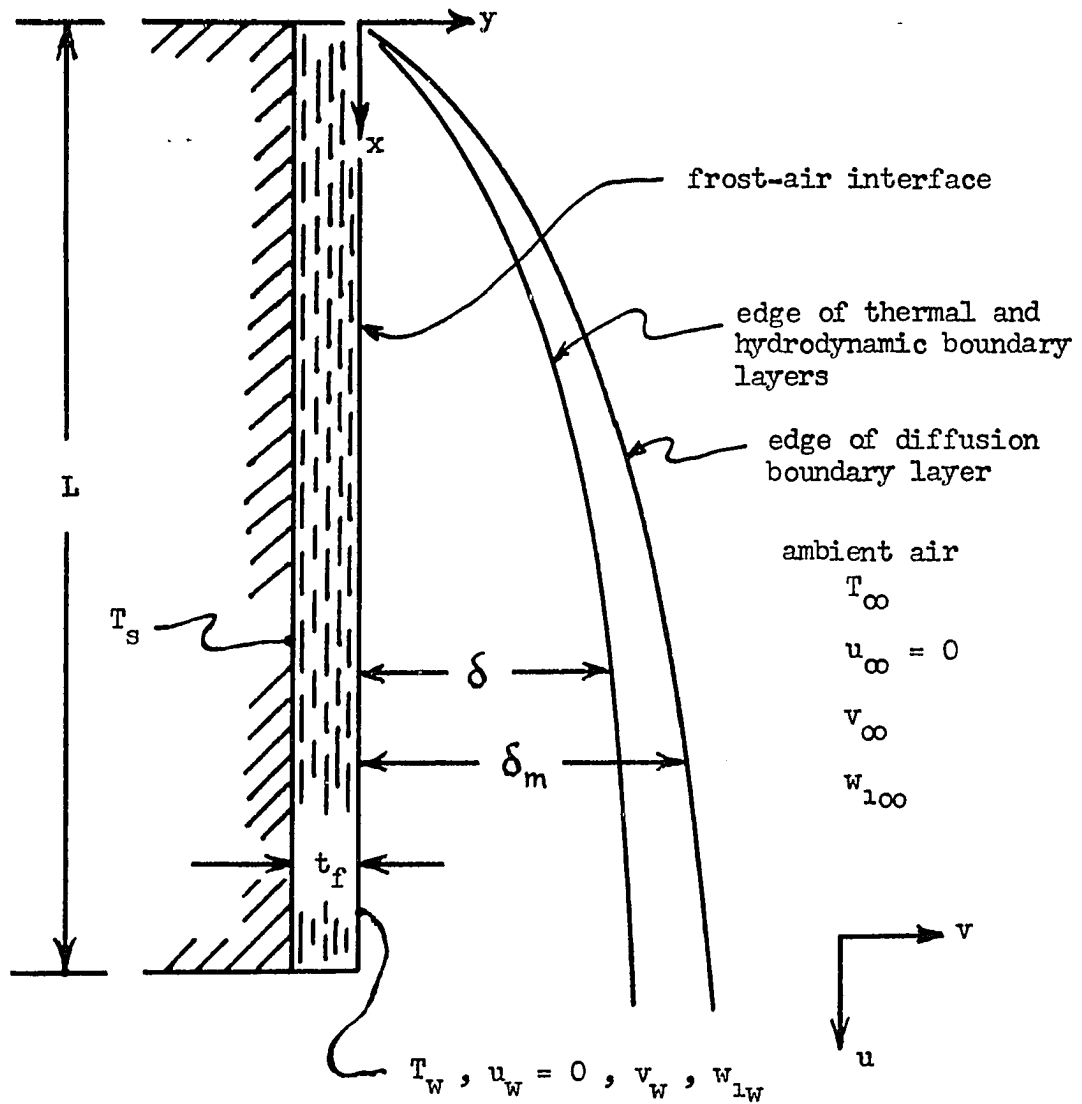


Figure 3. Physical system and system of coordinates.

(c) Diffusion equation:

$$\frac{d}{dx} \left[ \int_0^{\delta} \phi u dy \right] = - \left( \frac{1 - w_{1\infty}}{1 - w_{1w}} \right) D_{12} \left[ \left( \frac{d\phi}{dy} \right)_w + B_2 \left( \frac{d\theta}{dy} \right)_w \right] \quad (3-58)$$

### 3.3.1. Evaluation of the integrals

In order to complete the solution of the equations for the problem, the velocity, temperature, and mass fraction profiles must be known. The velocity  $u$  is zero at the frost surface and in the free stream; therefore, one function which satisfies this condition and the condition that the velocity gradient is zero at the edge of the boundary layer is:

$$u = u_m (y/\delta) (1 - y/\delta)^2 \quad (3-59)$$

where  $u_m$  is a function of the distance from the leading edge of the plate and is proportional to the maximum velocity in the boundary layer.

The function  $\theta$  is zero at the edge of the boundary layer and unity at the frost surface. In addition, the temperature gradient at the edge of the boundary layer is zero. One function which satisfies these conditions is

$$\theta = (1 - y/\delta)^2 \quad (3-60)$$

The concentration distribution is similar in its behavior to the temperature distribution; therefore, a function satisfying the condition

of  $\phi = 0$  at the edge of the concentration boundary layer and

$\phi = w_{1w} - w_{1\infty}$  at the frost surface is

$$\phi = (w_{1w} - w_{1\infty}) (1 - y/\delta)^2 \quad (3-61)$$

Using these distribution functions for the velocity, temperature, and mass fraction distributions in the boundary layer, the following integrals and derivatives may be evaluated.

$$\int_0^\delta u^2 dy = (u_m^2 \delta)/105 \quad (3-62)$$

$$\int_0^\delta \theta dy = \delta/3 \quad (3-63)$$

$$\int_0^{\delta_m} \phi dy = (w_{1w} - w_{1\infty})(\delta_m/3) \quad (3-64)$$

$$\left( \frac{du}{dy} \right)_w = \frac{u_m}{\delta} \quad (3-65)$$

$$\int_0^\delta \theta u dy = (u_m \delta)/30 \quad (3-66)$$

$$\left( \frac{d\theta}{dy} \right)_w = -\frac{2}{\delta} \quad (3-67)$$

$$\left( \frac{d\phi}{dy} \right)_w = -\frac{2(w_{1w} - w_{1\infty})}{\delta_m} \quad (3-68)$$

$$\int_0^{\delta_m} \phi u dy = u_m (w_{1w} - w_{1\infty})(\delta_m/30) \quad (3-69)$$

### 3.3.2. Solution of the integral equations

Let the ratio of the diffusion boundary layer thickness  $\delta_m$  to the thermal and velocity boundary layer thickness  $\delta$  be defined as

$$\xi = \delta_m/\delta \quad (3-70)$$

and assume that this ratio is independent of the coordinates  $x$  and  $y$ . If the expressions given in Eqs. (3-62) through (3-70) are substituted into the momentum, energy, and diffusion equations, Eqs. (3-56), (3-57), and (3-58), there is obtained the following expressions.

(a) Momentum equation:

$$\frac{1}{105} \frac{d(u_m^2 \delta)}{dx} = \frac{1}{3} g [\beta_t (T_\infty - T_w) + \beta_m (w_{1\infty} - w_{1w})(\xi)] - (v u_m / \delta) \quad (3-71)$$

(b) Energy equation:

$$\frac{1}{30} \frac{d(u_m \delta)}{dx} = \frac{2\alpha}{\delta} \left\{ 1 + \left( \frac{D_{12}}{\alpha} \right) \left[ \frac{(w_{1w} - w_{1\infty})}{\xi} + B_2 \right] \left[ \frac{1}{(1 - w_{1w})} + B_1 \right] \right\} \quad (3-72)$$

(c) Diffusion equation:

$$\frac{\xi}{30} \frac{d(u_m \delta)}{dx} = \frac{2 D_{12}}{\delta} \left[ \frac{1 - w_{1\infty}}{1 - w_{1w}} \right] \left[ \frac{1}{\xi} + \frac{B_2}{(w_{1w} - w_{1\infty})} \right] \quad (3-73)$$

In order to solve the boundary layer equations, the dependence of the parameters  $u_m$  and  $\delta$  on the coordinate  $x$  must be known. From the similarity solutions of Pohlhausen, it can be shown that these



parameters are exponential functions of the coordinate  $x$  for laminar flow.

$$u_m = C_1 x^{1/2} \quad (3-74)$$

$$\delta = C_2 x^{1/4} \quad (3-75)$$

where the quantities  $C_1$  and  $C_2$  must be determined.

If the expressions for  $u_m$  and  $\delta$  are substituted into the momentum equation, Eq. (3-71), and the indicated differentiation carried out, the following algebraic equation is obtained.

$$\begin{aligned} \frac{C_1^2 C_2}{84} &= \frac{1}{3} g [\beta_t (T_\infty - T_w) + \beta_m (w_{1\infty} - w_{1w})(\xi)] C_2 - \\ &\quad - (\nu C_1 / C_2) \end{aligned} \quad (3-76)$$

A second algebraic equation is obtained by making the same substitutions into the energy equation, Eq. (3-72).

$$C_1 C_2^2 = 80\alpha \left\{ 1 + \frac{\text{Pr}}{\text{Sc}} \left[ B_2 - \frac{(w_{1\infty} - w_{1w})}{\xi} \right] \left[ B_1 + \frac{1}{(1 - w_{1w})} \right] \right\} \quad (3-77)$$

where the ratio of Prandtl number to Schmidt number was substituted for the ratio  $(D_{12}/\bar{\alpha})$ . The third algebraic equation is obtained similarly from the diffusion equation, Eq. (3-73).

$$C_1 C_2^2 (\xi)^2 = 80 D_{12} \left[ \frac{1 - w_{1\infty}}{1 - w_{1w}} \right] \left[ 1 - \frac{B_2(\xi)}{(w_{1\infty} - w_{1w})} \right] \quad (3-78)$$

At this point, the ratio of the diffusion boundary layer thickness to the thermal boundary layer thickness can be obtained from Eqs. (3-77) and (3-78). The solution for this parameter would involve the solution of a quadratic equation if carried out directly; however, a much simpler expression is obtained if the solution is carried out by the method of successive approximations, which is quite accurate for the small mass fractions  $w_1$  involved in this problem. By dividing Eq. (3-78) by Eq. (3-77), the following expression is obtained.

$$\xi^2 = \left( \frac{D_{12}}{\alpha} \right) \frac{\left[ \frac{1 - w_{1\infty}}{1 - w_{1W}} \right] \left[ 1 - \frac{B_2(\xi)}{(w_{1\infty} - w_{1W})} \right]}{1 + \left( \frac{\text{Pr}}{\text{Sc}} \right) \left[ B_2 - \frac{(w_{1\infty} - w_{1W})}{\xi} \right] \left[ B_1 + \frac{1}{(1 - w_{1W})} \right]} \quad (3-79)$$

It is noted from Eq. (3-79) that, for small values of  $w_1$ ,  $B_1$ , and  $B_2$ , the boundary layer thickness ratio is approximately equal to

$$\xi = (D_{12}/\alpha)^{1/2} = (\text{Pr}/\text{Sc})^{1/2} \quad (3-80)$$

Substitution of this expression for  $\xi$  on the right side of Eq. (3-79) results in an expression for the boundary layer thickness ratio which is simpler to use in calculations than the quadratic solution and is accurate within the third place for mass fractions less than 0.10, as is usually encountered in air humidity calculations.

$$\xi^2 = \frac{\left(\frac{\text{Pr}}{\text{Sc}}\right) \left[ \frac{1 - w_{1\infty}}{1 - w_{1W}} \right] \left[ 1 - \frac{B_2 (\text{Pr}/\text{Sc})^{1/2}}{(w_{1\infty} - w_{1W})} \right]}{1 + \left(\frac{\text{Pr}}{\text{Sc}}\right) \left[ B_2 - \frac{w_{1\infty} - w_{1W}}{(\text{Pr}/\text{Sc})^{1/2}} \right] \left[ B_1 + \frac{1}{(1 - w_{1W})} \right]} \quad (3-81)$$

From Eq. (3-77) one may solve for  $C_2$  in terms of  $C_1$  and other parameters. If this expression for  $C_2$  is then substituted into Eq. (3-76), one may then solve for the parameter  $C_1$  to obtain:

$$C_1 = \frac{(80/3)^{1/2} \nu \left\{ \frac{g [\beta_t (T_\infty - T_W) + \beta_m (w_{1\infty} - w_{1W})(\xi)]^{1/2}}{\nu^2} \right\}}{\left[ \frac{20}{21} + \text{Pr} \left\{ 1 + \left(\frac{\text{Pr}}{\text{Sc}}\right) \left[ B_2 - \frac{(w_{1\infty} - w_{1W})}{\xi} \right] \left[ B_1 + \frac{1}{(1 - w_{1W})} \right] \right\}^{-1} \right]^{1/2}} \quad (3-82)$$

Using this expression for  $C_1$  in Eq. (3-77), the remaining parameter  $C_2$  may be determined.

$$C_2 = \frac{(80)^{1/2} B_3^{1/2} [(20/21) + (\text{Pr}/B_3)]^{1/4}}{(80/3)^{1/4} (\text{Pr})^{1/2} \left\{ \frac{g [\beta_t (T_\infty - T_W) + \beta_m (w_{1\infty} - w_{1W})(\xi)]^{1/4}}{\nu^2} \right\}} \quad (3-83)$$

where

$$B_3 = 1 + \left(\frac{\text{Pr}}{\text{Sc}}\right) \left[ B_2 - \frac{w_{1\infty} - w_{1W}}{\xi} \right] \left[ B_1 + \frac{1}{(1 - w_{1W})} \right] \quad (3-84)$$

### 3.3.3. Correlation for the heat transfer coefficient

A local heat transfer coefficient  $h_c$  for the sensible heat transfer may be obtained from the heat flux expression, Eq. (3-42), and Newton's Law of cooling.

$$q_x = -k \left( \frac{dT}{dy} \right)_w + \left[ \frac{a R M^2 T_w}{M_1 M_2} \right] j_{1w} = h_c (T_w - T_\infty) \quad (3-85)$$

In terms of the previously defined parameters,

$$h_c = -k \left( \frac{d\theta}{dy} \right)_w - \rho c_p D_{12} B_1 \left[ \left( \frac{d\phi}{dy} \right)_w + B_2 \left( \frac{d\theta}{dy} \right)_w \right] \quad (3-86)$$

Substituting the expressions for the derivatives, Eqs. (3-67) and (3-68), the following expression for the local heat transfer coefficient is obtained.

$$h_c = \frac{2k}{\delta} + \frac{2k D_{12} B_1}{\delta \alpha} \left[ B_2 - \frac{(w_{1\infty} - w_{1w})}{\xi} \right] \quad (3-87)$$

A local Nusselt number may be defined as:

$$Nu_x = \frac{h_c x}{k} = \frac{2x}{\delta} \left\{ 1 + \left( \frac{Pr}{Sc} \right) B_1 \left[ B_2 - \frac{(w_{1\infty} - w_{1w})}{\xi} \right] \right\} \quad (3-88)$$

Using the fact that  $\delta = C_2 x^{1/4}$ , the Nusselt number may be expressed in terms of the parameters entering into the expression for  $C_2$ , Eq. (3-83). At this point, a Grashof number which applies to combined heat and mass transfer situations may be defined.

$$Gr_x = \frac{g [\beta_t (T_\infty - T_w) + \beta_m (w_{1\infty} - w_{1w})(\xi)] x^3}{\nu^2} \quad (3-89)$$

The first term in the right side of Eq. (3-89) is the conventional Grashof number for zero mass transfer; whereas, the additional term represents the effect of the additional buoyancy obtained from the presence of a concentration gradient in the boundary layer along with a temperature gradient.

The final expression for the local Nusselt number for the combined heat and mass transfer problem is:

$$Nu_x = 0.508 \psi (Gr_x Pr)^{1/4} \quad (3-90)$$

where

$$\psi = \frac{(Pr)^{1/4} \left\{ 1 + (Pr/Sc) B_1 \left[ B_2 - \frac{(w_{1\infty} - w_{1w})}{\xi} \right] \right\}}{(B_3)^{1/4} [Pr + 0.952 B_3]^{1/4}} \quad (3-91)$$

and  $B_3$  has been previously defined by Eq. (3-84). For a flat plate in laminar flow, the average Nusselt number is 4/3 times the local Nusselt number evaluated at  $x = L$ ; therefore, the average Nusselt number is:

$$\overline{Nu} = 0.677 \psi (Gr_L Pr)^{1/4} \quad (3-92)$$

It is noted from the preceding equations that, for zero thermal diffusion ( $B_1 = B_2 = 0$ ), the heat transfer correlation is given by:

$$\overline{Nu} = \frac{0.677 (Pr)^{1/4} (Gr_L Pr)^{1/4}}{(B_3)^{1/4} [Pr + 0.952 B_3]^{1/4}} \quad (3-93)$$

where:

$$B_3 = 1 - \left( \frac{\text{Pr}}{\text{Sc}} \right) \frac{(w_{1\infty} - w_{1w})}{(1 - w_{1w})(\xi)} \quad (3-94)$$

$$\xi = \left[ \frac{(\text{Pr}/\text{Sc}) (1 - w_{1\infty})}{(1 - w_{1w}) - (\text{Pr}/\text{Sc})^{1/2} (w_{1\infty} - w_{1w})} \right]^{1/2} \quad (3-95)$$

### 3.3.4. Correlation for the mass transfer coefficient

A local mass transfer coefficient  $h_m$  may be defined from the mass flux expression, Eq. (3-40), including the convective mass transfer.

$$m_{1w} = j_{1w} + \rho v_w w_{1w} = \rho h_m (w_{1w} - w_{1\infty}) \quad (3-96)$$

Elimination of the normal velocity at the frost surface by Eq. (3-7) yields:

$$h_m = \frac{j_{1w}}{(w_{1w} - w_{1\infty})(1 - w_{1w}) \rho} \quad (3-97)$$

Substituting for the mass flux from Eq. (3-40),

$$h_m = - \frac{D_{12}}{(w_{1w} - w_{1\infty})(1 - w_{1w})} \left[ \left( \frac{d\phi}{dy} \right)_w + B_2 \left( \frac{d\theta}{dy} \right)_w \right] \quad (3-98)$$

Using the previously determined expressions for the derivatives, the following expression is obtained for the local Sherwood number.

$$\frac{h_m x}{D_{12}} = Sh_x = \frac{2 x}{\delta \xi (1 - w_{1w})} \left[ 1 - \frac{B_2}{(w_{1\infty} - w_{1w})} \right] \quad (3-99)$$

Substitution for the boundary layer thickness, as in the case of the heat transfer correlation, yields the following correlation for the local mass transfer coefficient.

$$Sh_x = \frac{0.508 (Pr)^{1/2} (Gr_x)^{1/4} \left[ 1 - \frac{B_2 \xi}{(w_{1\infty} - w_{1w})} \right]}{(1 - w_{1w})(\xi)(B_3)^{1/4} [Pr + 0.952 B_3]^{1/4}} \quad (3-100)$$

where  $B_3$  is defined by Eq. (3-84). The average Sherwood number for a flat plate and laminar flow is equal to 4/3 times the local Sherwood number evaluated at  $x = L$ ; therefore,

$$\overline{Sh} = \frac{\overline{h_m L}}{D_{12}} = \frac{0.677 (Pr)^{1/4} (Gr_L Pr)^{1/4} \left[ 1 - \frac{B_2 \xi}{(w_{1\infty} - w_{1w})} \right]}{(1 - w_{1w})(\xi)(B_3)^{1/4} [Pr + 0.952 B_3]^{1/4}} \quad (3-101)$$

For the special case of zero thermal diffusion, the average Sherwood number is given by

$$\overline{Sh} = \frac{0.677 (Pr)^{1/4} (Gr_L Pr)^{1/4}}{(1 - w_{1w})(\xi)(B_3)^{1/4} [Pr + 0.952 B_3]^{1/4}} \quad (3-102)$$

where  $B_3$  is given by Eq. (3-94) for this special case.

### 3.3.5. Correlation for the enthalpy transport coefficient

In the case of frost formation in which there is a change of phase of the diffusing gas at the surface of the plate, the total heat flux, exclusive of radiation, is made up of the sensible heat flux plus the latent heat flux, i.e.,

$$q_c + q_m = \bar{h}_c (T_w - T_\infty) + \rho \bar{h}_m i_{sg} (w_{1w} - w_{1\infty}) \quad (3-103)$$

As suggested by other authors (18, 19, 20), an enthalpy transport coefficient may be used to determine the total heat flux if the enthalpy difference is properly defined. The enthalpy transport coefficient is defined from

$$q_c + q_m = \rho \bar{h}_i (i_w - i_\infty) \quad (3-104)$$

A local enthalpy number is defined from

$$Ni_x = h_i x / \alpha \quad (3-105)$$

with the average enthalpy number given by

$$\bar{Ni} = \bar{h}_i L / \alpha \quad (3-106)$$

The general relation for the enthalpy number for all cases of frost formation, whether under forced or free convection conditions, turbulent or laminar flow, may be developed as follows. Equating the total heat flux given by Eqs. (3-103) and (3-104) results in the following general relation:

$$\bar{Ni} (i_w - i_\infty) = \bar{Nu} c_p (T_w - T_\infty) + (Pr/Sc) \bar{Sh} i_{sg} (w_{1w} - w_{1\infty}) \quad (3-107)$$



Comparing Eqs. (3-92) and (3-101), the relationship between the Nusselt number and the Sherwood number for laminar flow is obtained.

$$\overline{Sh} = \frac{\frac{\overline{Nu}}{(\xi)(1 - w_{1w})} \left[ 1 - \frac{B_2 \xi}{(w_{1\infty} - w_{1w})} \right]}{1 + (Pr/Sc) B_1 \left[ B_2 - \frac{(w_{1\infty} - w_{1w})}{\xi} \right]} \quad (3-108)$$

For the case of zero thermal diffusion,

$$\overline{Sh} = \frac{\overline{Nu}}{(\xi)(1 - w_{1w})} \quad (3-109)$$

Using Eq. (3-108), it is observed that, if an "enthalpy" is defined as follows:

$$i = c_p T + \frac{\frac{(Pr/Sc) i_{sg} w_1}{(\xi)(1 - w_{1w})} \left[ 1 - \frac{B_2 \xi}{(w_{1\infty} - w_{1w})} \right]}{1 + (Pr/Sc) B_1 \left[ B_2 - \frac{(w_{1\infty} - w_{1w})}{\xi} \right]} \quad (3-110)$$

then, the following identity is true:

$$\overline{Ni} = \overline{Nu} \quad (3-111)$$

$$\text{or,} \quad \overline{h}_i = \overline{h}_c / \rho c_p \quad (3-112)$$

For the case of zero thermal diffusion, the enthalpy expression is somewhat more compact.

$$i = c_p T + \frac{(Pr/Sc) i_{sg} w_1}{(\xi)(1 - w_1)} \quad (3-113)$$

#### 3.4. Solution for turbulent flow

In this section, the general equations of momentum, energy, and diffusion will be solved under the assumption that turbulent flow exists in the boundary layer on the plate. Since the basic mechanisms of thermal diffusion and diffusion thermo-effect in turbulent flow have not been investigated, and such an investigation is not within the scope of the present investigation, the effects of thermal diffusion and diffusion thermo-effect will not be included in the development of this section.

The physical system to be considered with the coordinates used for the solution of the problem is the same as for the case of laminar flow, i.e., Figure 3. The dimensionless temperature and mass fraction parameters defined by Eqs. (3-51) and (3-52) are used, as for the case of laminar flow.

According to Reference (21), the measured velocity and temperature profiles for free convection heat transfer without mass transfer can be approximated by the following expressions:

$$\theta = 1 - (y/\delta)^{1/7} \quad (3-114)$$

$$u = u_m (y/\delta)^{1/7} [1 - (y/\delta)]^4 \quad (3-115)$$

These equations cannot be expected to yield the shear stress and heat flux at the surface from the velocity and temperature gradients at the surface, because these expressions apply only for the turbulent boundary layer and do not apply in the laminar sub-layer at the surface of the plate. The form of the velocity profile equation was chosen so that in the vicinity of the surface, the equation has the form  $u = u_m (y/\delta)^{1/7}$ , which is similar to the equation proposed by Prandtl for forced convection in turbulent flow over a flat plate. The concentration boundary layer in turbulent flow was assumed to be similar to the thermal boundary layer, as was done for the laminar flow problem; therefore, the mass fraction distribution in the turbulent boundary layer was chosen to be

$$\phi = (w_{1w} - w_{1\infty}) [1 - (y/\delta_m)^{1/7}] \quad (3-116)$$

From the experimental investigations of Prandtl for flow over flat plates in turbulent flow, the shear stress at the frost surface was assumed to be given by

$$(\tau_w/\rho) = 0.0228 u_m^2 (\delta/\nu)^{-1/4} \quad (3-117)$$

Applying the Colburn analogy between momentum and heat transfer,

$$\frac{\tau_w}{u_m^2 \rho} = \frac{q_w (Pr)^{2/3}}{\rho c_p u_m (T_w - T_\infty)} \quad (3-118)$$

the corresponding equation for the heat flux at the frost surface for turbulent flow is obtained.

$$\frac{q_w}{c_p} = \frac{0.0228 u_m (T_w - T_\infty)}{(Pr)^{2/3} (u_m \delta / \nu)^{1/4}} \quad (3-119)$$

Applying the Colburn analogy between heat and mass transfer,

$$\frac{q_w (Pr)^{2/3}}{\rho c_p u_m (T_w - T_\infty)} = \frac{m_{1w} (Sc)^{2/3}}{\rho u_m (w_{1w} - w_{1\infty})} \quad (3-120)$$

the corresponding equation for the mass flux at the frost surface for turbulent flow is given by

$$\frac{m_{1w}}{\rho} = \frac{0.0228 u_m (w_{1w} - w_{1\infty})}{(Sc)^{2/3} (u_m \delta_m / \nu)^{1/4}} \quad (3-121)$$

Using the preceding expressions and the assumption of constant fluid properties, the momentum, energy, and diffusion equations for turbulent flow may be written as follows.

(a) Momentum equation

$$\begin{aligned} \frac{d}{dx} \left[ \int_0^\delta u^2 dy \right] &= g (T_\infty - T_w) \left[ \beta_t \int_0^\delta \theta dy \right] - g \beta_m \int_0^{\delta_m} \phi dy - \\ &- 0.0228 u_m^2 (u_m \delta / \nu)^{-1/4} \end{aligned} \quad (3-122)$$

(b) Energy equation

$$\begin{aligned} \frac{d}{dx} \left[ \int_0^\delta \theta u dy \right] &= 0.0228 (Pr)^{-2/3} (u_m \delta / \nu)^{-1/4} u_m + \\ &+ 0.0228 (Sc)^{-2/3} (u_m \delta_m / \nu)^{-1/4} u_m \end{aligned} \quad (3-123)$$

(c) Diffusion equation

$$\frac{d}{dy} \left[ \int_0^{\delta_m} \phi u dy \right] = \frac{0.0228 (Sc)^{-2/3} (1 - w_{1\infty})(w_{1W} - w_{1\infty})u_m}{(1 - w_{1W})(u_m \delta_m / \nu)^{1/4}} \quad (3-124)$$

#### 3.4.1. Evaluation of the integrals

Using the functions for the velocity, temperature, and mass fraction distributions given by Eqs. (3-114), (3-115), (3-116), the following integrals were evaluated:

$$\int_0^{\delta} u^2 dy = 0.05231 u_m^2 \delta \quad (3-125)$$

$$\int_0^{\delta} \theta dy = \delta/8 \quad (3-126)$$

$$\int_0^{\delta_m} \phi dy = (w_{1W} - w_{1\infty})(\delta_m/8) \quad (3-127)$$

$$\int_0^{\delta} \theta u dy = 0.03663 u_m \delta \quad (3-128)$$

$$\int_0^{\delta_m} \phi u dy = 0.03663 u_m \delta_m \quad (3-129)$$

#### 3.4.2. Solution of the integral equations

Substitution of the expressions given in Eqs. (3-125) through (3-129) into the momentum, energy, and diffusion equations, and introducing the ratio of diffusion boundary layer thickness to thermal boundary layer thickness,  $\xi = \delta_m/\delta$ , resulted in the following expressions.

(a) Momentum equation

$$0.05231 \frac{d(u_m^2 \delta)}{dx} = \frac{1}{8} g [\beta_t (T_\infty - T_w) + \beta_m (w_{1\infty} - w_{1w})(\xi)] - 0.0228 u_m^2 (u_m \delta / \nu)^{-1/4} \quad (3-130)$$

(b) Energy equation

$$0.03663 \frac{d(u_m \delta)}{dx} = 0.0228 u_m (u_m \delta / \nu)^{-1/4} (\text{Pr})^{-2/3} \left[ 1 + \left( \frac{\text{Pr}}{\text{Sc}} \right)^{2/3} \frac{(w_{1w} - w_{1\infty})}{(1 - w_{1w})(\xi)^{1/4}} \right] \quad (3-131)$$

(c) Diffusion equation

$$0.03663 (\xi)^{5/4} \frac{d(u_m \delta)}{dx} = \frac{(1 - w_{1\infty}) 0.0228 u_m (\text{Sc})^{-2/3}}{(1 - w_{1w}) (u_m \delta / \nu)^{1/4}} \quad (3-132)$$

As in the case for laminar flow, the dependence of the parameters  $u_m$  and  $\delta$  on the coordinate  $x$  must be known to complete the solution. According to Reference (22), these parameters can be expressed as exponential functions of the coordinate  $x$  for turbulent flow as follows.

$$u_m = C_1 x^{1/2} \quad (3-133)$$

$$\delta = C_2 x^{7/10} \quad (3-134)$$

where the quantities  $C_1$  and  $C_2$  must be determined.

If the expressions for  $u_m$  and  $\delta$  are substituted into the momentum equation, Eq. (3-130), and the indicated differentiation carried out, the following algebraic equation is obtained:

$$0.08893 C_1^2 C_2 = \frac{1}{8} g [\beta_t (T_\infty - T_w) + \beta_m (w_{1\infty} - w_{1w})(\xi)] - 0.0228 C_1^2 (C_1 C_2 / \nu)^{-1/4} \quad (3-135)$$

A second algebraic equation is obtained by making the same substitutions into the energy equation, Eq. (3-131).

$$0.04396 C_2 = 0.0228 (Pr)^{-2/3} (C_1 C_2 / \nu)^{-1/4} \left[ 1 + \left( \frac{Pr}{Sc} \right)^{2/3} \frac{(w_{1w} - w_{1\infty})}{(1 - w_{1w})(\xi)^{1/4}} \right] \quad (3-136)$$

The third algebraic equation is obtained similarly from the diffusion equation, Eq. (3-132).

$$0.04396 C_2 \xi^{5/4} = \frac{0.0228 (1 - w_{1\infty})(Sc)^{-2/3}}{(1 - w_{1w})(C_1 C_2 / \nu)^{1/4}} \quad (3-137)$$

By dividing Eq. (3-137) by Eq. (3-136), the following expression is obtained for the boundary layer thickness ratio.

$$(\xi)^{5/4} = \frac{\left( \frac{1 - w_{1\infty}}{1 - w_{1w}} \right) \left( \frac{Pr}{Sc} \right)^{2/3}}{1 - \left[ \frac{(w_{1\infty} - w_{1w})}{(1 - w_{1w})(\xi)^{1/4}} \right] \left( \frac{Pr}{Sc} \right)^{2/3}} \quad (3-138)$$

It is noted from Eq. (3-138) that for small values of mass fraction, the boundary layer thickness ratio is approximately given by

$$\xi \doteq (\text{Pr}/\text{Sc})^{8/15} \quad \text{or} \quad (\xi)^{1/4} \doteq (\text{Pr}/\text{Sc})^{2/15} \quad (3-139)$$

Substitution of this expression for  $\xi$  on the right side of Eq. (3-138) results in the following expression for the boundary layer thickness ratio for turbulent flow.

$$\xi = \frac{\left(\frac{\text{Pr}}{\text{Sc}}\right)^{8/15} \left(\frac{1 - w_{1\infty}}{1 - w_{1W}}\right)^{4/5}}{\left[1 - \left(\frac{\text{Pr}}{\text{Sc}}\right)^{8/15} \frac{(w_{1\infty} - w_{1W})}{(1 - w_{1W})}\right]^{4/5}} \quad (3-140)$$

From Eq. (3-136) one may solve for  $C_2$  in terms of  $C_1$  and other parameters. If this expression is then substituted into Eq. (3-135), one may solve for the parameter  $C_1$  to obtain

$$C_1 = 1.186 \nu \frac{\{g [\beta_t (T_\infty - T_W) + \beta_m (w_{1\infty} - w_{1W})(\xi)]/\nu^2\}^{1/2}}{1 + \frac{0.494 (\text{Pr})^{2/3}}{\left[1 - \left(\frac{\text{Pr}}{\text{Sc}}\right)^{2/3} \frac{(w_{1\infty} - w_{1W})}{(1 - w_{1W})(\xi)^{1/4}}\right]}}$$

Using this expression for  $C_1$  in Eq. (3-136), the remaining parameter  $C_2$  may be determined.



$$C_2 = \frac{0.571 [1 + 0.494 (Pr)^{2/3} / (B_4)]^{1/10} (1 + B_4)^{4/5}}{(Pr)^{8/15} \left\{ \frac{g [\beta_t (T_\infty - T_w) + \beta_m (w_{1\infty} - w_{1w})(\xi)]}{v^2} \right\}^{1/10}} \quad (3-142)$$

where:

$$B_4 = \left( \frac{Pr}{Sc} \right)^{2/3} \frac{(w_{1w} - w_{1\infty})}{(1 - w_{1w})(\xi)} \quad (3-143)$$

### 3.4.3. Correlation for the heat transfer coefficient

A local heat transfer coefficient and local Nusselt number for sensible heat transfer may be defined as follows:

$$Nu_x = h_c x / k = q_w x / (T_w - T_\infty) k \quad (3-144)$$

Substitution of the expression for the heat flux at the surface given by Eq. (3-119) results in the following expression for the local Nusselt number.

$$Nu_x = 0.0228 (Pr)^{1/3} (u_m x / \nu)^{3/4} (x / \delta)^{1/4} \quad (3-145)$$

Using the fact that  $u_m = C_1 x^{1/2}$  and  $\delta = C_2 x^{1/4}$  and substituting for the parameters  $C_1$  and  $C_2$  from Eqs. (3-141) and (3-142), the following expression is obtained for the local Nusselt number.

$$Nu_x = \frac{0.0295 (Pr)^{7/15} (1 + B_4)^{1/5} (Gr_x)^{2/5}}{[1 + 0.494 (Pr)^{2/3} + B_4]^{2/5}} \quad (3-146)$$

where  $B_4$  is given by Eq. (3-143). The average Nusselt number is 5/6 times the local Nusselt number evaluated at  $x = L$ ; therefore,

$$\bar{Nu} = \bar{h}_c L / k = \frac{0.0246 (Pr)^{1/15} (1 + B_4)^{1/5} (Gr_L Pr)^{2/5}}{[1 + 0.494 (Pr)^{2/3} + B_4]^{2/5}} \quad (3-147)$$

Or, for turbulent flow,

$$\bar{Nu} = 0.0246 \psi (Gr_L Pr)^{2/5} \quad (3-148)$$

#### 3.4.4. Correlation for the mass transfer coefficient

A local mass transfer coefficient and local Sherwood number may be defined from

$$Sh_x = h_m x / D_{12} = m_1 x / \rho (w_{1w} - w_{1\infty}) D_{12}$$

Substitution of the expression for the mass flux at the surface given by Eq. (3-121) results in the following expression for the local Sherwood number.

$$Sh_x = 0.0228 (Sc)^{1/3} (u_m x / \nu)^{3/4} (x / \delta)^{1/4} (\xi)^{-1/4} \quad (3-149)$$

Substitution for the parameters  $u_m$  and  $\delta$ , as in the case of the heat transfer correlation, yields the following correlation for the local Sherwood number:

$$Sh_x = \frac{0.0295 (Pr)^{2/15} (Sc)^{1/3} (1 + B_4)^{1/5} (Gr_x)^{2/5}}{(\xi)^{1/4} [1 + 0.494 (Pr)^{2/3} + B_4]^{2/5}} \quad (3-150)$$

The average Sherwood number for a flat plate in turbulent flow is equal to 5/6 times the local Sherwood number evaluated at  $x = L$ ; therefore, the average Sherwood number is given by

$$\overline{Sh} = \overline{h_m} L / D_{12} = \frac{0.0246 (Pr)^{2/15} (Sc)^{1/3} (1 + B_4)^{1/5} (Gr_L)^{2/5}}{(\xi)^{1/4} [1 + 0.494 (Pr)^{2/3} + B_4]^2/5} \quad (3-151)$$

where  $B$  is given by Eq. (3-143).

#### 3.4.5. Correlation for the enthalpy transport coefficient

As in the case for laminar flow, an enthalpy transport coefficient and an enthalpy number may be defined from

$$\overline{Ni} = h_i L / \alpha = L (q_c + q_m) / \rho (i_w - i_\infty) \quad (3-152)$$

Comparing Eqs. (3-147) and (3-151), the following relationship between the average Nusselt number and average Sherwood number for turbulent flow is obtained.

$$\overline{Sh} = \overline{Nu} (Sc/Pr)^{1/3} (\xi)^{-1/4} \quad (3-153)$$

Making this substitution into the general expression for enthalpy number, Eq. (3-107), there is obtained

$$\overline{Ni} (i_w - i_\infty) = \overline{Nu} \left[ c_p (T_w - T_\infty) + \left( \frac{Pr}{Sc} \right)^{2/3} \frac{i_{sg}(w_{1w} - w_{1\infty})}{(\xi)^{1/4}} \right] \quad (3-154)$$

From Eq. (3-154) it is evident that, if the identity  $\overline{Ni} = \overline{Nu}$  or

$\overline{h_i} = \overline{h_c} / \rho c_p$  is to be valid, then the correct enthalpy to be used for turbulent flow is defined by

$$i = c_p T + \left( \frac{\text{Pr}}{\text{Sc}} \right)^{2/3} \frac{i_{sg} w_1}{(\xi)^{1/4}} \quad (3-155)$$

where the boundary layer thickness ratio is given by Eq. (3-140).

### 3.5. Transition Grashof number

An estimate of the value of the Grashof number at which the flow pattern changes from laminar to turbulent flow may be obtained by determining the Grashof number at which the laminar flow heat transfer correlation, Eq. (3-93), yields the same value for Nusselt number as the turbulent flow heat transfer correlation, Eq. (3-147). Equating the two expressions for the average Nusselt number results in the following expression for the transition Grashof number:

$$(\text{Gr}_L)_{\text{trans.}} = \frac{(3.94)(10^9)(\text{Pr})^{2/9} [1 + 0.494 (\text{Pr})^{2/3} + B_4]^{8/3}}{(1 + B_4)^{4/3} (B_3)^{5/3} (\text{Pr} + 0.952 B_3)^{5/3}} \quad (3-156)$$

A numerical value for the transition Grashof number may be calculated for the following typical values of the parameters:

$$\begin{array}{ll} T_w = -300^\circ\text{F} & w_{1w} = 0.000\dots \\ T_\infty = +80^\circ\text{F} & w_{1\infty} = 0.020 \\ \text{Pr} = 0.740 & \text{Pr}/\text{Sc} = 1.414 \end{array}$$

Using these values, the boundary layer thickness ratios are

$$\xi = 1.191 \text{ for laminar flow}$$

$$\xi = 1.207 \text{ for turbulent flow}$$

The other parameters in Eq. (3-156) are

$$B_3 = 0.976$$

$$B_4 = -0.0240$$

Substituting these values into Eq. (3-156) yields the transition Grashof number.

$$(Gr_L)_{trans} = 3.42 \times 10^9$$

The product of Grashof and Prandtl number (Rayleigh number) at transition is

$$(Gr_L Pr)_{trans} = (3.42)(10^9)(0.740) = 2.53 \times 10^9$$

According to Reference (23), the transition values of  $(Gr_L Pr)$  for free convection without mass transfer is  $10^9$ ; whereas, Reference (24) suggests a transition value of  $(Gr_L Pr)$  of between  $10^8$  and  $10^{10}$ ; therefore, the value calculated from the equations developed in this investigation agrees quite well with these references.

## CHAPTER IV

### EXPERIMENTAL APPARATUS AND PROCEDURE

#### 4.1. Description of experimental apparatus

A schematic of the test apparatus used to verify the analytical expressions for heat and mass transfer is shown in Figure 4.

The test set-up consisted of four parts:

- (a) Test plates
- (b) Reservoir vessel with associated guard vessel and guard shield
- (c) Boil-off measurement system
- (d) Frost thickness and temperature measurement probe

The major considerations taken into account in the design of the apparatus were: elimination of as much stray heat in-leak to the reservoir vessel as possible, accurate measurement of frost thickness and temperature profile in the boundary layer near the frost surface, and elimination of thermal stresses resulting from severe temperature differentials.

##### 4.1.1. Test plates

Two test plates were used in the investigation: (a) a "short" plate, 4 inches high, 12 inches long, and 0.75 inches thick, and (b) a "long" plate, 10 inches high, 12 inches long, and 0.75 inches thick. The height of the short plate was selected such that laminar

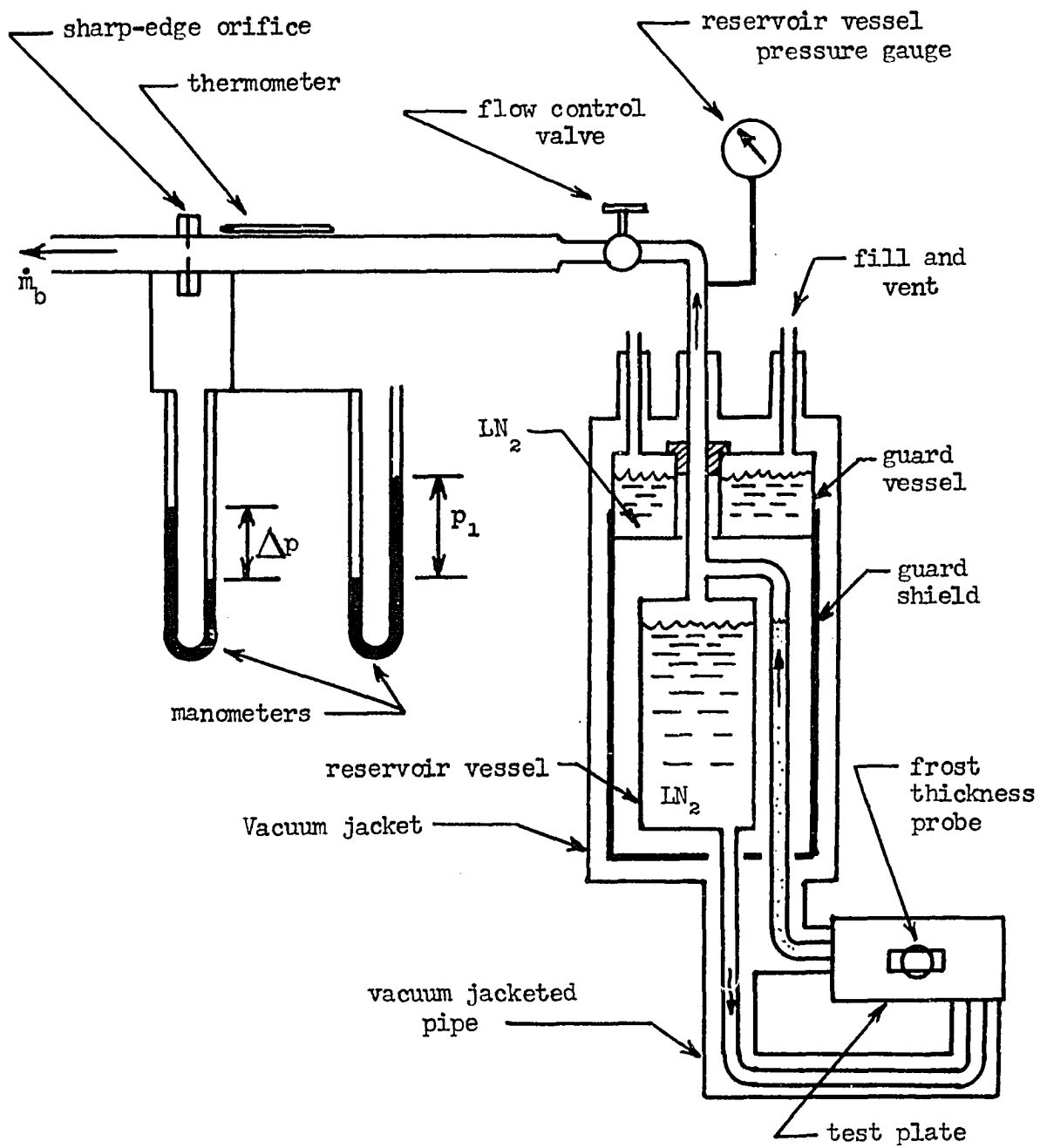


Figure 4. Schematic of test apparatus.

flow would prevail over the entire plate surface, while the height of the long plate assured turbulent flow over a major portion of the plate surface. Both plates were made of aluminum and were of welded construction.

The plates were hollow with a cavity of 3 in. x 11 in. x 0.50 in. for the short plate and 9 in. x 11 in. x 0.50 in. for the long plate. Each plate was connected to a vacuum-jacketed, multilayer insulated line at an inlet and an outlet by an O-ring sealed flange. The cryogenic liquid was fed by gravity to the plate at the inlet on the bottom, while the resulting vapor was carried away through the outlet at the upper corner of the plate. The area above the plate was free from any protuberances which would interfere with the flow pattern over the plate.

In order to prevent frost formation on the surface of the plate during the cool-down process, a special box covering of Styrofoam (an expanded urethane foam) was placed over the plate during this process. The Styrofoam box fit snugly over the whole plate surface except the areas at the side and bottom at which the inlet and outlet connections were made. When a run was to begin, the Styrofoam box was suddenly removed, and the timer started.

Frost was deposited on both sides of the plate in a symmetrical manner; therefore, thickness and temperature profile measurements were made on only one side of the plate.



#### 4.1.2. Reservoir vessel

A cylindrical stainless steel vessel 11 inches long and 6.625 inches in diameter was used as the reservoir vessel to contain the cryogenic fluid used to cool the plates during a run. As shown in Figure 4, the cryogenic fluid flowed from the bottom of the reservoir or inner vessel to the plates and returned to the fill and vent line of the reservoir vessel through a tee to equalize the static pressure in the system. The entire inner vessel and its contents were supported by a single tube (the fill and vent tube), which was 3/4 inch nominal schedule 5 stainless steel pipe. Horizontal motion of the inner vessel was constrained to some extent by a support ring placed between the fill and vent tube of the inner vessel and the guard vessel; however, the entire piping system was flexible enough to accommodate thermal strains encountered in cooling the apparatus down to operating temperature.

The inner vessel was surrounded by a second vessel (the guard vessel) and a copper shield. The purpose of the guard vessel and copper shield was to reduce any extraneous heat inleaks from ambient to the inner vessel. Since this was one of the critical parts of the design, an analysis is presented in Appendix C to demonstrate that the inner vessel was indeed well shielded from ambient heat inleaks. The guard vessel was filled with the same cryogenic liquid used in cooling the plate but was not pressurized. All surfaces of the guard vessel, inner vessel, copper shield, and inner surface of the vacuum jacket were polished before assembly in an attempt to further reduce heat transfer to these containers. The guard vessel was

supported by two 3/4 inch nominal schedule 5 stainless steel pipes which served as the vent and fill lines for the guard vessel.

The guard vessel and reservoir vessel were enclosed within a vacuum jacket 12.75 inches in diameter and 22 inches long. Six inch-long stand-offs (extensions of the vacuum jacket) were used on the fill and vent lines for the guard vessel and reservoir vessel to reduce conduction heat transfer along these pipes to the cold region. In the space between the jacket and the inner and reservoir vessels, the pressure was reduced by an oil diffusion pump through a CryoLab valve to a value of approximately  $10^{-5}$  mm Hg absolute to eliminate gaseous convection and reduce gaseous conduction to a minimum. As shown in Appendix C, the radiant heat flux to the guard vessel and shield was estimated at 5.84 Btu/hr-ft<sup>2</sup> for the guard vessel at liquid nitrogen temperature (140°R or -320°F). Using the Knudsen equation (25) for free molecular conduction and unity accommodation coefficients, the gaseous conduction heat flux may be estimated as follows. The Knudsen equation is

$$q_g = \left( \frac{\gamma + 1}{\gamma - 1} \right) F_a (g_c R / 8\pi T_a)^{1/2} p (T_a - T_c) \quad (4-1)$$

where :  $q_g$  = heat flux due to gaseous conduction,  $\gamma$  = ratio of specific heats = 1.40 for air,  $F_a$  = accommodation coefficient factor, given by:

$$F_a = \frac{1}{(1/a_1) + (A_1/A_2) [(1/a_2) - 1]} \quad (4-2)$$

$a_1$  = accommodation coefficient for the enclosed surface = 1 in this case,  $a_2$  = accommodation coefficient for the enclosure = 1 in this case,  $A_1$  = surface area of the enclosed cylinder,  $A_2$  = surface area of the enclosure,  $g_c$  = conversion factor in Newton's Second Law of Motion =  $32.174 \text{ ft-lb}_m / \text{lb}_f\text{-sec}^2$  in the British system of units,  $R$  = gas constant =  $53.35 \text{ ft-lb}_f / \text{lb}_m\text{-}^\circ\text{R}$  for air,  $T_a$  = temperature of the enclosure,  $T_c$  = temperature of the enclosed surface, and  $p$  = absolute pressure of the gas between the two surfaces =  $10^{-5} \text{ mm Hg}$  =  $1.934 \times 10^{-7} \text{ psia}$ . For unity accommodation coefficients, the accommodation coefficient factor is also unity. Substitution of the preceding factors into Eq. (4-1) and using  $T_a = 75^\circ\text{F}$  and  $T_c = -320^\circ\text{F}$  yields the following value for the gaseous conduction heat flux.

$$q_g = 0.109 \text{ Btu/hr-ft}^2$$

The supply and return line to the test plate from the reservoir vessel was not enclosed by the shield; however, both lines were vacuum jacketed and the inner line was covered with a multilayer insulation having a thermal conductivity of approximately  $2.5 \times 10^{-5} \text{ Btu/hr-ft-}^\circ\text{F}$  to reduce heat inleak to these elements.

#### 4.1.3. Boil-off measurement system

The heat transfer rate to the test plate was determined by measuring the rate at which liquid was boiled away within the plate. In order to measure this boil-off rate, a sharp-edge orifice was connected to the vent line of the reservoir vessel, as indicated in Figure 4. The orifice plate had a 1/4 inch diameter orifice in it

and was placed between an upstream section of 1 inch pipe 36 inches long and a downstream section of 1 inch pipe 12 inches long. Vena contracta taps were used in conjunction with a water manometer to measure the pressure drop across the orifice. From the pressure measurement at the orifice and upstream temperature measurement, the vapor mass flow rate was determined from the equations given in the ASME Fluid Meters Book (26).

#### 4.1.4. Frost thickness and temperature measurement probe

The frost thickness and temperature measurement probe consisted essentially of a micrometer with a thermocouple and two small rods mounted on it, as shown in Figure 5. The micrometer had a smallest division of 0.0005 inch, and the thermocouple used to measure the temperature distribution in the boundary layer was a copper and constantan thermocouple.

The probe unit was mounted on a slide on an apparatus-stand in front of the plate. The whole unit could be moved horizontally along the entire width of the plate, and could be moved a limited amount ( $\pm 1/2$  inch) vertically by placing small plates under the probe unit. Two platforms were provided on the apparatus-stand for the probe assembly so that measurement at two positions on the larger plate could be carried out.

A reference junction in an ice bath was used with the thermocouple, and the thermocouple output was read by a self-balancing potentiometer on a continuous recorder. The span of the recorder was adjusted so that the entire range of the recorder scale was used in

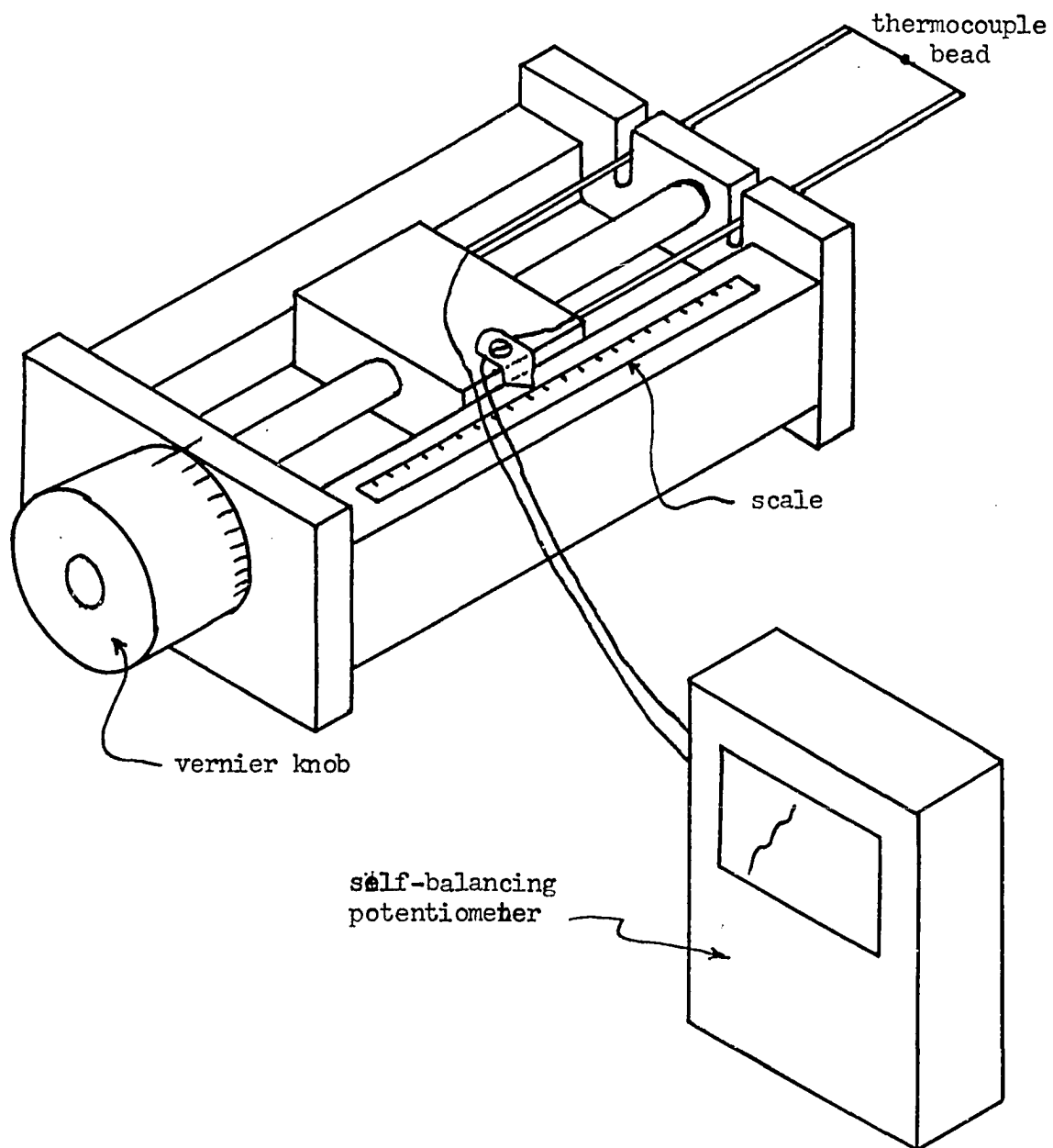


Figure 5. Frost thickness and temperature measurement probe.

traversing from the ambient temperature region to the cold plate surface.

The measurement of the frost thickness was carried out with the probe unit by shining a small flashlight on the surface of the frost near the tip of the pointed rod holding the thermocouple wire, and noting the reading of the micrometer when the shadow of the pointed rod and the rod point just touched.

#### 4.2. Experimental procedure

The typical procedure used in obtaining the experimental data is outlined in this section. Readings of temperature profile, frost thickness, pressure within reservoir vessel, and flow rate measurements were taken at 10 minute intervals for the smaller plate and at 5 minute intervals for the larger plate.

##### 4.2.1. Cool-down of apparatus

The first step in the experimental procedure was to cool down the apparatus by filling the reservoir vessel and guard vessel with the cooling liquid. The vessels were filled simultaneously to eliminate the possibility of thermal strains at the support point between the two vessels.

Both containers were filled by hand from dewar vessels. Since the reservoir vessel had only a single pipe for both filling and venting, some difficulty was experienced at first in filling this vessel. The difficulty was overcome by filling the inner vessel through a long copper tube which was inserted down the fill and vent

line of the reservoir vessel. At the upper end of this fill tube, a metal funnel was attached, and the cooling liquid was poured into the funnel to fill the inner container. The fill tube was smaller in diameter than the fill and vent line; therefore, the vapor evolved during the cool-down process flowed up the annular space between the fill tube and the fill and vent line, while the liquid flowed down within the fill tube. The guard vessel had two pipes attached to it, so no problem was experienced in filling the guard vessel through one pipe while the vapor evolved during cool-down escaped through the other pipe.

As mentioned previously, the test plate was covered by a Styrofoam box during the cool-down operation, in order that no frost formed on the surface of the plate. Prior to placing the Styrofoam box over the plate, a zero reading on the frost thickness probe was made to determine the position of the plate surface at initial time before frost formed on the plate surface.

The cool-down operation required approximately one hour to complete, primarily due to the slow rate at which the inner vessel could be filled with liquid. Approximately 22 lb<sub>m</sub> of stainless steel, 9 lb<sub>m</sub> of aluminum, and 26 lb<sub>m</sub> of copper had to be cooled from ambient temperature to the cryogenic temperature during the cool-down process. From the mass of solid and enthalpy changes of the various solid elements, it was estimated that approximately 4 gallons (15 liters) of liquid nitrogen was required for the cool-down operation. The capacity of the reservoir vessel was approximately 2

gallons; therefore, 8 gallons or 30 liters of liquid nitrogen was required to cool down the apparatus and fill the inner and guard vessels prior to a test run.

The filling operation was completed when a spray of liquid was observed in the venting vapor issuing from the vent line. When this occurred, the copper fill tube was withdrawn from the reservoir vessel, and the flow meter section was connected to the fill and vent line of the reservoir vessel by means of an O-ring sealed flanged connection. Since liquid nitrogen boils at approximately 6°F below the condensation point of air at atmospheric pressure, it was necessary to build up the pressure within the reservoir vessel to 10 psig to bring the saturation temperature of the boiling nitrogen slightly above the condensation temperature of ambient air. This was accomplished by means of a valve in the flow-meter section. The pressure within the reservoir vessel was held constant during a run and was monitored by observing a Bourdon pressure gauge and adjusting the control valve.

Immediately prior to beginning a test run, the barometric pressure and the wet and dry bulb temperatures of the ambient air in the room were measured. The wet and dry bulb temperatures were measured by a conventional sling psychrometer. This measurement was repeated at the conclusion of a test run, and an average value was used in the reduction of the data. The readings before and after a test run were very close to each other; usually varying less than 1 degree F. All test runs were made in the interferometer room in



Robinson Laboratory, Ohio State University, because this room could be isolated from the air conditioning system of the building. Before removing the Styrofoam box from the test plate to start a test run, the air supply to the interferometer room was shut off, thereby eliminating stray air currents from this source, which would seriously affect the free convection heat transfer data.

One set of runs was made with approximately 55% relative humidity in the test room, and another set of runs was made with near 100% relative humidity for approximately the same dry bulb temperature of the room in both cases. The high humidity was obtained by boiling water in the room for one hour during the time in which the apparatus was being cooled down.

#### 4.2.2. Frost thickness and temperature profile measurements

The first two or three minutes of each run was spent in adjusting the control valve in the flow-meter section to maintain a constant pressure of 10 psig in the reservoir vessel. At the end of this time, the pressure stabilized, and the frost thickness probe was positioned at approximately 0.3 inches from the plate surface.

At intervals of 10 minutes for the smaller plate and 5 minutes for the larger plate, temperature profile and frost thickness measurements were made. The temperature profile measurements were made by advancing the thermocouple bead between the two rods in the thickness probe in steps of 0.025 inches by turning the micrometer on the probe while the chart drive was moving the strip chart on the self-

balancing potentiometer used to indicate temperature. A prior measurement showed that the time constant for the thermocouple was approximately 5 seconds; therefore, the thermocouple bead was allowed to remain at each position for 10 or 15 seconds before advancing it further. The temperature profile measurement required between 2 and 3 minutes to complete due to this restriction. The temperature at each position was indicated by plateaus in the temperature curve drawn on the strip chart by the potentiometer. The frost surface temperature was determined by plotting the temperature profile and extrapolating this profile to the frost surface, since the temperature profile became approximately linear adjacent to the surface.

When the probe rod tip approached the frost surface, a flashlight was turned on to illuminate the frost surface near the pointed tip of the rod. The rod was advanced until the shadow of the rod tip on the frost surface just touched the rod tip, and the reading of the micrometer was noted at this time; thereby giving an indication of the frost thickness.

#### 4.2.3. Boil-off rate measurement

Immediately after taking a frost thickness measurement, the frost thickness probe was withdrawn to approximately 0.3 inches from the plate surface, and a reading of boil-off rate was taken. The boil-off rate was determined from readings of the pressure drop across the orifice in the flow-meter section, the upstream pressure of the effluent vapor before the orifice, and the upstream temperature before reaching the orifice plate by passing the vapor through a length of pipe exposed to ambient air.

The boil-off rate was calculated from these measurements by the orifice equation given in the ASME Fluid Meters Handbook:

$$\dot{m}_D = F_m F_a F_C Y (\rho_1 \Delta p)^{1/2} \quad (4-3)$$

where  $\dot{m}$  = mass flow rate of vapor, lb<sub>m</sub>/hr,  $F_m$  = orifice factor = 13.495 for a 0.250 inch diameter orifice installed in a 1.049 inch ID pipe,  $F_a$  = orifice diameter contraction factor = 1,000 for a gas temperature between 32°F and 84°F,  $F_C$  = Reynolds number correction factor, given by

$$F_C = 1 + (E/Re_o) \quad (4-4)$$

where  $E = 156.6$  for a 0.250 inch orifice in a 1.049 inch ID pipe, and  $Re_o$  = orifice Reynolds number based on the orifice diameter and flow rate per unit orifice cross sectional area. The quantity  $Y$  is the expansion factor, which accounts for compressibility effects of the flowing gas. For the small pressure differences used in the present investigation, the expansion factor could be calculated from

$$Y = 1 - 0.01057 (\Delta p/p_1) \quad (4-5)$$

where:  $\Delta p$  = pressure drop across the orifice, inches of water, and  $p_1$  = upstream pressure of the flowing gas before the orifice, psia. The quantity  $\rho_1$  in Eq. (4-3) is the density of the gas upstream of the orifice.

Since the Reynolds number used in calculating the Reynolds number correction factor was dependent upon the mass flow of gas through

the orifice, and this quantity was not known, the determination of the gas mass flow rate was an iterative process; however, since the Reynolds number correction factor was near unity, only two or three trials were required before a satisfactory solution was obtained.

The total heat transfer rate to the test plate and the boil-off rate are related by (see, e.g., Scott (25), pg. 203).

$$\dot{Q} = \frac{i_{fg} \dot{m}_b}{1 - (\rho_g / \rho_f)} \quad (4-6)$$

where:  $i_{fg}$  = heat of vaporization of the cooling fluid at the operating pressure,  $\rho_g$  = density of the saturated vapor at the operating pressure within the reservoir vessel, and  $\rho_f$  = density of the saturated liquid at the same condition. The factor in the denominator of Eq. (4-6) accounts for the fact that not all of the vapor evolved in vaporizing a unit mass of liquid leaves the reservoir vessel. For example, if one ft<sup>3</sup> of liquid is vaporized, one ft<sup>3</sup> of vapor remains behind to occupy the space left by the liquid; therefore, the boil-off vapor mass flow rate  $\dot{m}_b$  is smaller than the rate of liquid boil-off rate by the factor in the denominator of Eq. (4-6). The value of heat transfer rate as determined by Eq. (4-6) was the total heat transfer rate made up of a convective portion, a radiation portion, and a latent heat transport portion.

#### 4.2.4. Density and mass transfer measurement

The measurement of the thickness of frost as a function of time together with a knowledge of the surface area of the plate allowed the

determination of the volumetric rate at which frost was deposited on the plate surface; however, in order to determine the mass transfer rate, the frost density was required. The frost density was measured in this investigation at three points: at thirty-minute intervals for the small plate, and at 15 minute intervals for the large plate. At the end of a run, the first frost density measurement was made by scraping of the accumulated frost into a graduated vial, allowing the frost to melt, and measuring the volume of water resulting from the melted frost. From this measurement, the total mass of frost deposited on one side of the plate was determined. Since the thickness of the frost (and, hence, the volume of frost) was known at the end of the run, a mean frost density could be calculated from the ratio of mass of frost to volume of frost.

For the two intermediate measurements, the test run was repeated, except that the frost was scraped off of one side of the plate at the end of the previously mentioned time interval, and then after the next time interval, the frost was scraped off of the other side of the plate.

The mass transfer rate of water vapor to the plate was determined by plotting the mass of frost accumulated as determined from the product of frost density and frost volume as a function of time and graphically differentiating the curve. The frost build-up data was smoothed before carrying out this differentiation.

#### 4.2.5. Determination of heat transfer rates

The individual components of energy transfer were determined by the following method. As mentioned in 4.2.3., the measured value of

heat transfer rate was the total of three components: a convective or sensible heat transport, a radiation energy transport, and a latent heat transport associated with the mass transfer. The last component, the latent heat transport  $q_m$  was determined from

$$q_m = m_1 i_{sg} \quad (4-7)$$

where  $m_1$  is the water vapor mass flux as determined from the frost thickness and frost density measurements. The radiation heat flux was calculated from

$$q_r = \sigma e_f (T_\infty^4 - T_w^4) \quad (4-8)$$

where the frost surface temperature  $T_w$  was determined from the temperature profile measurements, and the emissivity of the frost surface for thermal radiation  $e_f$  was taken as 0.92, as suggested by Holten (11). The sensible heat flux was finally calculated as the difference between the total measured heat flux and the sum of the radiation and latent transport components.

The radiation component of the total heat flux amounted to approximately 25% of the total heat flux, while the latent heat flux was less than 5% of the total heat flux. For this reason, the value of frost emissivity assumed had a significant effect on the calculated value of the convective or sensible heat flux. Dorsey (27) measured the emissivity of white frost layers 0.1 to 0.2 mm thick (0.025 to 0.050 inches thick) at a temperature of +14.7°F and found this value to be  $0.985 \pm 0.030$ . Kamei (2) assumed a value of 0.984

for the frost emissivity in his calculations. Both of these investigations were carried out at temperatures much above the cryogenic range used in this work, however. At cryogenic temperatures, it was felt that the emissivity of the frost surface would be somewhat lower than the values near 32°F; therefore, the value of 0.92 suggested by Holten was chosen.

## CHAPTER V

### DISCUSSION OF RESULTS

#### 5.1. Effect of thermal diffusion

The effect of thermal diffusion on the convective heat transport is determined by the magnitude and algebraic sign of the parameters  $B_1$  and  $B_2$  in Eq. (3-91). These thermal diffusion parameters were defined in Eqs. (3-53) and (3-54) as follows:

$$B_1 = \frac{a R M^2}{M_1 M_2 c_p [1 - (T_\infty/T_w)]} \quad (5-1)$$

$$B_2 = a w_{1w} (1 - w_{1w}) [1 - (T_\infty/T_w)] \quad (5-2)$$

It is apparent from the above definitions that the thermal diffusion parameters depend upon the thermal diffusion constant  $a$ , the mass fraction of component 1 at the interface  $w_{1w}$ , and the ratio of free stream temperature to interface temperature  $T_\infty/T_w$ . For mixtures in which the thermal diffusion constant is positive and the plate is cooled ( $T_\infty/T_w$  greater than unity), both of the parameters  $B_1$  and  $B_2$  are negative. A positive value of the thermal diffusion constant indicates a transport of energy to the plate, as may be observed from Eq. (3-42), if the plate is at a lower temperature than its surroundings; therefore, the convective heat transfer rate is increased by thermal diffusion in this case.



On the other hand, if the thermal diffusion constant is negative (as is the case for air-water-vapor mixtures) and if the plate is cooled, the parameters  $B_1$  and  $B_2$  are both positive. A negative value of the thermal diffusion constant indicates a flux of energy away from the plate for the cooled plate; therefore, the effect of thermal diffusion is to reduce the convective heat transfer component. The magnitude of this effect depends upon the magnitude of the thermal diffusion parameters.

In order to ascertain if thermal diffusion would contribute significantly to the heat transfer for the case of water vapor diffusing through air, one may calculate numerical values for the thermal diffusion parameters. The author was unable to find experimental values for the thermal diffusion constant for mixtures of air and water vapor, so this property was calculated from theoretical models, as outlined in Appendix B. The Sutherland model, in which the molecules are assumed to be elastic spheres which attract each other with a force inversely proportional to the seventh power of the intermolecular spacing, yields results for the transport properties which agree fairly well with experimental measurements; therefore, this model was chosen in evaluating the thermal diffusion constants. From Appendix B, the thermal diffusion constant for water vapor and air mixtures was found to be  $a = -0.0856$ .

In order to illustrate the effect of thermal diffusion in this case, let the following values be selected:

- (a) Interface temperature,  $T_w = 160^\circ\text{R} = -300^\circ\text{F}$

(b) Free stream temperature,  $T_\infty = 600^\circ\text{R} = 140^\circ\text{F}$

(c) Mass fraction of water vapor at the interface,  $w_{1W} = 0$ .

The saturation mass fraction of water vapor in air at  $-300^\circ\text{F}$  is approximately  $5 \times 10^{-24}$ ; therefore, for purposes of illustration, it may be taken as zero.

(d) For small mass fractions of water vapor,  $(M^2/M_1 M_2) = (M_2/M_1)$  and  $R = 0.0684 \text{ Btu/lb}_m\text{-}^\circ\text{R}$ .

(e) Specific heat,  $c_p = 0.240 \text{ Btu/lb}_m\text{-}^\circ\text{R}$ .

Substitution of these numbers in Eqs. (5-1) and (5-2) results in the following values for the thermal diffusion parameters:

$$B_1 = + 0.0143$$

$$B_2 = 0$$

These quantities are quite small, so one would expect that the effect of thermal diffusion is small in this case.

Substitution of the values for  $B_1$  and  $B_2$  into Eq. (3-92) would illustrate the magnitude of the effect of thermal diffusion on the convective heat flux. For  $\text{Pr} = 0.735$ ,  $(\text{Pr}/\text{Sc}) = 1.403$ , and  $w_{1\infty} = 0.10$ , the following values are calculated.

(a) Boundary layer thickness ratio

With thermal diffusion . . . . .  $\xi = 1.199$

Without thermal diffusion . . . . .  $\xi = 1.198$

(b) The function  $\overline{\text{Nu}}/(\text{Gr}_L \text{Pr})^{1/4}$

With thermal diffusion . . . . . 0.577

Without thermal diffusion . . . . . 0.578

From this numerical example, it is apparent that thermal diffusion plays a very minor role in heat transfer for the case of frost formation on a plate exposed to ambient air, since the heat transfer rate is reduced by  $(0.578 - 0.577)/(0.577) = 0.17\%$  as a result of thermal diffusion. The reason for this small effect lies not in the small numerical value for the thermal diffusion constant, but primarily in the fact that the mass fraction of water vapor at the interface is so small for frost at cryogenic temperatures. Since the thermal diffusion ratio is expressed at  $k_T = a w_1 (1 - w_1)$ , if the mass fraction  $w_1$  is practically zero (say on the order of  $10^{-22}$ ), then the thermal diffusion ratio will also be practically zero. The statement is made in some treatments of mass transfer (see Reference 13, pg. 452, for example) that extreme temperature gradients result in appreciable mass flow due to thermal diffusion; however, this statement is true only for cases in which the mass fraction at the interface is not insignificant. In spite of the large temperature gradients at the frost interface (gradients on the order of  $5000^\circ\text{F}/\text{inch}$ ), thermal diffusion plays a minor part in the energy transport because the thermal diffusion ratio is practically zero at the interface.

## 5.2. Effect of mass transfer on heat transfer

According to Eq. (3-92) the heat transfer correlation may be written in the following form for laminar flow without thermal diffusion:

$$\frac{\overline{Nu}}{(Gr_L Pr)^{1/4}} = \frac{0.677 (Pr)^{1/4}}{(B_3)^{1/4} [Pr + 0.952 B_3]^{1/4}} \quad (5-3)$$

where the parameter  $B_3$  is defined as follows:

$$B_3 = 1 - \left( \frac{\text{Pr}}{\text{Sc}} \right) \frac{(w_{1\infty} - w_{1w})}{(1 - w_{1w})(\xi)} \quad (5-4)$$

and

$$\xi = \left[ \frac{(\text{Pr}/\text{Sc})(1 - w_{1\infty})}{(1 - w_{1w}) - (\text{Pr}/\text{Sc})^{1/2} (w_{1\infty} - w_{1w})} \right]^{1/2} \quad (5-5)$$

It is noted that the right side of Eq. (5-3) is a function of properties of the surrounding gas ( $\text{Pr}$ ,  $\text{Sc}$ ) and the mass fractions of component 1 in the free stream and at the interface; therefore, the right side is independent of the dimensions of the plate. For the case of zero mass transfer, according to Reference (21), pg. 315,

$$\frac{\overline{\text{Nu}}}{(\text{Gr}_L \text{Pr})^{1/4}} = \frac{0.677 (\text{Pr})^{1/4}}{(\text{Pr} + 0.952)^{1/4}} \quad (5-6)$$

From a comparison of Eqs. (5-3) and (5-6), it is seen that the effect of mass transfer on the convective portion of the heat flux (as determined by the effect on the convection coefficient  $h_c$ ) may be observed by plotting the right side of Eq. (5-3) as a function of the mass fraction of component 1 in the free stream for various values of  $\text{Pr}$ ,  $\text{Sc}$ , and  $w_{1w}$ . For the case of frost formation on a plate cooled to cryogenic temperatures, the mass fraction of water vapor at the frost interface is practically zero, so this variable

is eliminated for this special case. For laminar flow, the ratio of the convective coefficient for non-zero mass transfer to the convective coefficient for the same conditions except with zero mass transfer is given by

$$\frac{\overline{h}_c}{(\overline{h}_c)_{m=0}} = \frac{(\text{Pr} + 0.952)^{1/4}}{(\text{Pr} + 0.952 B_3)^{1/4} (B_3)^{1/4}} \quad (5-7)$$

For the problem of frost formation,  $B_3$  is a quantity less than unity; therefore, the effect of mass transfer is to increase the convection heat transfer coefficient.

Similarly, for turbulent flow with non-zero mass transfer,

$$\frac{\overline{\text{Nu}}}{(\text{Gr}_L \text{Pr})^{2/5}} = \frac{0.0246 (\text{Pr})^{1/15} (1 + B_4)^{1/5}}{[1 + 0.494 (\text{Pr})^{2/3} + B_4]^{1/5}} \quad (5-8)$$

as given by Eq. (3-147), where

$$B_4 = \left( \frac{\text{Pr}}{\text{Sc}} \right)^{2/3} \frac{(w_{1w} - w_{1\infty})}{(1 - w_{1w})(\xi)^{1/4}} \quad (5-9)$$

$$\xi = \frac{\left( \frac{\text{Pr}}{\text{Sc}} \right)^{8/15} \left( \frac{1 - w_{1\infty}}{1 - w_{1w}} \right)^{4/5}}{\left[ 1 - \left( \frac{\text{Pr}}{\text{Sc}} \right)^{8/15} \frac{(w_{1\infty} - w_{1w})}{(1 - w_{1w})} \right]^{4/5}} \quad (5-10)$$

For the case of zero mass transfer in turbulent flow, according to Reference (21), pg. 324,

$$\frac{\overline{Nu}}{(Gr_L Pr)^{2/5}} = \frac{0.0246 (Pr)^{1/15}}{[1 + 0.494 (Pr)^{2/3}]^{2/5}} \quad (5-11)$$

The ratio of the convective heat transfer coefficient with mass transfer to the convective coefficient without mass transfer is then given by:

$$\frac{\overline{h}_c}{(\overline{h}_c)_{m=0}} = \frac{[1 + 0.494 (Pr)^{2/3}]^{2/5} (1 + B_4)^{1/5}}{[1 + 0.494 (Pr)^{2/3} + B_4]^{2/5}} \quad (5-12)$$

The effect of mass transfer on the convective heat transfer coefficient for laminar and turbulent flows is illustrated in Figures 6 and 7 for  $Pr = 0.735$  and  $(Pr/Sc) = 1.403$ . As noted from both of these plots, the effect of mass transfer to the plate on the film coefficient is to increase the film coefficient. This effect is slightly more pronounced for laminar flow than for turbulent flow. For a mass fraction  $w_{1\infty} = 0.10$  for laminar flow,  $(\overline{h}_c/\overline{h}_{c,m=0}) = 1.046$ ; whereas, for turbulent flow,  $(\overline{h}_c/\overline{h}_{c,m=0}) = 1.043$ . For the small mass fraction, the effect of mass transfer is seen to be fairly small (on the order of 4% to 5%). The specific humidity for moist air corresponding to a mass fraction of 0.10 is

$$W = \frac{w_1}{1 - w_1} = \frac{0.10}{0.90} = 0.1111 \text{ lb}_m \text{ water/lb}_m \text{ dry air}$$

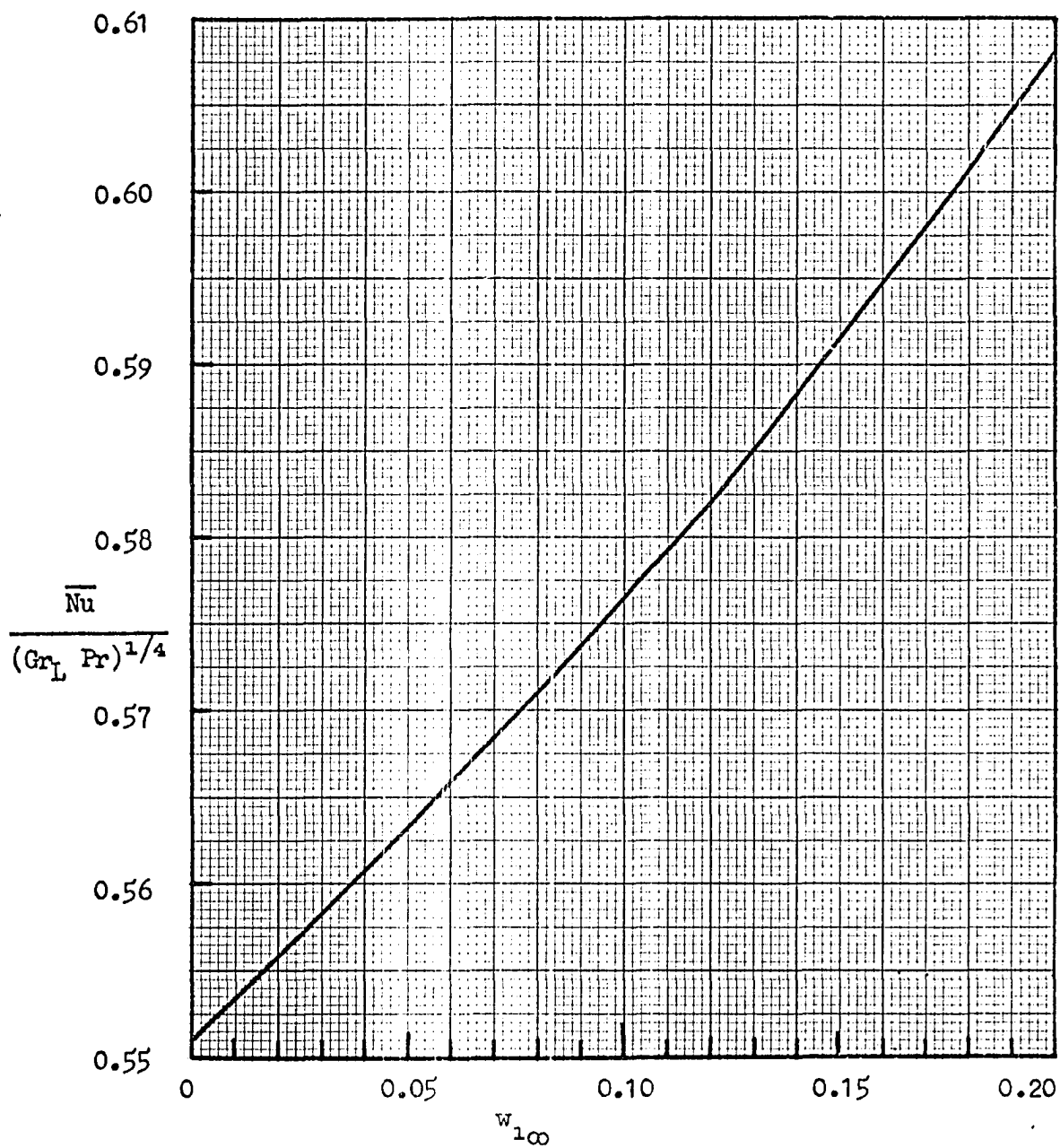


Figure 6. Variation of  $\overline{Nu}/(Gr_L Pr)^{1/4}$  with  $w_{1\infty}$  for laminar flow.

The curve is plotted for  $Pr = 0.735$ ,  $(Pr/Sc) = 1.403$ , and

$$w_{1w} = 0.$$

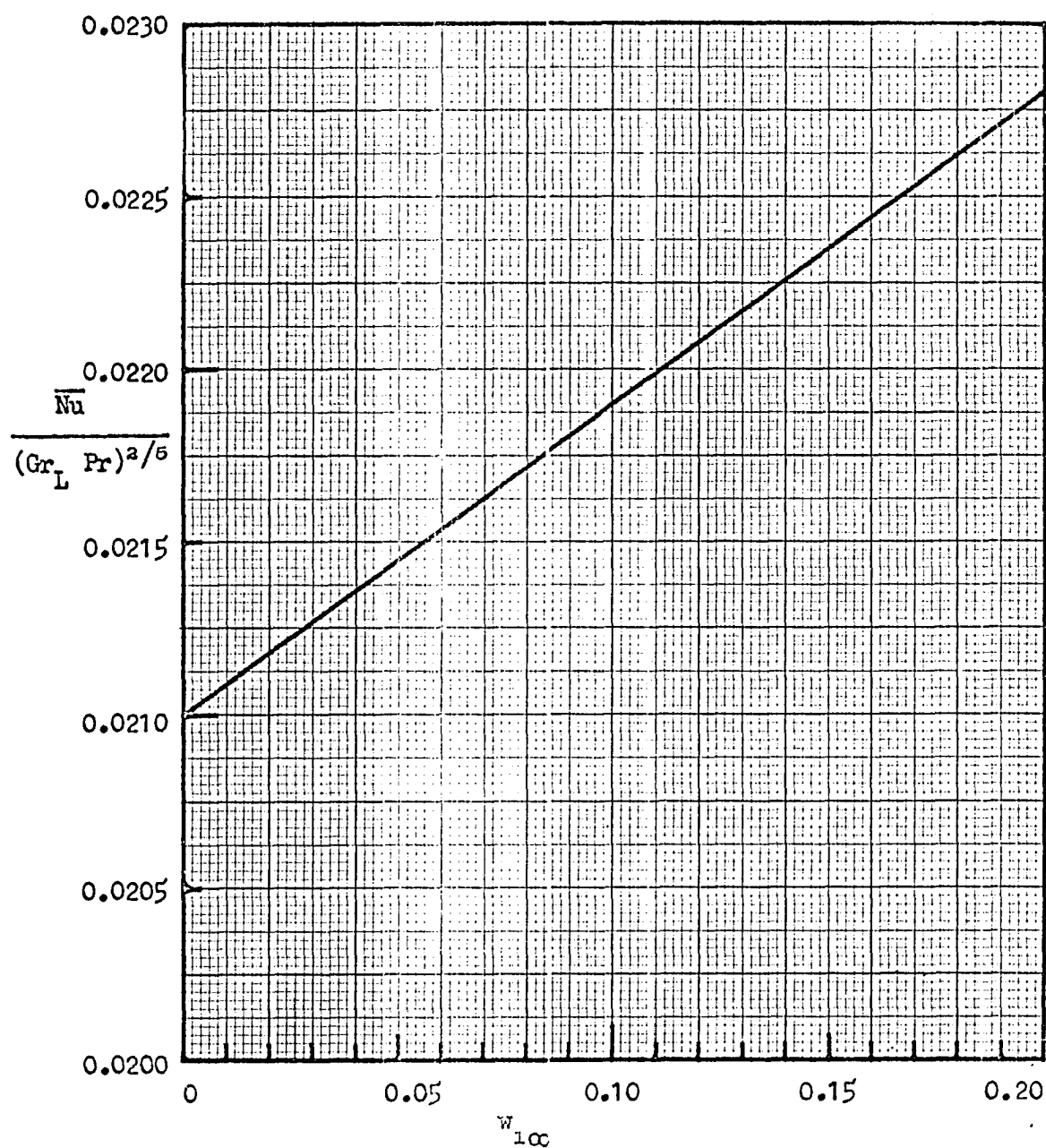


Figure 7. Variation of  $\overline{Nu}/(Gr_L Pr)^{2/5}$  with  $w_{1\infty}$  for turbulent flow.

The curve is plotted for  $Pr = 0.735$ ,  $(Pr/Sc) = 1.403$ , and

$w_{1w} = 0$ .



In order to attain this specific humidity even for saturated air, the dry bulb temperature would be slightly less than 130°F; therefore, mass transfer should have a relatively small effect on the free convection heat transfer coefficient for frost formation on a cryogenically cooled surface, for which the mass fraction at the interface is practically zero.

### 5.3. Experimentally measured heat transfer rates

A typical plot of the experimentally measured total heat flux and the three components of the total heat flux is shown in Figure 8. As would be expected, the total heat flux decreased with time as the insulating layer of frost was deposited on the surface of the plate. In comparing the theoretical expressions and the experimentally measured values, the assumption of quasi-steady-state was used. This assumption is justified in Appendix D, in which it is shown that the time required to reach steady-state is on the order of 1 second for a sudden change in surface temperature.

At the end of 10 minutes, the total heat flux was distributed as follows: (a) convective portion = 82.7%, (b) radiation portion = 16.8%, and (c) mass transfer portion = 0.5%. At the end of 88 minutes, the total heat flux was distributed as follows: (a) convective portion = 78.3%, (b) radiation portion = 21.1%, and (c) mass transfer portion = 0.6%. It is seen from these numbers that the contribution of latent heat transport to the total heat flux was small for frost formation on a cryosurface, and that the predominant contribution was the convective component. Since it was necessary

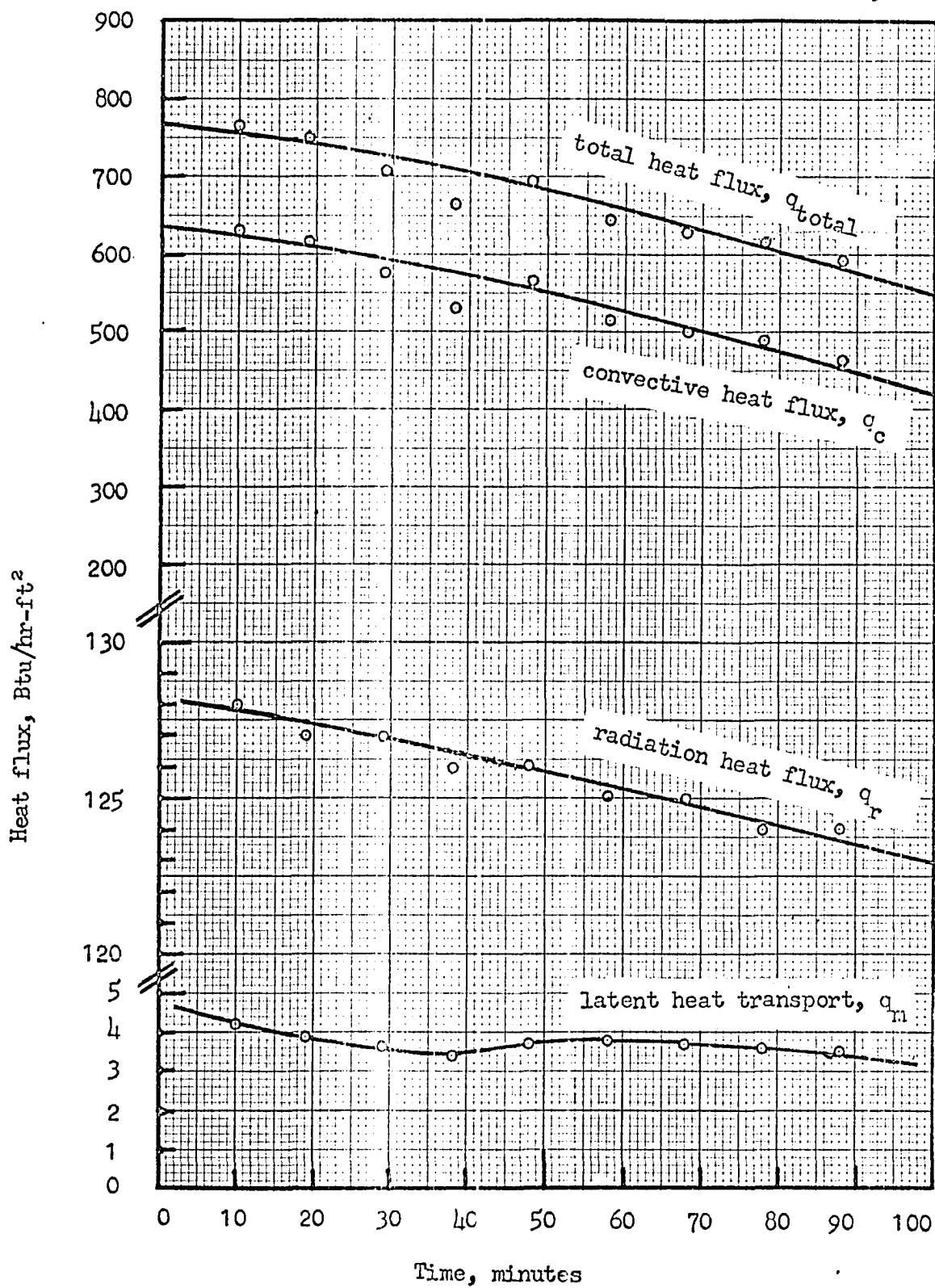


Figure 8. Heat transfer measurements. Run No. 1,  $L = 4$  inches,

$$T_{\infty} = 75.0^{\circ}\text{F}, w_{1\infty} = 0.01011$$

to pressurize the liquid nitrogen used to cool the plate and transfer of liquid nitrogen under pressure to the cryostat could not be carried out, the time of the individual runs was limited by the capacity of the reservoir vessel in the cryostat to approximately 90 minutes for the smaller plate and 30 to 45 minutes for the larger plate. Some scatter was noted in the measurement of the total heat flux due to the inability of controlling the flow precisely to maintain a constant pressure within the reservoir vessel. It is generally noted, however, that a point which is lower than the average curve is usually followed by a point which is above the average curve. This was a result of the adjustment of the control valve as the pressure within the reservoir vessel was observed to decrease slightly below or above the set point of 10 psig. A low point resulted when the reservoir vessel pressure fell below 10 psig, and the following high point resulted when the control valve was opened slightly to allow the pressure to decrease when the pressure rose above the 10 psig value.

In Figure 9 the average Nusselt number is plotted as a function of the Rayleigh number (product of Grashof and Prandtl numbers). The experimental correlation fell somewhat below the theoretical correlation. The slope of the experimental curve in the laminar flow regime did approach the theoretical value of  $1/4$ . The number of points in the turbulent flow regime was insufficient to determine a definite value for the slope of the experimental curve; however, the points did lie near a curve with a slope of  $2/5$  as indicated by theory.

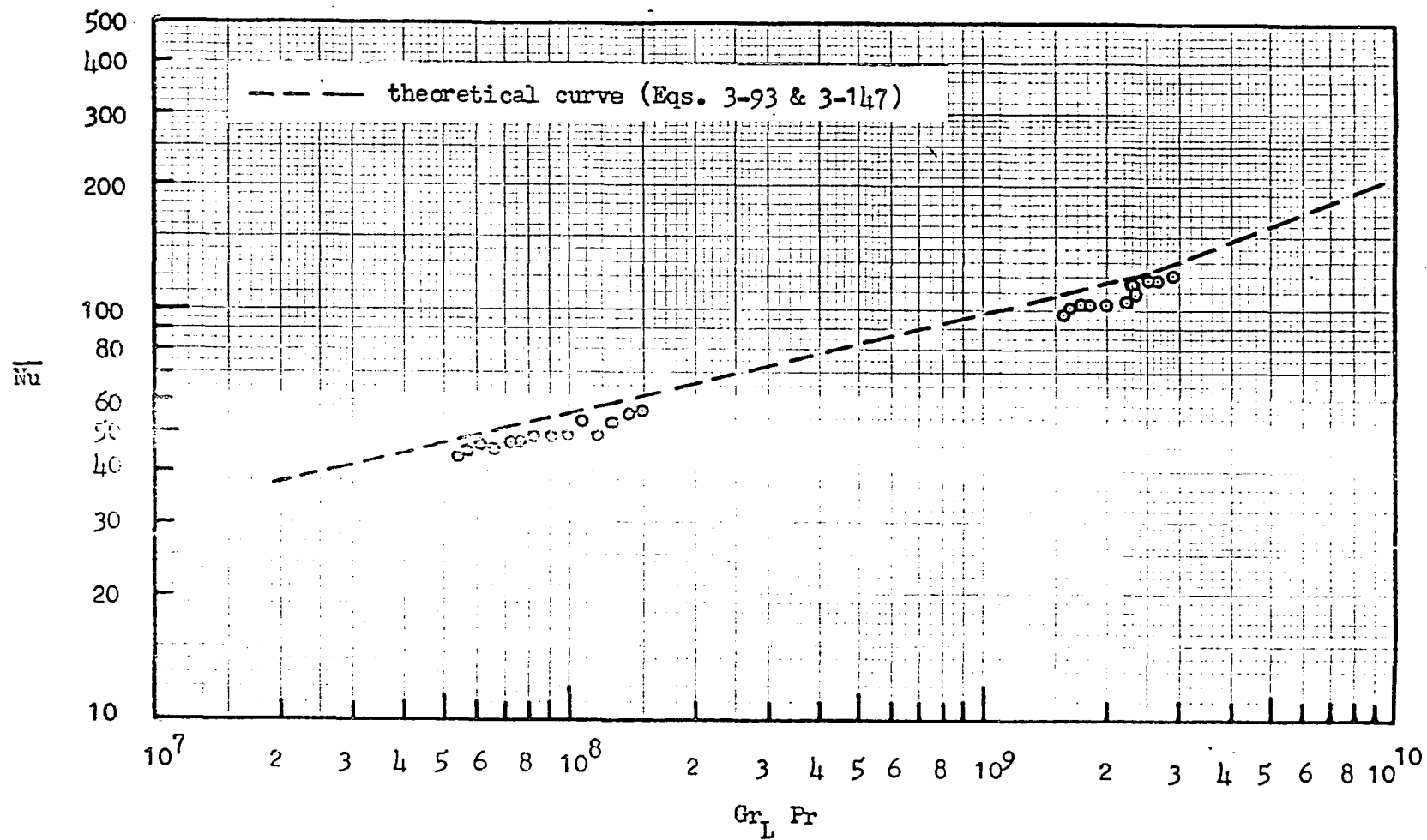


Figure 9. Experimental heat transfer correlation.

As shown in Appendix F, the constant coefficient in Eq. (3-92) taken from an average of 23 different points was found to be 0.616 instead of the predicted value of 0.677, which represents a departure from the theoretical value of 9%. In the theoretical solution, however, a parabolic temperature distribution was assumed. Since the temperature distribution was not quite parabolic, some departure from the theoretical value was to be expected. For air with a Prandtl number of 0.714 and no mass transfer, Schmidt and Beckmann (28) calculated exactly the following correlation:

$$\overline{Nu} = 0.523 (Gr_L Pr)^{1/4} \quad (5-13)$$

In the experimental runs for this investigation, the Prandtl number evaluated at the mean film temperature was 0.729 to 0.741. Using the average values, the experimental curve for the laminar flow regime could be represented by

$$\overline{Nu} = 0.503 (Gr_L Pr)^{1/4} \quad (5-14)$$

In this case, the coefficient in Eq. (5-14) differed from the one in Eq. (5-13) by approximately 4%.

In the turbulent flow regime, the average numerical coefficient as given in Eq. (3-147) was 0.0246 from theoretical considerations, and was 0.0248 from an average of 9 experimental points.

In view of the agreement between the experimental and theoretical results, it was indicated that the flat plate results could be extended to other geometrical shapes. For example, for frost formation on a horizontal cylinder, using a characteristic length of

$L = 2.5 D$  as suggested in Reference (21), pg. 318, the free convection heat transfer coefficient correlation may be written for laminar flow as follows:

$$\overline{Nu} = \frac{\overline{h}_c D}{k} = \frac{0.538 (Pr)^{1/2} (Gr_D)^{1/4}}{[Pr + 0.952 B_3]^{1/4} (B_3)^{1/4}} \quad (5-15)$$

where  $B_3$  is defined by Eq. (5-4), and  $Gr_D$  is the Grashof number based on the diameter of the cylinder.

#### 5.4. Mass transfer results

A plot of the experimentally measured mass flux is shown in Figure 10. It is noted from this plot that the higher mass transfer rates occurred for the larger values of ambient mass fraction of water vapor, as would be expected. In three of the four cases, a maximum in the mass transfer rate occurred. If it had been possible to extend the time of the run for which no maximum was recorded, it is likely that a similar maximum would have been evidenced. This maximum in mass transfer rate has been observed previously by Holten (11) in his work on frost formation on spherical surfaces. As in the case of Holten's work, the maximum in the mass flux vs. time curve was sharpest for the larger values of ambient mass fraction of water vapor. It has previously been suggested (11) that the occurrence of a maximum in the mass transfer rate at a time later than at initial time was the result of the interaction of two mechanisms. Since

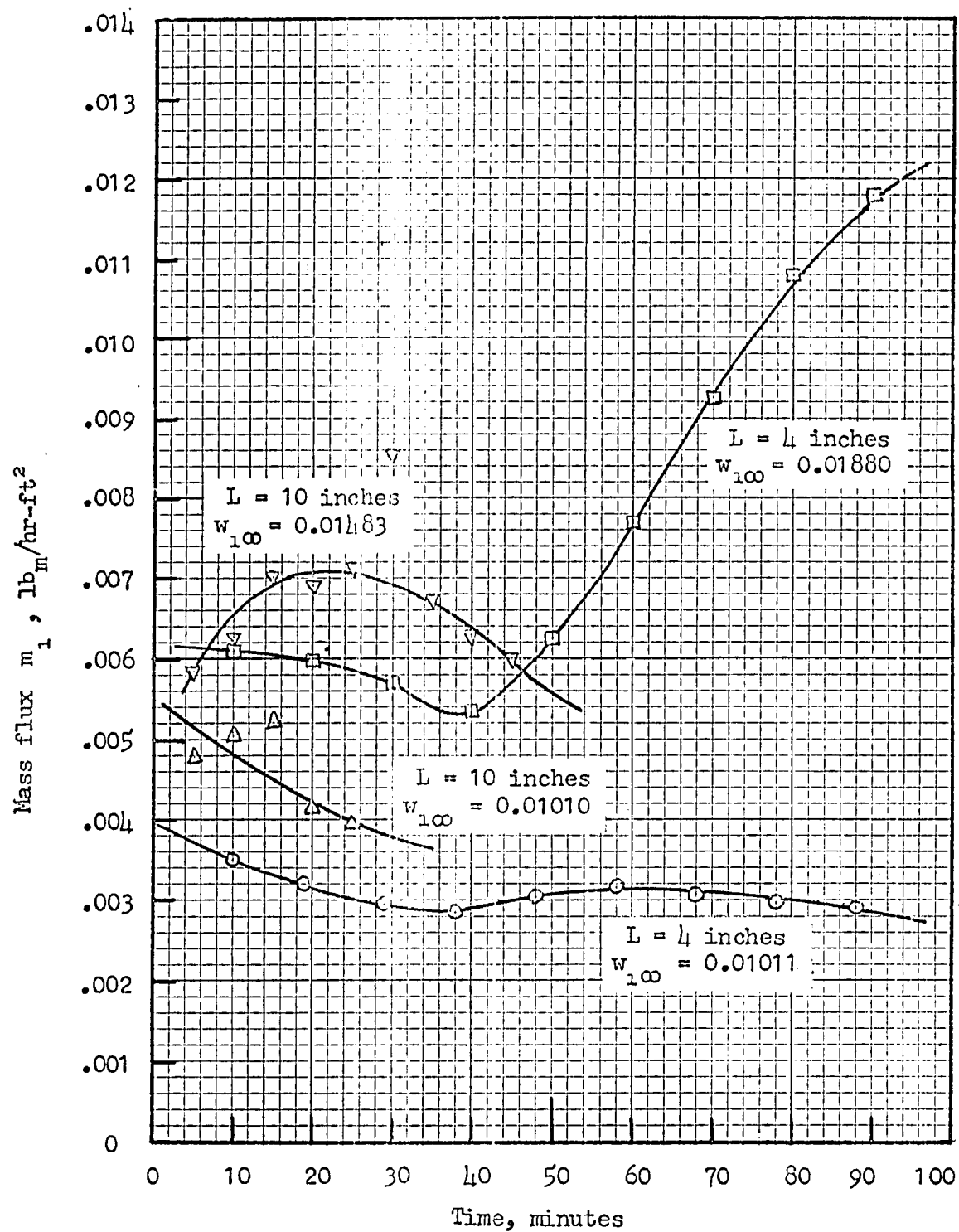


Figure 10. Experimentally measured mass flux.

the rate of frost formation could depend upon the type of surface over which the air in the boundary layer was moving, the fact that the surface was irregular instead of smooth would result in a larger number of nucleation sites for condensation to take place. In this investigation, the frost surface was observed to be highly irregular, with columnar growth of frost at random sites with a finer layer of frost being formed between the small columns. For this situation, as the frost columns grew, more area was available for the depositing of frost; therefore, the mass transfer rate should increase as a result of this mechanism.

On the other hand, the frost interface temperature constantly increased as a result of the insulating effect of the frost layer. This increase in frost interface temperature results in a decrease in the temperature difference between the ambient air and the frost interface, thereby reducing the Grashof number. The decrease in Grashof number would result in a decrease in the mass transfer rate for free convection as a result of this mechanism. The interaction of these two mechanisms could result in an initial increase in mass transfer as the first mechanism (columnar growth) predominated, followed by a decrease in mass transfer as the second mechanism (increase in frost interface temperature) began to predominate.

In Figure 11 the theoretical and experimental correlations for mass transfer are compared. From the scatter of the data, it was difficult to arrive at a definite value for the exponent in a power correlation,  $\overline{Sh} = C (Gr_L Pr)^n$ ; however, it is obvious from Figure 11



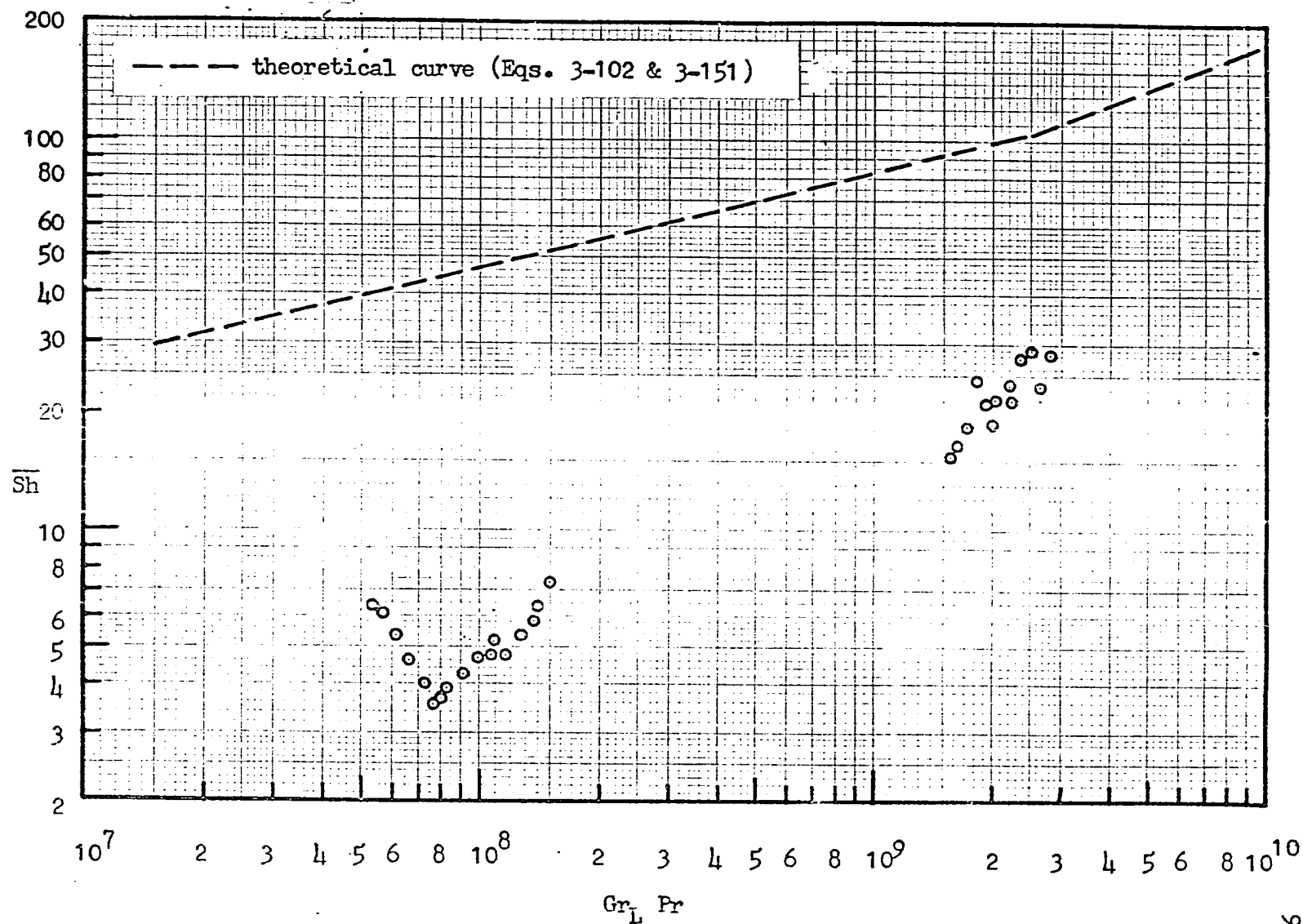


Figure 11. Experimental mass transfer correlation.

that the magnitude of the mass transfer rate measured experimentally was approximately one order of magnitude less than the theoretically predicted correlation. This result has been observed by Holten (11) on frost formation on spheres and by Ruccia and Mohr (10) of frost formation on large liquid oxygen containers.

It was stated by Holten that the condensation of water vapor in the boundary layer prior to reaching the container wall caused the discrepancy between theory and experiment. It is possible that the denser particles of frost, which were observed to form in the boundary layer in this investigation, too, did not move at the same velocity as the gas in the boundary layer; however, because of the fact that there were no forced convection currents, the difference in velocity should be small enough that this mechanism would not result in a difference of an order of magnitude. The formation of frost particles in the boundary layer could decrease the mass transfer rate through another mechanism, however. In the theoretical correlation, the diffusion coefficient for water vapor molecules diffusing through air molecules was used. Since the boundary layer near the frost interface contains particles or "macromolecules" of frost, the water vapor molecules must diffuse through both the air molecules and these particles of frost. Since the frost particles are much larger than the air molecules, the frost particles would offer a greater resistance to diffusion of water vapor molecules than would the air molecules; therefore, the mass transfer rate would be reduced significantly. For rigid sphere molecules (29), the

expression for the diffusion coefficient is

$$D_{12} = \left( \frac{k_b T}{2\pi m_r} \right)^{1/2} \frac{1.5}{n (d_1 + d_2)^2} \quad (5-16)$$

where  $k_b$  = Boltzmann constant,  $T$  = absolute temperature,  $m_r$  = reduced mass of the molecules,

$$m_r = (1/m_1 + 1/m_2)^{-1} \quad (5-17)$$

$n$  = number of molecules per unit volume, and  $d$  = diameter of the molecules. If it is desired to show the effect of the presence of macromolecules of frost, the following argument may be used. The mass of a macromolecule is much larger than the mass of either the air molecules or the water vapor molecules; therefore, the reduced mass of the three-particle system will not be much different from the reduced mass of the two-particle system. For similar conditions, the total number of molecules will be approximately the same, since the number of air molecules is much greater than either the number of water vapor molecules or the total of water vapor molecules and macromolecules. From this reasoning, therefore, the diffusion coefficient is inversely proportional to the square of the sum of molecular diameters.

From Appendix B, the diameter of the water vapor molecule was found to be  $d_1 = 4.21 \times 10^{-8}$  cm and the diameter of the air molecule was  $d_2 = 3.74 \times 10^{-8}$  cm. Suppose the ratio of diffusion coefficient with frost particles present to the diffusion coefficient without

frost particles is taken as 0.100. Since  $(d_1 + d_2) = 7.95 \times 10^{-8} \text{ cm}$ , the sum of molecular diameters for the case of frost being present is

$$(d_3 + \bar{d}) = (7.95)(10^{-8})/(0.100)^{1/2} = 25.1 \times 10^{-8} \text{ cm}$$

where  $\bar{d}$  is a mean diameter, say  $\bar{d} = 0.5 (d_1 + d_2) = 3.98 \times 10^{-8} \text{ cm}$ . The diameter of the macromolecule of frost is then

$$d_3 = (25.1 - 4.0)(10^{-8}) = 21.1 \times 10^{-8} \text{ cm}$$

This magnitude is approximately the size of smoke particles (30). If it is assumed that the water vapor condenses in the hexagonal-close-packed crystal arrangement (as evidence by the hexagonal symmetry of snowflakes), the previously calculated macromolecule diameter corresponds to a cluster of water vapor molecules  $(21.1)/(4.21) = 5$  molecules across or a cluster of 63 water vapor molecules.

Since the human eye cannot detect particles smaller than 10 microns in diameter (30), and the diameter calculated previously was 0.0021 micron, this value must represent an average diameter, because frost particles were visible in the boundary layer. If 63 water vapor molecules per macromolecule represents an average cluster, there must be present in the boundary layer particles on the order of 5 microns to 50 microns, which is the range of particle size in fog (30).

For large macromolecules, the number of water vapor molecules making up the cluster is on the order of  $(d_3/d_1)^3$ . The average number

of water vapor molecules per particle may be estimated from

$$\frac{(1)n_1 + (d_3/d_1)^3 n_3}{(n_1 + n_3)}$$

where  $n_1$  = number of water vapor molecules per unit volume not in a cluster, and  $n_3$  = number of macromolecules per unit volume. Since  $n_1$  is so much larger than  $n_3$ , the denominator of the preceding equation may be written as  $(n_1 + n_3) \doteq n_1$ . For air at 14.7 psia, 350°R, and a mass fraction of 0.010, the mixture density is 0.1133 lb<sub>m</sub>/ft<sup>3</sup>, and the partial density of the water vapor is 1.133 x 10<sup>-3</sup> lb<sub>m</sub>/ft<sup>3</sup>. The number density of water vapor molecules for these conditions is

$$n_1 = (N_o \rho_1)/M_1 = (2.73)(10^{26})(1.133)(10^{-3})/(18)$$

$$n_1 = 1.72 \times 10^{22} \text{ water vapor molecules/ft}^3$$

where  $N_o$  = Avagadro's number. Assuming a macromolecule size of 0.001 inch (25.4 micron), the number density of macromolecules may be determined, using an average number of 63 water vapor molecules per particle.

$$63 = 1 + (d_3/d_1)^3 (n_3/n_1)$$

$$n_3 = 62 (d_1/d_3)^3 n_1 = (62)(4.21 \times 10^{-8}/2.54 \times 10^{-3})^3 (1.72 \times 10^{22})$$

$$n_3 = 4.85 \times 10^9 \text{ macromolecules/ft}^3$$

Another estimate of the number density of macromolecules can be made by assuming that the macromolecules effectively block off a portion of the area of the plate from the water vapor molecules. Assuming that the macromolecules are uniformly distributed within the boundary layer, the volume occupied by one macromolecule is  $(1/n_3)$ , and the projected area (projected to the plate surface) of this volume is  $(1/n_3)^{2/3}$ . The projected area of the single macromolecule occupying the aforementioned volume is  $(\pi/4)(d_3)^2$ . If  $\delta$  is the boundary layer thickness, the number of layers of macromolecules perpendicular to the plate surface is  $(n_3)^{1/3}(\delta)$ ; therefore, the projected area of all the macromolecules in the boundary layer divided by the plate surface area is

$$\frac{(\pi/4)(d_3)^2 (n_3^{1/3}\delta)}{(1/n_3)^{2/3}} = (\pi/4) \delta n_3 d_3^2$$

Using the following values, the average boundary layer thickness may be determined from Eq. (3-75), in which the average boundary layer thickness is 4/5 time the boundary layer thickness at  $x = L$  :

$(Gr_L Pr) = 10^8$ ,  $Pr = 0.740$ ,  $(Pr/Sc) = 1.414$ , and  $w_{1\infty} = 0.010$ . Performing the calculation, the average boundary layer thickness was found to be  $0.01287 \text{ ft} = 0.1543 \text{ in.}$  With an average macromolecule size of 25.4 microns, and assuming that 90% of the plate surface is covered by macromolecules (which would result in a reduction of the mass transfer rate by a factor of 0.10), the number density of macromolecules may be determined.

$$0.90 = (\pi/4) \delta n_3 d_2^2$$

$$n_3 = (4)(0.90)(1728)/(\pi)(0.1543)(0.001)^2$$

$$n_3 = 1.28 \times 10^9 \text{ macromolecules/ft}^3$$

From the first estimate of the number density of macromolecules, a value of  $n_3 = 4.85 \times 10^9$  macromolecules/ft<sup>3</sup> was obtained, which is of the same order of magnitude as the estimate using the area blocked off by the macromolecules. From these calculations, it is concluded that the difference between the theoretical and experimental mass transfer rates was due to the presence of large clusters of frost within the boundary layer. The frost clusters reduced the diffusion coefficient for no frost present by an order of magnitude by blocking much of the area available for motion of water vapor molecules to the frost surface. The size of the frost particles was estimated to be of the order of 0.001 inch, since the particles could be seen with the naked eye.

The presence of macromolecules of frost within the boundary layer would also explain the fact that the mass transfer could not be treated as a quasi-steady-state process, as could the heat transfer process. The slope of the  $\overline{Sh}$  vs.  $(Gr_L Pr)$  curve was nearer unity than 0.25 for the laminar flow runs; however, the two curves for the two different size plates did not coincide. This fact indicated that the mass transfer rate was smaller for longer times than for short times. This behavior would be reasonable in view of the fact that at short periods of time (near the initial time), the majority of the particles

of frost could consist of particles 5 molecules across, say; whereas, as time proceeded, additional molecules would condense on the surface of the frost particles, thereby increasing the particle diameter to 7 molecules, and so on. As the frost particles grew larger, the diffusion coefficient and the mass transfer rate would correspondingly decrease, as was evidenced by the experimental measurements, with the exception of the latter points in run no. 2 at high humidity.

It is noted that some of the points in Figure 11 do not follow this trend. These points were obtained at the latter times for the run with a high humidity and a short plate. It is noted for this run, as shown in Figure 12, that the thickness of frost increased near the end of the run in a manner different from that of the other runs. Whether this anomalous behavior was due to extraneous effects could not be discerned by the author, but the test points taken near the end of this run did not follow the pattern of the remainder of the test runs; therefore, it is recommended that these points be considered doubtful in the interpretation of the data.

There was much more scatter in the mass transfer data than in the heat transfer data because of the mechanical failure of the frost layer and the irregular nature of the frost interface. During the entire run, small patches of frost would sometimes fall from the surface of the plate. This mechanical failure made correlation of the data quite difficult; however, frost thickness measurements were made at areas in which frost remained intact in order to attempt to alleviate this problem.



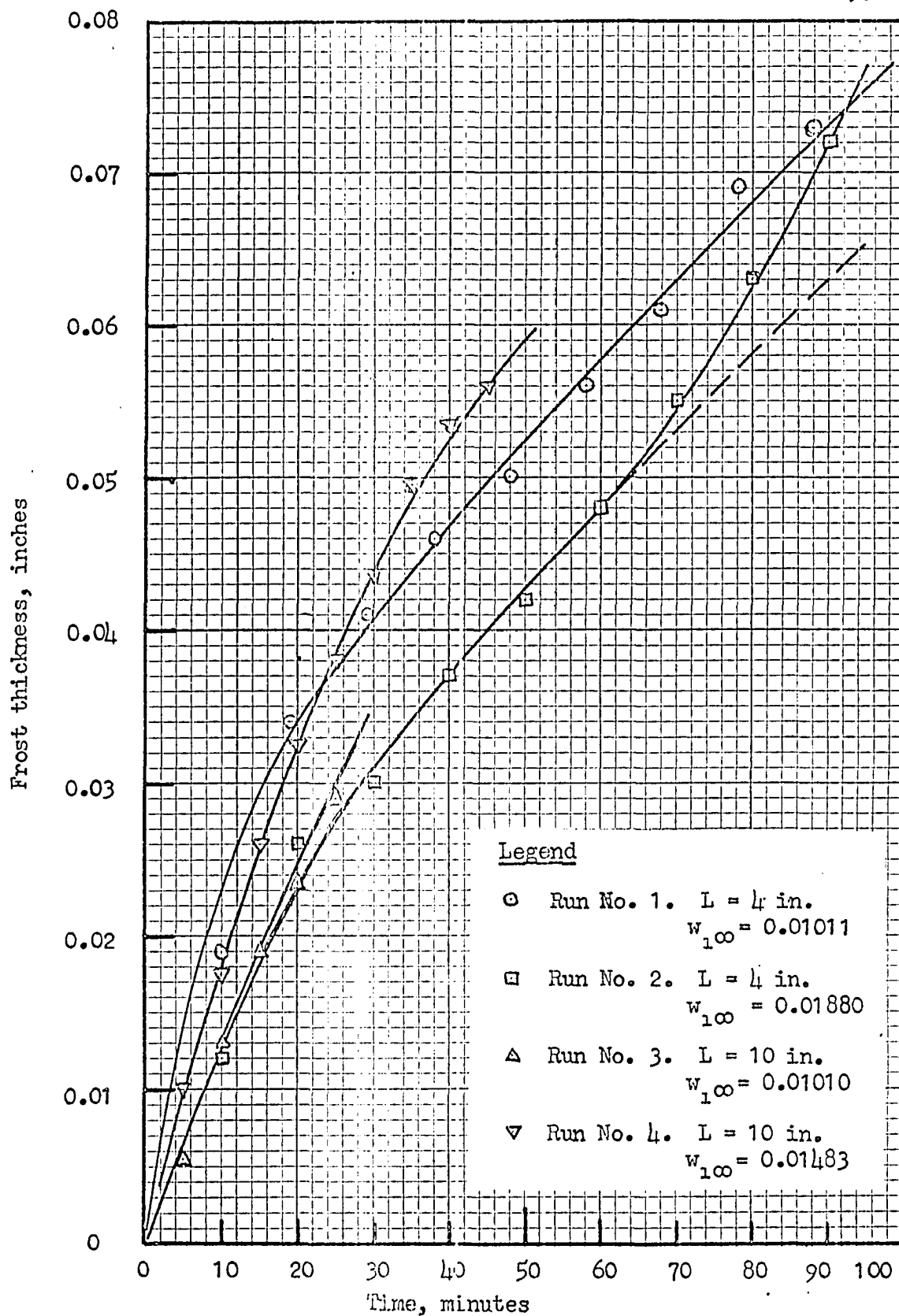


Figure 12. Frost thickness vs. time.

The irregularity of the frost surface presented an even greater obstacle in accurately determining the frost thickness, since the peak-to-valley roughness was estimated at as high as 20% in some cases. An attempt was made to determine the average thickness by locating the frost thickness probe in the area adjacent to a peak in the frost surface instead of measuring the peak or valley thickness. From Figure 12, it is observed that the frost thickness grew faster for the runs with higher ambient mass fraction of water vapor, as would be expected in view of the higher mass flux for this situation.

#### 5.5. Frost thermal conductivity

Although it was not one of the factors to be investigated in this study, it is appropriate to mention the frost thermal conductivity at this point, since this property is involved in determining the frost interface temperature. The plate surface temperature was not measured in this investigation; however, this temperature could be determined from experimental curves of pool boiling of liquid nitrogen which appear in the literature (31, 32, 33). With this value of temperature  $T_s$  and the measured experimental data, the frost thermal conductivity was calculated from the Fourier rate equation for conduction heat transfer.

$$k_f = \frac{q_{\text{total}} t_f}{(T_w - T_s)} \quad (5-18)$$

A plot of the values of frost thermal conductivity determined by this method is given in Figure 13. It is noted from this plot that the frost thermal conductivity decreased during the initial period of frost formation, and there appeared to have been an approach to a minimum in the frost thermal conductivity followed by an increase in conductivity. This behavior was observed for one run with a high ambient mass fraction and the short plate; whereas, the trend could not be confirmed for the other runs due to the limited time available for the run. As mentioned in Chapter II, from the data of Smith et al. (8) for frost formation in forced convection across a tube cooled to cryogenic temperatures, the frost thermal conductivity was observed to increase with time in an exponential manner, in contrast to the behavior observed in this investigation. No definite explanation for this difference was apparent to the author.

The frost thermal conductivity is plotted against the mean frost temperature in Figure 14, along with the data of Holten (11). There was much scatter in the data shown in Figure 14, and the value of frost thermal conductivity also appeared to be a function of ambient mass fraction of water vapor as well as mean frost temperature. The data of Holten taken from large liquid oxygen vessels at higher mean frost temperatures showed a large scatter also; however, the trend of the thermal conductivity was increasing with increasing mean frost temperature. In the present investigation, the frost thermal conductivity decreased during the initial stages of frost

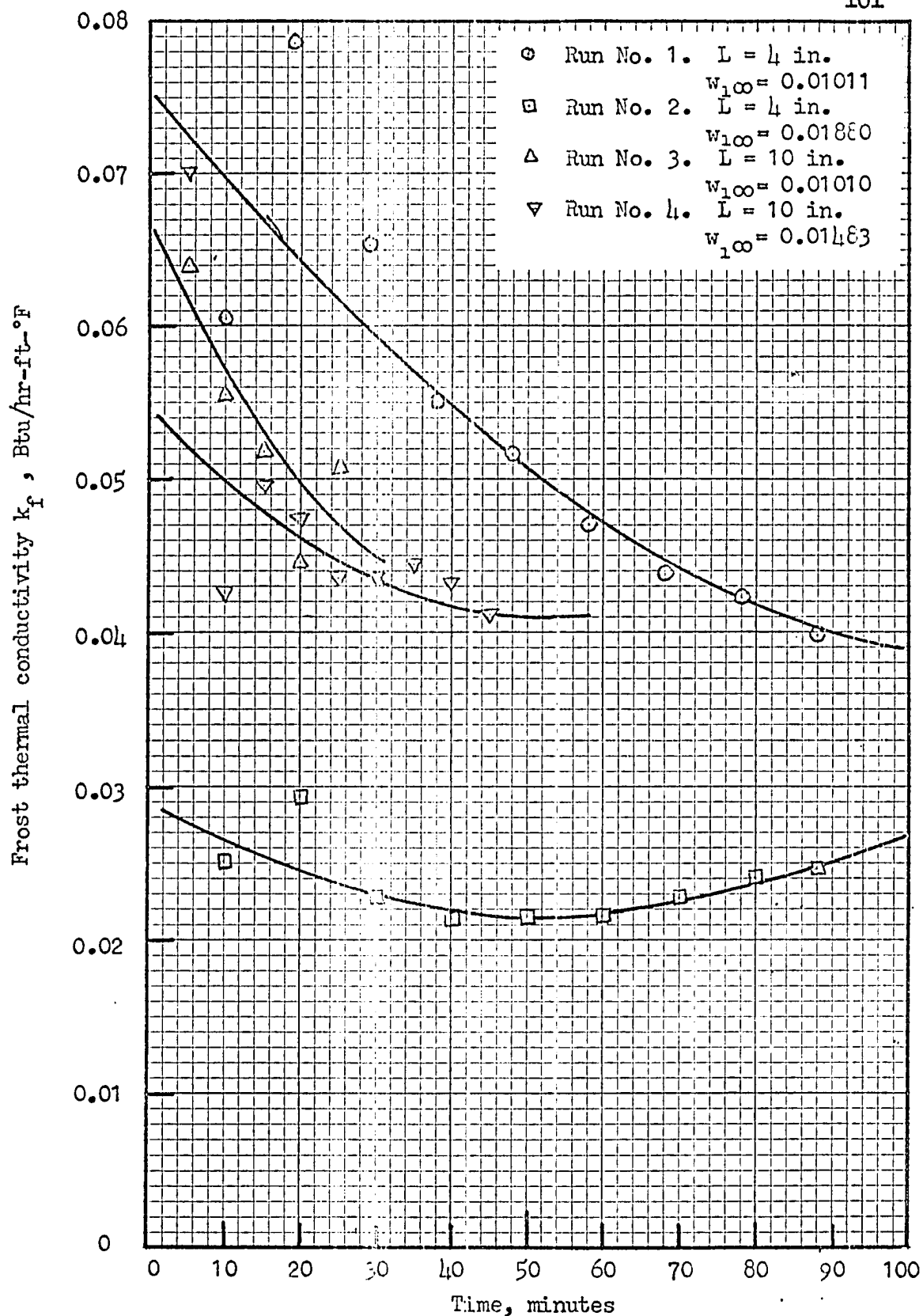


Figure 13. Frost thermal conductivity vs. time.

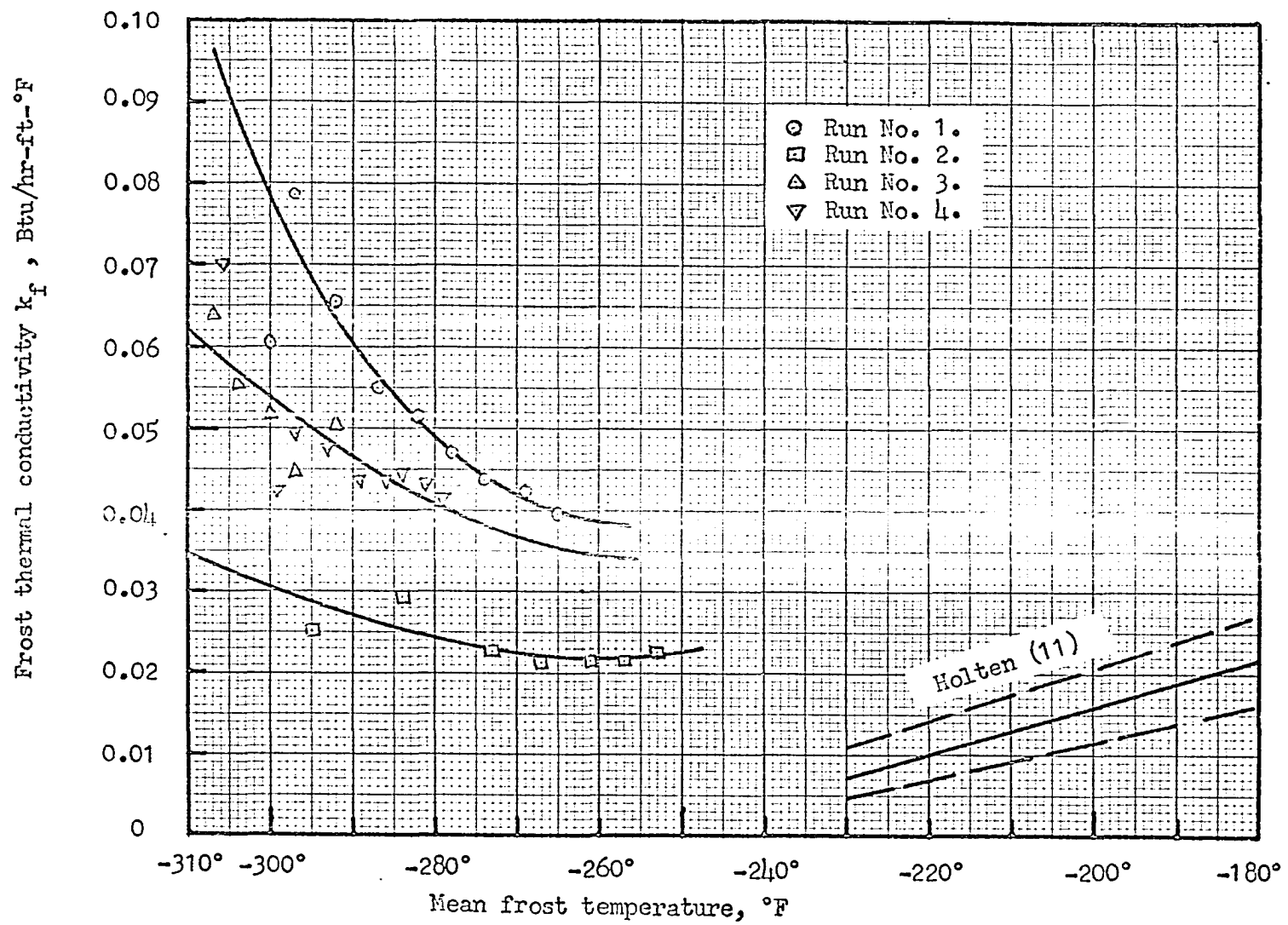


Figure 14. Frost thermal conductivity vs. mean frost temperature.

formation, and appeared to approach a minimum, after which the thermal conductivity increased with increasing frost temperature. It appears that the mechanism of energy transport through the frost was more complicated than simple conduction. This is one area in which further basic research is required to separate the various mechanisms responsible for energy transport within the frost layer.

In Figure 15 the frost thermal conductivity is plotted vs. the frost density. The data points seemed to fall near a single line for all runs, which indicated that the mechanisms responsible for the change in frost density and frost thermal conductivity have a similar effect on these two properties. It appeared that diffusion of water vapor through the porous frost contributed to the energy transmission through the frost during the initial stages, resulting in higher values of frost apparent thermal conductivity as calculated by Eq. (5-18). The low density of the frost during the initial stages of frost formation indicated an open porous structure, which would not offer as much resistance to diffusion of water vapor as a denser structure. As the frost layer became more dense, the resistance to internal diffusion became greater, the diffusion current became smaller and the frost thermal conductivity decreased. With further increase in frost density, the solid conduction mechanism became predominant, since there was more solid material to transmit energy and less open spaces to retard the conduction mechanism, and the apparent thermal conductivity increased as the frost density increased.

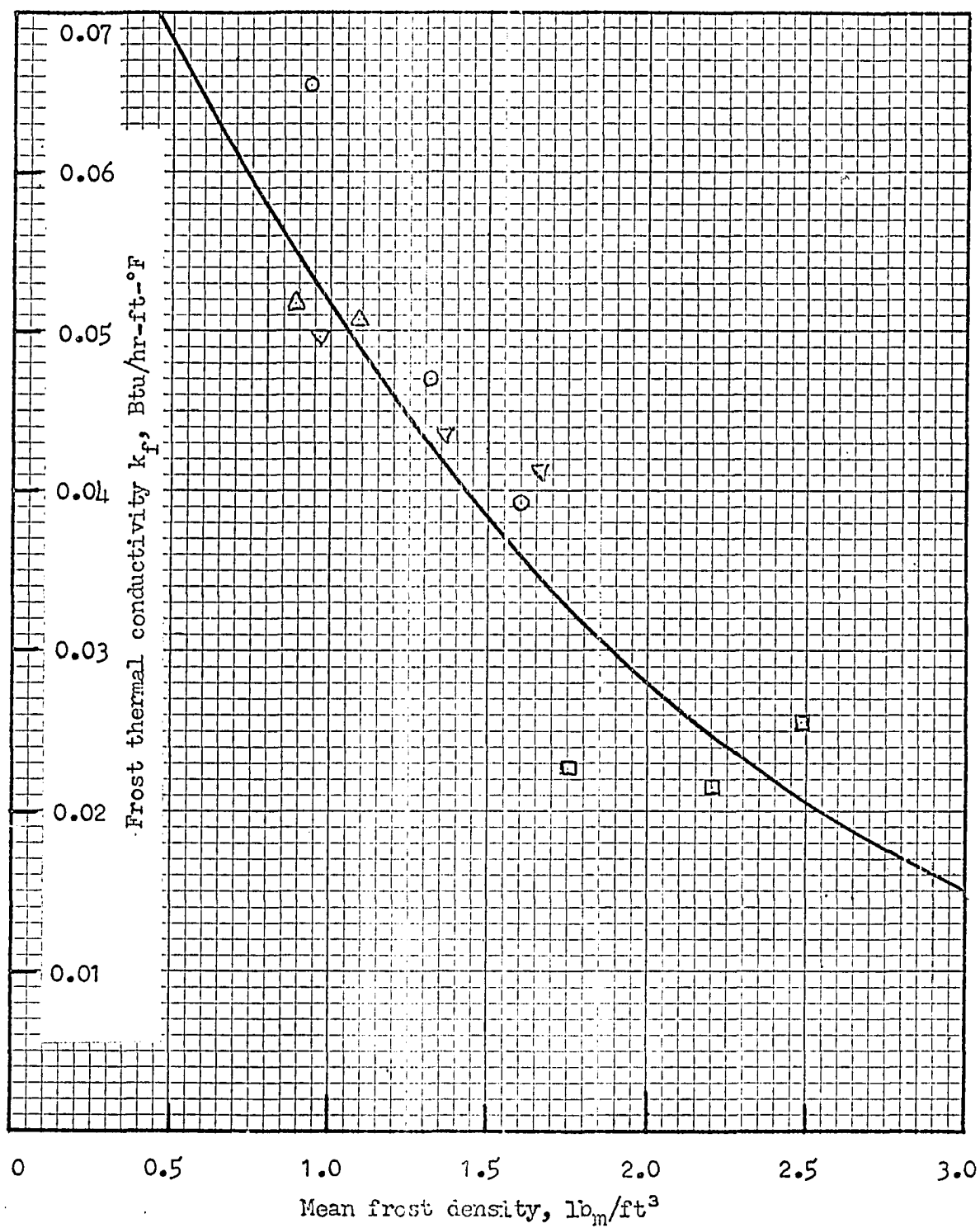


Figure 15. Frost thermal conductivity vs. frost density.

### 5.6. Application of the results

An example problem is worked out in Appendix E, in which the results of this investigation are used to predict the heat transfer and frost growth on a vertical flat plate cooled to cryogenic temperatures. By assuming a series of frost surface temperatures, the heat transfer and mass transfer rates can be determined from the experimental correlations presented in this chapter. When the total heat transfer rate is known, the frost thermal conductivity, density, and thickness may be determined from Eq. (5-18) and the experimental curves. The time required for the frost surface temperature and frost thickness to change by the assumed increment can then be determined from

$$\Delta\tau = \rho_f \Delta t_f / m_1 \quad (5-19)$$

The numerical calculation is then repeated until the frost surface temperature reaches 32°F, at which time steady-state operation is achieved.



## CHAPTER VI

### SUMMARY AND CONCLUSIONS

An analytical expression for the convective heat flux and mass flux to a vertical flat plate in free convection with simultaneous heat and mass transfer (frost formation) was developed for both the laminar and turbulent flow regimes. In the expression for laminar flow, the effect of thermal diffusion and diffusion thermo-effect was included. Since the mechanism for thermal diffusion in turbulent flow has not been established, the turbulent flow correlation did not include this effect. In order to verify the analytical correlations, a series of experimental runs were made for two different size plates cooled to liquid nitrogen temperatures under different conditions of ambient humidity.

The following conclusions may be drawn from this investigation:

- (1) From values of the thermal diffusion constant for mixtures of water vapor and air and the application of the theoretical heat flux correlation, it was concluded that thermal diffusion and diffusion thermo-effect produced a negligible effect on the convective heat and mass flux for frost formation in free convection at cryogenic temperatures. The reason for this behavior was that the thermal diffusion ratio was practically zero at the frost interface as a result of the extremely small mass fraction of water vapor at the interface.

(2) From the theoretical analysis, it was concluded that the simultaneous mass transfer does have a small effect on the convective heat flux (on the order of 5% for an ambient mass fraction of water vapor of 0.10) for both laminar and turbulent flow. The effect of mass transfer to the plate was to increase the convective heat transfer coefficient, and the effect increases with increasing mass fraction of water vapor (or, correspondingly, with increasing specific humidity).

(3) From the experimental portion of the investigation, it was concluded that the convective heat transfer correlation for frost formation under free convection conditions for a vertical plate could be expressed as follows:

(a) For laminar flow:

$$\overline{Nu} = \frac{\bar{h}_c L}{k} = \frac{0.616 (Pr)^{1/4} (Gr_L Pr)^{1/4}}{[Pr + 0.952 B_3]^{1/4} (B_3)^{1/4}} \quad (6-1)$$

where:

$$B_3 = 1 - \left( \frac{Pr}{Sc} \right) \frac{(w_{1\infty} - w_{1w})}{(1 - w_{1w})(\xi)} \quad (6-2)$$

$$\xi = (\delta_m / \delta) = \left[ \frac{(Pr/Sc)(1 - w_{1\infty})}{(1 - w_{1w}) - (Pr/Sc)^{1/2} (w_{1\infty} - w_{1w})} \right]^{1/2} \quad (6-3)$$

(b) For turbulent flow:

$$\overline{Nu} = \frac{0.0248 (Pr)^{1/15} (1 + B_4)^{1/5} (Gr_L Pr)^{2/5}}{[1 + 0.494 (Pr)^{2/3} + B_4]^{2/5}} \quad (6-4)$$

where:

$$B_4 = \left( \frac{Pr}{Sc} \right)^{2/3} \frac{(w_{1W} - w_{1\infty})}{(1 - w_{1W})(\xi)^{1/4}} \quad (6-5)$$

$$\xi = \left( \frac{Pr}{Sc} \right)^{8/15} \left( \frac{1 - w_{1\infty}}{1 - w_{1W}} \right)^{4/5} \left[ 1 - \left( \frac{Pr}{Sc} \right)^{8/15} \frac{(w_{1\infty} - w_{1W})}{(1 - w_{1W})} \right]^{-4/5} \quad (6-6)$$

In the preceding equations, all fluid properties are evaluated at the mean film temperature,  $T_m = 0.5 (T_\infty + T_w)$ . The transition Grashof-Prandtl number product from Eqs. (6-1) and (6-4) is:

$$(Gr_L Pr)_{trans} = \frac{(2.00)(10^9)(Pr)^{11/9} [1 + 0.494 (Pr)^{2/3} + B_4]^{8/3}}{(B_3)^{5/3} (1 + B_4)^{4/3} (Pr + 0.952 B_3)^{5/3}} \quad (6-7)$$

Under typical conditions ( $Pr = 0.740$ ,  $Pr/Sc = 1.141$ ,  $w_{1\infty} = 0.020$ ) for a plate at cryogenic temperatures, the transition value of  $(Gr_L Pr)$  is approximately  $(Gr_L Pr)_{trans} = 2 \times 10^9$ .

The Grashof number used in this investigation included both the bouyancy effects due to temperature differences and concentration differences, as follows:

$$Gr_L = \frac{g[\beta_t (T_\infty - T_w) + \beta_m (w_{1\infty} - w_{1w})(\xi)] L^3}{\nu^2} \quad (6-8)$$

where the concentration coefficient of expansion is defined as follows:

$$\beta_m = \frac{[(M_2/M_1) - 1]}{1 + w_1 [(M_2/M_1) - 1]} \quad (6-9)$$

(4) From the theoretical analysis for zero thermal diffusion and diffusion thermo-effect, the mass transfer coefficient was found to be related to the convective heat transfer coefficient by the following expressions.

(a) Laminar flow:

$$\overline{Sh} = \frac{\overline{h}_m L}{D_{12}} = \frac{\overline{Nu}}{(\xi)(1 - w_{1w})} \quad (6-10)$$

(b) Turbulent flow:

$$\overline{Sh} = \overline{Nu} (Sc/Pr)^{1/3} (\xi)^{-1/4} \quad (6-11)$$

In these equations, the mass transfer coefficient is defined by

$$m_1 = \rho \overline{h}_m (w_{1\infty} - w_{1w}) \quad (6-12)$$

The experimentally measured mass transfer rate, however, was an order of magnitude smaller than that predicted by the theoretical equations when the diffusion coefficient for water vapor diffusing through air was used. It was postulated that the actual diffusion coefficient in the vicinity of the frost interface was an order of magnitude smaller than that used in the calculations because of the presence of frost particles in the boundary layer near the interface. These frost particles offered an additional resistance to mass transfer over and above that due to the presence of air molecules alone.

(5) From the relationship between the heat and mass transfer coefficients obtained analytically, an enthalpy coefficient may be defined from

$$q_c + q_m = \rho \bar{h}_i (i_\infty - i_w) \quad (6-13)$$

An enthalpy number may be defined and under proper definition of the enthalpy, the following relationship holds true for both laminar and turbulent flow:

$$\overline{Ni} = \bar{h}_i L / \alpha = \overline{Nu} \quad (6-14)$$

$$\text{or,} \quad \bar{h}_i = \bar{h}_c / \rho c_p \quad (6-15)$$

The correct enthalpy definitions are these:

(a) Laminar flow:

$$i = c_p T + \frac{(\text{Pr}/\text{Sc}) i_{sg} w_1}{(\xi)(1 - w_{1w})} \quad (6-16)$$

(b) Turbulent flow:

$$i = c_p T + \frac{(Pr/Sc)^{2/3} i_{sg} w_1}{(\xi)^{1/4}} \quad (6-17)$$

Because of the difference between the theoretical and experimental mass flux, the enthalpy correlation could not be used to predict the total energy transfer. Values of  $(q_c + q_m)$  calculated from the theoretical equations were 20% to 25% too large.

(6) The predominant component of energy transfer for frost formation on a cryogenically cooled plate was the free convection component of the total energy flux, with radiation contributing 15% to 20%, and latent heat transport making a contribution of approximately 1%.

(7) Values of apparent frost thermal conductivity were calculated from the Fourier rate equation for conduction heat transfer, and it was observed that the frost thermal conductivity was primarily a function of frost density. No definite correlation could be achieved between frost thermal conductivity and mean frost temperature. From this result, it was concluded that the mechanism for energy transport through the porous frost was not pure solid conduction, but other mechanisms, such as diffusion, contributed to the energy transport. The resistance to diffusion through the frost was a function of frost density, which was related to the ambient air temperature and specific humidity, the plate surface temperature, and the time elapsed from starting the frosting operation.

Since the predominant component of heat transfer under frosting conditions was the convective portion, which was determined to a large extent in free convection by the difference in temperature between ambient air and the frost interface, it was felt that further basic research is needed in determining the mechanisms for energy transport through the frost layer, because the apparent thermal conductivity of the frost is one of the factors which determines the frost interface temperature.

## APPENDIX A

### PROPERTIES OF AIR AT LOW TEMPERATURES

In order that all of the properties of air at low temperatures be readily available, several property values are tabulated at 10°F increments in this Appendix. The property group  $(g\beta_t/v^2)$  entering in the Grashof number was obtained by plotting values given in W. H. McAdams, Heat Transmission, 4th Ed, on semi-log paper and interpolating from this plot. Other property values except the heat of sublimation and saturation mass fraction were obtained from National Bureau of Standards Circular 564. The values of heat of sublimation and saturation mass fraction were calculated from data given by the Heating Ventilating and Air Conditioning Guide.

The tabulated property values apply for dry air at a pressure of 14.7 psia. At pressures ordinarily encountered in frost formation, the viscosity, specific heat, thermal conductivity, Prandtl number, and Schmidt number are essentially independent of pressure. The density is directly proportional to the absolute pressure; whereas, the thermal diffusivity, kinematic viscosity, and diffusion coefficient are inversely proportional to the absolute pressure.

The dependence of the property values on the mass fraction of water vapor is somewhat more complex in some cases. For the small values of mass fraction usually encountered in humid air, the thermal diffusivity and kinematic viscosity are approximately independent of



the mass fraction. From the perfect gas equation of state, it can be shown that the density of an air-water-vapor mixture may be determined from

$$\rho = \frac{\rho_2}{(1 + 0.611 w_1)} \quad (\text{A-1})$$

For nonreactive mixtures (as is the case for water vapor and air), the specific heat is given by

$$c_p = w_1 c_{p1} + w_2 c_{p2} \quad (\text{A-2})$$

For water vapor and air mixtures, the specific heat is given by

$$c_p = c_{p2} (1 + 0.875 w_1) \quad (\text{A-3})$$

The expressions for viscosity and thermal conductivity are somewhat more complicated than the previous expressions. Using an expression for the viscosity of binary mixtures of gases given by Wilke (34), the following expression was developed for air and water vapor mixtures.

$$\mu = \mu_2 \left[ \frac{1 + 2.62 (w_1/w_2) + 1.603 (w_1/w_2)^2}{1 + 3.24 (w_1/w_2) + 2.63 (w_1/w_2)^2} \right] \quad (\text{A-4})$$

For small values of mass fraction of water vapor ( $w < 0.02$ ), the following expression may be used within slide-rule accuracy:

$$\mu = \mu_2 (1 - 0.603 w_1 - 9.09 w_1^2) \quad (\text{A-5})$$

Using an expression for the thermal conductivity of binary mixtures given by Lindsay and Bromley (35), the following expression was developed for air and water vapor mixtures.

$$k = k_2 \left[ \frac{1 + 2.27 b_1 (w_1/w_2) + 1.311 b_{12} (w_1/w_2)^2}{1 + (1.234 b_1 + 1.273/b_2)(w_1/w_2) + 1.573 b_{12} (w_1/w_2)^2} \right] \quad (\text{A-6})$$

where:

$$b_1 = (T + S_1)/(T + S_{12})$$

$$b_2 = (T + S_2)/(T + S_{12})$$

$$b_{12} = (T + S_1)/(T + S_2)$$

$T$  = absolute temperature

$S_1$  = 1020°R for  $H_2O$  vapor (The Sutherland constant)

$S_2$  = 200°R for air

$S_{12}$  = 331°R

For small mass fractions of water vapor, the thermal conductivity may be calculated within slide-rule accuracy by:

$$k = k_2 (1 + 0.0344 w_1) \quad (\text{A-7})$$

TABLE 1  
PROPERTIES OF DRY AIR AT 14.7 PSIA

Temperature, °F	$(g \beta_t / v^2)$ ft <sup>3</sup> -°F <sup>-1</sup>	Pr	Sc	Pr/Sc
-300	665 x 10 <sup>6</sup>	0.774	0.450	1.720
-290	519	0.772	0.460	1.680
-280	397	0.770	0.470	1.638
-270	302	0.768	0.480	1.600
-260	230	0.766	0.488	1.570
-250	179 x 10 <sup>6</sup>	0.765	0.493	1.550
-240	142	0.763	0.497	1.536
-230	114	0.761	0.501	1.520
-220	93.1	0.759	0.504	1.506
-210	75.5	0.758	0.507	1.495
-200	62.6 x 10 <sup>6</sup>	0.756	0.510	1.483
-190	53.0	0.754	0.512	1.473
-180	44.8	0.752	0.514	1.463
-170	37.5	0.750	0.516	1.454
-160	31.1	0.749	0.517	1.448
-150	26.4 x 10 <sup>6</sup>	0.747	0.519	1.439
-140	23.1	0.745	0.520	1.432
-130	20.1	0.743	0.521	1.427
-120	17.5	0.742	0.522	1.422
-110	15.3 x 10 <sup>6</sup>	0.740	0.523	1.414

TABLE 1 (Contd.)

Temperature, °F	$(g \beta_t / \nu^2)$ $\text{ft}^{-3} \text{ } ^\circ\text{F}^{-1}$	Pr	Sc	Pr/Sc
-100	$13.3 \times 10^6$	0.738	0.524	1.409
-90	11.9	0.736	0.524	1.403
-80	10.4	0.735	0.525	1.400
-70	9.26	0.733	0.525	1.397
-60	8.19	0.731	0.526	1.391
-50	$7.20 \times 10^6$	0.729	0.526	1.387
-40	6.48	0.727	0.526	1.382
-30	5.70	0.726	0.527	1.378
-20	5.08	0.724	0.527	1.373
-10	4.57	0.722	0.527	1.369
0	$4.11 \times 10^6$	0.720	0.527	1.366
+10	3.73	0.719	0.527	1.363
+20	3.39	0.717	0.527	1.360
+30	3.12	0.716	0.527	1.357
+40	2.85	0.714	0.528	1.353
+50	$2.58 \times 10^6$	0.713	0.528	1.350
+60	2.36	0.711	0.528	1.346
+70	2.16	0.709	0.528	1.343
+80	1.99	0.708	0.528	1.340
+90	1.84	0.707	0.528	1.338
+100	$1.71 \times 10^6$	0.706	0.528	1.336

TABLE 2

## THERMAL AND DYNAMIC PROPERTIES OF DRY AIR AT 14.7 PSIA

Temperature, °F	k	$\nu$	$\alpha$	$D_{12}$
	Btu/hr-ft-°F	ft <sup>2</sup> /hr	ft <sup>2</sup> /hr	ft <sup>2</sup> /hr
-300	0.00478	0.0574	0.0743	0.1277
-290	0.00505	0.0656	0.0850	0.1427
-280	0.00534	0.0741	0.0962	0.1577
-270	0.00563	0.0838	0.1090	0.1743
-260	0.00592	0.0935	0.1220	0.1914
-250	0.00621	0.1026	0.134	0.208
-240	0.00650	0.1128	0.148	0.227
-230	0.00680	0.1233	0.162	0.246
-220	0.00709	0.1347	0.177	0.267
-210	0.00737	0.1450	0.191	0.286
-200	0.00766	0.158	0.208	0.309
-190	0.00794	0.168	0.223	0.330
-180	0.00822	0.181	0.240	0.352
-170	0.00850	0.193	0.257	0.374
-160	0.00877	0.206	0.275	0.398
-150	0.00905	0.219	0.293	0.422
-140	0.00933	0.233	0.313	0.448
-130	0.00961	0.247	0.332	0.473
-120	0.00990	0.260	0.351	0.499
-110	0.01017	0.275	0.372	0.526

TABLE 2 (Contd.)

Temperature, °F	k	$\nu$	$\alpha$	$D_{12}$
	Btu/hr-ft-°F	ft <sup>2</sup> /hr	ft <sup>2</sup> /hr	ft <sup>2</sup> /hr
-100	0.01045	0.291	0.394	0.554
-90	0.01071	0.305	0.415	0.582
-80	0.01100	0.320	0.436	0.610
-70	0.01126	0.336	0.458	0.640
-60	0.01153	0.352	0.482	0.671
-50	0.01180	0.368	0.505	0.701
-40	0.01207	0.384	0.529	0.732
-30	0.01234	0.402	0.554	0.764
-20	0.01261	0.419	0.579	0.796
-10	0.01287	0.437	0.605	0.829
0	0.01313	0.455	0.632	0.863
+10	0.01340	0.473	0.659	0.899
+20	0.01365	0.491	0.685	0.931
+30	0.01392	0.508	0.710	0.963
+40	0.01418	0.530	0.742	1.004
+50	0.01445	0.549	0.770	1.040
+60	0.01468	0.568	0.800	1.076
+70	0.01492	0.588	0.829	1.115
+80	0.01516	0.609	0.861	1.153
+90	0.01540	0.630	0.892	1.193
+100	0.01564	0.650	0.921	1.230

TABLE 3

HEAT OF SUBLIMATION OF ICE AND SATURATION MASS FRACTION OF WATER

Temp., °F	$i_{sg}$	$w_{1sat}$	Temp., °F	$i_{sg}$	$w_{1sat}$
	Btu/lb <sub>m</sub>			Btu/lb <sub>m</sub>	
-200	1207.0	$5.90 \times 10^{-12}$	-50	1220.3	$0.413 \times 10^{-4}$
-190	1208.4	$2.94 \times 10^{-11}$	-40	1220.5	0.787
-180	1209.8	$1.03 \times 10^{-10}$	-30	1220.5	1.456
-170	1211.1	$5.62 \times 10^{-10}$	-20	1220.5	2.62
-160	1212.4	$2.12 \times 10^{-9}$	-10	1220.3	4.58
-150	1213.6	$6.93 \times 10^{-9}$	0	1220.1	$7.97 \times 10^{-4}$
-140	1214.7	$2.11 \times 10^{-8}$	+10	1219.77	13.08
-130	1215.7	$6.00 \times 10^{-8}$	+20	1219.3	21.4
-120	1216.6	$1.61 \times 10^{-7}$	+30	1218.7	34.3
-110	1217.4	$4.06 \times 10^{-7}$	+40	--	51.7
-100	1218.1	$9.77 \times 10^{-7}$	+50	--	$75.8 \times 10^{-4}$
-90	1218.8	$2.24 \times 10^{-6}$	+60	--	109.3
-80	1219.3	$4.93 \times 10^{-6}$	+70	--	155.3
-70	1219.8	$1.04 \times 10^{-5}$	+80	--	217.7
-60	1220.1	$2.12 \times 10^{-5}$	+90	--	$301.3 \times 10^{-4}$
			+100	--	$414 \times 10^{-4}$

APPENDIX B  
DETERMINATION OF THE THERMAL DIFFUSION CONSTANT  
FOR WATER VAPOR AND AIR

No values of the thermal diffusion coefficient have been reported in the literature for water vapor and air mixtures, as far as can be discerned by the author; therefore, in order to assess the effect of thermal diffusion in this case, a value of the thermal diffusion coefficient was calculated from two theoretical models:

- (a) The rigid elastic sphere model, and
- (b) The Sutherland model, or the case in which the force field between the molecules is an inverse 7th power of the distance between the molecules.

Theoretical expressions for the thermal diffusion constant, defined by

$$a = k_T / w_1 w_2 = (D_T / D_{12}) / w_1 (1 - w_1) \quad (B-1)$$

have been worked out by Chapman (36). In general,

$$a = \frac{C M \left[ (w_1 / M_1) S_1 - (w_2 / M_2) S_2 \right]}{(M_2 / M_1) w_1^2 Q_{11} + w_1 w_2 Q_{12} + (M_1 / M_2) w_2^2 Q_{22}} \quad (B-2)$$

where:

$C = 1$  for rigid elastic spheres

$C = 1/3$  for Sutherland molecules



The other quantities entering into Eq. (B-2) are defined as follows.

$$S_1 = \frac{E_1 \left( 1 + \frac{M_2}{M_1} \right) - 4 A (M_2/M_1) - 3 (M_2/M_1) \left[ \frac{M_2}{M_1} - 1 \right]}{\left( 1 + \frac{M_2}{M_1} \right)^2} \quad (\text{B-3})$$

$$S = \frac{E_2 (M_2/M_1) \left( 1 + \frac{M_2}{M_1} \right) - 4 A (M_2/M_1) - 3 \left( 1 - \frac{M_2}{M_1} \right)}{\left( 1 + \frac{M_2}{M_1} \right)^2} \quad (\text{B-4})$$

$$Q_1 = \frac{E_1 [6 (M_2/M_1)^2 + (5 - 4B) + 8 A (M_2/M_1)]}{\left( 1 + \frac{M_2}{M_1} \right)^2} \quad (\text{B-5})$$

$$Q_{2..} = \frac{E_2 [6 + (5 - 4B)(M_2/M_1)^2 + 8 A (M_2/M_1)]}{\left( 1 + \frac{M_2}{M_1} \right)^2} \quad (\text{B-6})$$

$$Q_{12} = \frac{3(5 - 4B) \left(1 - \frac{M_2}{M_1}\right)^2 + 4 A(11 - 4B) (M_2/M_1)}{\left(1 + \frac{M_2}{M_1}\right)^2} + 2 E_1 E_2 \quad (B-7)$$

where:

$$E_1 = \frac{16 F \left(1 + \frac{M_2}{M_1}\right)^{1/2} \left(\frac{d_1}{d_1 + d_2}\right)^2}{5 (2M_2/M_1)^{1/2}} \quad (B-8)$$

$$E_2 = \frac{16 F \left(1 + \frac{M_2}{M_1}\right)^{1/2} \left(\frac{d_2}{d_2 + d_1}\right)^2}{5 \sqrt{2}} \quad (B-9)$$

The quantities  $d_1$  and  $d_2$  are the molecular diameters, which may be calculated from viscosity data (37) by the expression:

$$d^2 = \frac{0.1792 (k_b m T)^{1/2}}{\mu} \quad (B-10)$$

where  $\mu$  = viscosity,  $k_b$  = Boltzmann constant =  $1.38 \times 10^{-16}$  erg/°K,  $m$  = mass of the molecule ( $m_1 = 30.1 \times 10^{-24}$  gm for water vapor,  $m_2 = 48.4 \times 10^{-24}$  gm for air), and  $T$  = absolute temperature. Using

values of viscosity of  $\mu_1 = 1.130 \times 10^{-4}$  poise for water vapor at 80°F (300°K) and  $\mu_2 = 1.849 \times 10^{-4}$  poise for air at 80°F (300°K), the following values for the molecular diameters are calculated:

$$d_1 = 4.21 \times 10^{-8} \text{ cm for water vapor}$$

$$d_2 = 3.74 \times 10^{-8} \text{ cm for air}$$

The quantities  $M_1$  and  $M_2$  are the molecular weights of the two gases,

$$M_1 = 18 \text{ for water vapor}$$

$$M_2 = 28.96 \text{ for air}$$

The remaining factors in the equations depend upon the molecular force model assumed, and have the following values.

	Rigid elastic spheres	Sutherland molecules
A . . . . .	0.400	0.493
B . . . . .	0.600	0.711
F . . . . .	1.000	1.231

The parameters entering in the expression for the thermal diffusion constant were calculated from Eqs. (B-3) through (B-9) for the two models mentioned, and the following values were obtained.

Rigid elastic spheres			Sutherland molecules
$E_1$	. . . . .	0.824	1.015
$E_2$	. . . . .	0.807	0.995
$S_1$	. . . . .	-0.496	-0.510
$S_2$	. . . . .	+0.389	+0.417
$Q_1$	. . . . .	2.81	3.58
$Q_2$	. . . . .	2.12	2.62
$Q_{12}$	. . . . .	5.01	6.26

Substitution of the above values in Eq. (B-2) results in the following expressions for the thermal diffusion constant:

(a) Rigid sphere model:

$$a = \frac{(-0.0276 w_1 - 0.01342 w_2) M}{(4.53 w_1^2 + 5.01 w_1 w_2 + 1.316 w_2^2)} \quad (\text{B-11})$$

(b) Sutherland model:

$$a = \frac{(-0.00945 w_1 - 0.00480 w_2) M}{(5.77 w_1^2 + 6.26 w_1 w_2 + 1.626 w_2^2)} \quad (\text{B-12})$$

For very small values of  $w_1$  and for  $w_2$  approaching unity, the value of the thermal diffusion constant approaches the following values:

- (a) Rigid sphere model . . . .  $a = - 0.296$   
 (b) Sutherland model . . . .  $a = - 0.0856$

In Eqs. (B-2), (B-11), and (B-12), the molecular weight  $M$  is the molecular weight of the mixture, given by:

$$M = \frac{M_2}{1 + w_1 [(M_2/M_1) - 1]} = \frac{28.96}{(1 + 0.611 w_1)} \quad (\text{B-13})$$

The thermal diffusion ratio  $k_T = a w_1 w_2$  and the thermal diffusion constant  $\underline{a}$  are plotted in Figures 16 and 17 as a function of the mass fraction of water vapor  $w_1$ . Since no experimental values of the thermal diffusion ratio for water vapor and air appear in the literature, no comparison between the calculated and experimental values could be made. A comparison of the theoretical and experimental values of the thermal diffusion ratio for hydrogen and carbon dioxide mixtures was made by Jost (38), and the Sutherland model was in closer agreement with the experimental values than the rigid sphere model; therefore, the Sutherland model was chosen for the present investigation.

It is noted that the values of the thermal diffusion ratio as calculated by both theoretical models is a negative number. This result indicates that the mass flux due to thermal diffusion will be from the cold region (the frost surface, in the present case) to the warm region (ambient air, in this case) for transport of water vapor molecules. This conclusion may be reached by consideration of Eq.

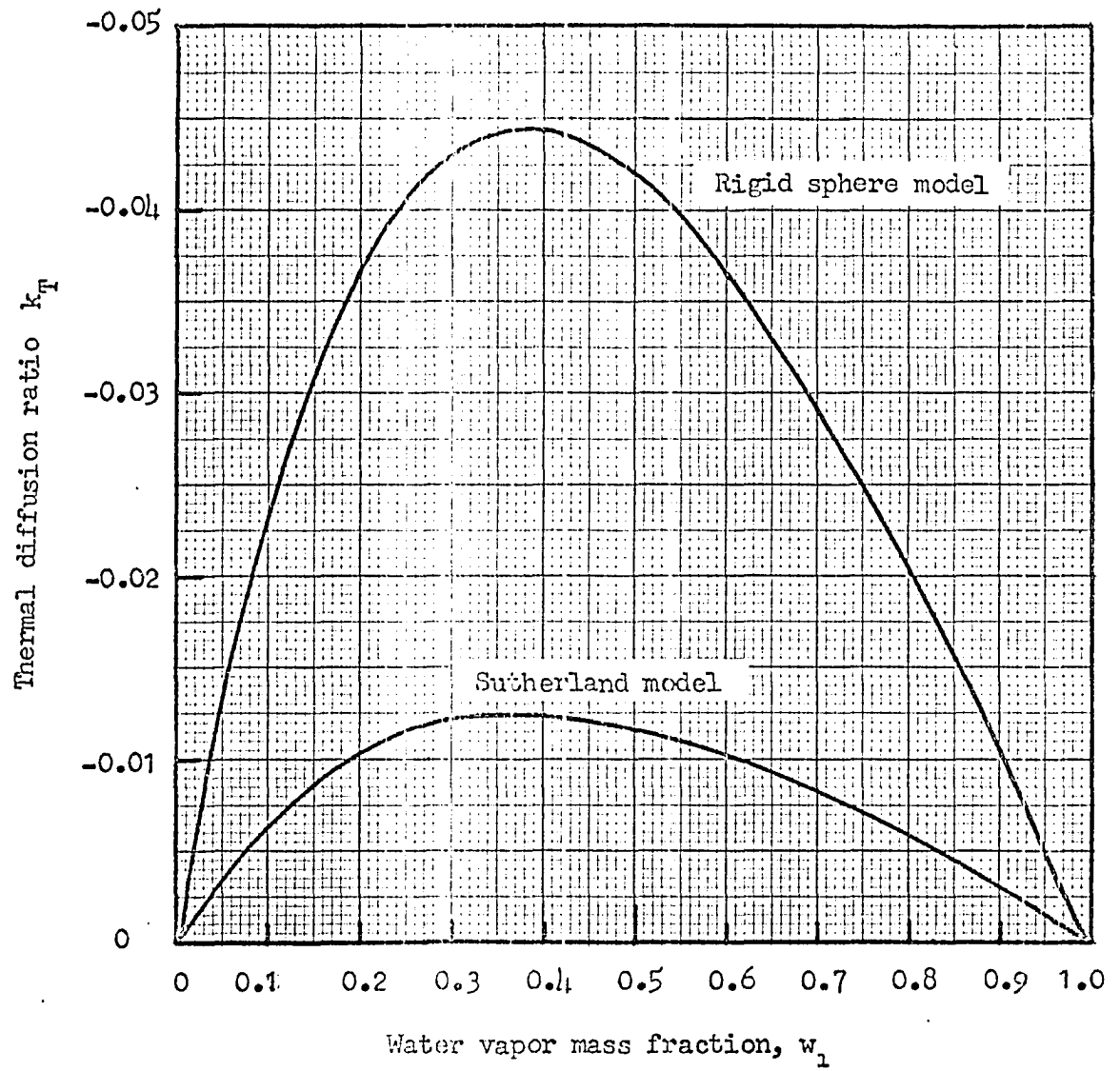


Figure 16. Variation of thermal diffusion ratio with  $w_1$ .

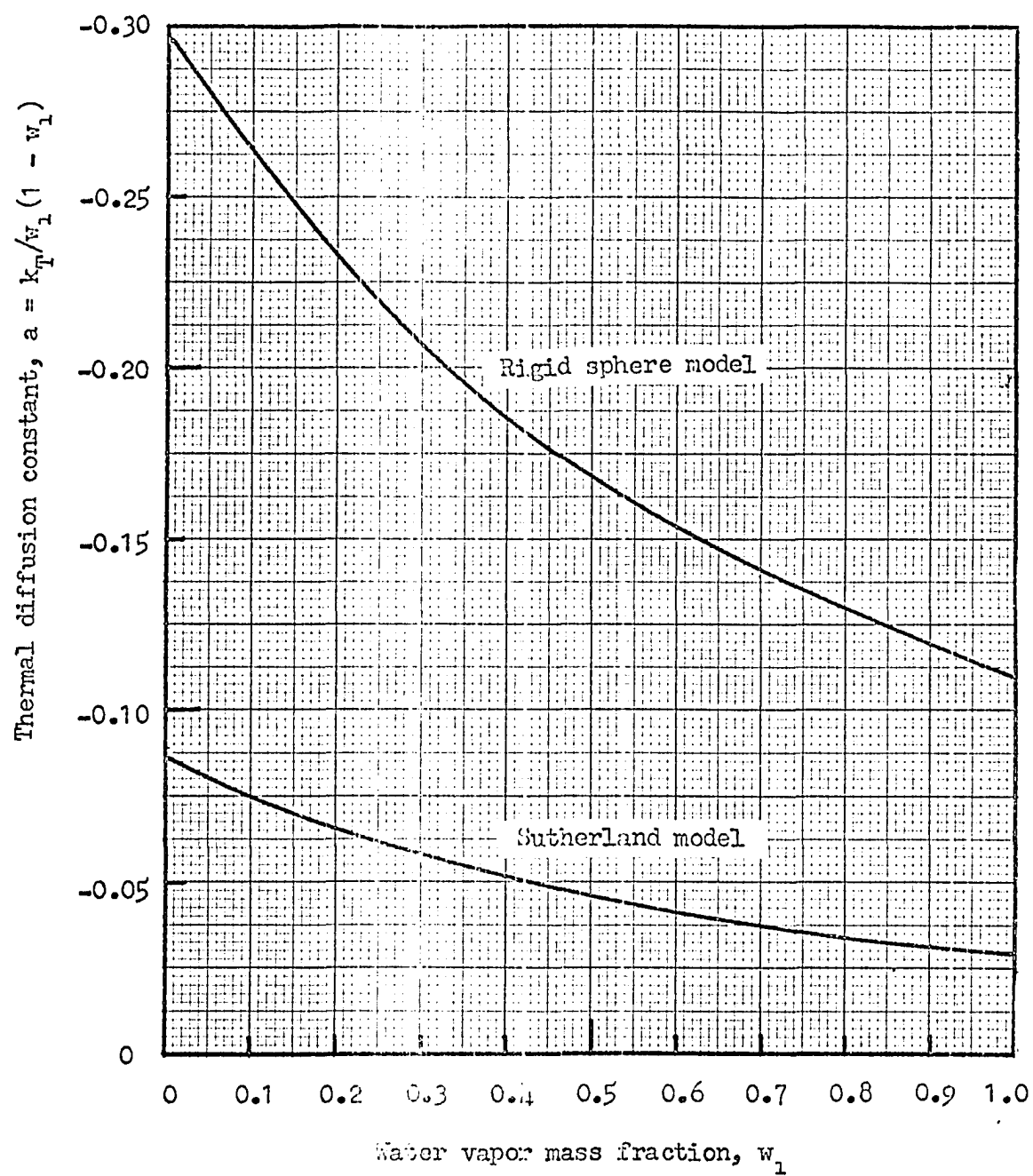


Figure 17. Variation of thermal diffusion constant with  $w_1$ .

(3-40), in which a positive value for the mass flux indicates a mass flux away from the frost surface. For a positive temperature gradient (which is the case for the cooled plate) and a negative value of the thermal diffusion constant, the second term on the right side of Eq. (3-40) or the thermal diffusion term is positive.

For negative values of the thermal diffusion constant and positive concentration gradients (as is the case for frost formation), the diffusion thermo-effect results in a transport of energy away from the frost surface, as indicated by Eq. (3-41). The first term on the right side is positive, thereby denoting a heat flux away from the frost surface.

The fact that, in general, the heavier molecules (air in this case) tend to concentrate in the colder region under the influence of thermal diffusion has been observed for other gas mixtures (39).



## APPENDIX C

### DETERMINATION OF GUARD SHIELD TEMPERATURE RISE

One of the critical factors in accurate determination of the heat transfer rate by the boil-off method, as used in the present investigation, was the elimination of heat fluxes from other sources than the test plate. One of the major sources of heat in-leak in an ordinary set-up would be the heat flux to the vessel used to store the cryogenic fluid during a run, or the inner cylinder in this case. In an attempt to eliminate as much undesirable heat transfer to this vessel as possible, the entire inner vessel was surrounded by a radiation shield cooled by liquid in an auxiliary container (the guard vessel). In order to demonstrate that the heat transfer rate to the inner vessel from sources other than the test plate was small, the maximum temperature rise of the guard shield was determined analytically.

Consider the guard shield and guard vessel, as shown in Figure 18. The guard shield consisted of a copper cylinder of diameter  $D$ , thickness  $t$ , and length  $L$  with one end of the cylinder soldered to the guard vessel, and the other end closed by a disc of copper of the same thickness as the cylindrical portion. It was assumed that the temperature of the shield at the point at which it was soldered to the guard vessel was the same as the fluid temperature in the guard vessel  $T_0$ . Since heat was added to the shield from the jacket

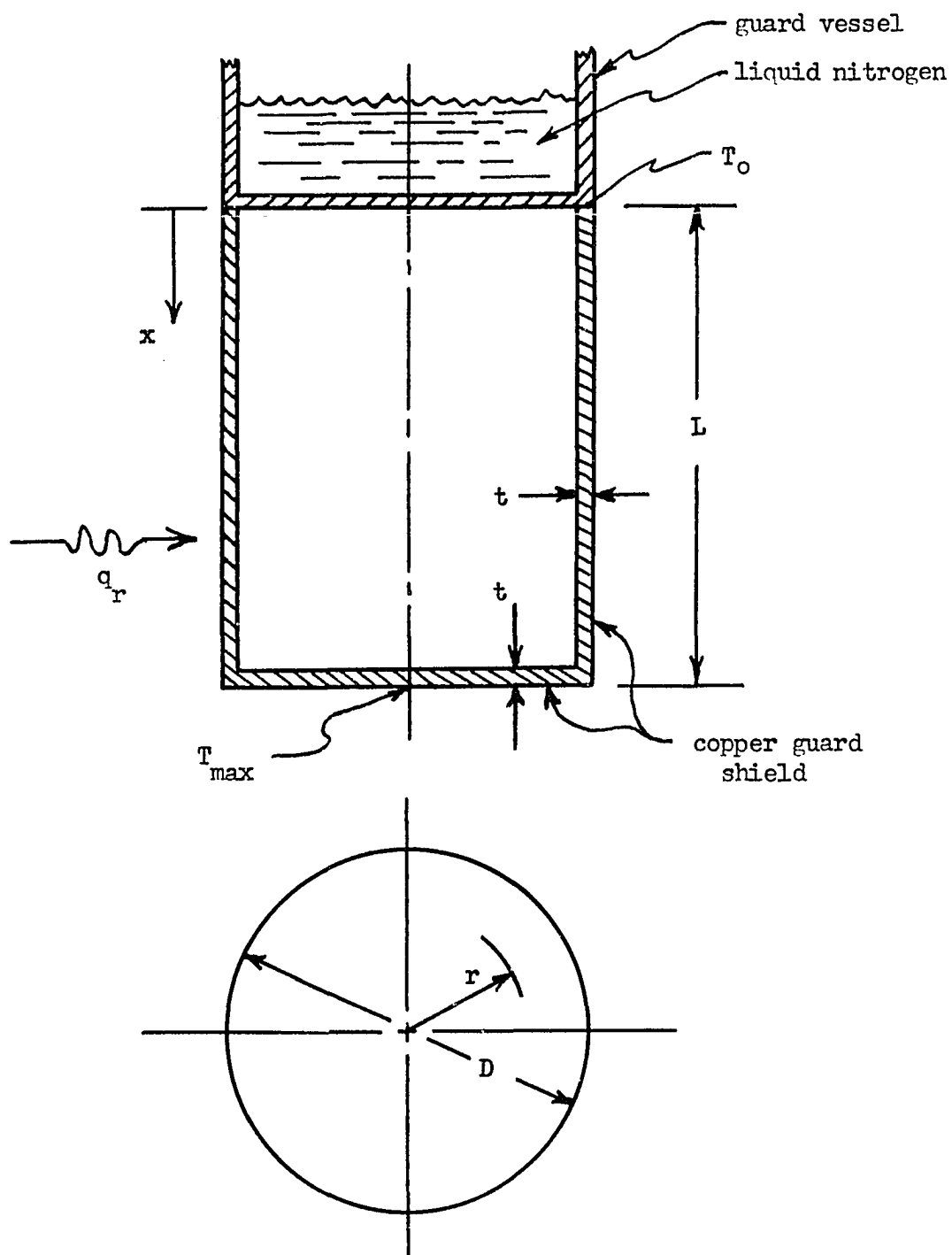


Figure 18. Model and coordinate system for analysis of guard shield temperature distribution.

of the apparatus, and this energy was conducted to the guard vessel, the maximum temperature of the shield occurred at the center of the disc closing the end of the shield.

Two sets of coordinate systems were set up to describe the temperature field: (a) an  $x$ -coordinate system with the origin at the junction between the shield and the guard vessel and extending parallel to the axis of the shield, and (b) a  $r$ -coordinate system with the origin at the center of the end disc.

The space between the jacket and the shield, guard vessel, and inner vessel was highly evacuated (approximately  $10^{-5}$  mm Hg abs. pressure); therefore, the energy transferred by gaseous conduction or convection was assumed negligible compared to the heat transferred by radiation. In order to be conservative in the estimate of the guard shield temperature rise, the small amount of heat transferred from the shield to the inner vessel was neglected in determining the shield temperature distribution. In addition, if the shield temperature were almost constant, then the thermal conductivity of the shield material  $k_s$  could be assumed constant. The shield thickness was small compared to the shield diameter; therefore, temperature variations across the thickness of the shield were neglected.

With these assumptions in mind, the following energy balances may be written for a differential element in the cylindrical portion of the shield and for the end closure:

$$\begin{aligned} \text{(a) For } 0 \leq x \leq L. \quad & d^2T \\ & - \pi D t k_s \frac{d^2T}{dx^2} dx = q_r (\pi D) dx \end{aligned} \quad \text{(C-1)}$$

(b) For  $0 \leq r \leq D/2$ .

$$- 2\pi t k_s \frac{d}{dr} \left( r \frac{dT}{dr} \right) dr = q_r (2\pi r) dr \quad (C-2)$$

where  $q_r = \sigma F_e (T_a^4 - T^4) \quad (C-3)$

$\sigma$  = Stefan-Boltzmann constant

$F_e$  = emissivity factor for radiation

$T_a$  = absolute temperature of the vacuum jacket

$T$  = absolute temperature of the shield at any point

In anticipation of the result that the shield temperature will not vary more than  $10^\circ$  or  $20^\circ R$ , and noting that the jacket temperature is near ambient temperature, one can show that the radiation flux  $q_r$  remains practically constant if the shield temperature is near liquid nitrogen temperature ( $-320^\circ F$  or  $140^\circ R$ ). With this additional assumption, the temperature field equations given below were solved.

(a) For  $0 \leq x \leq L$ .

$$\frac{d^2 T}{dx^2} = - \frac{q_r}{k_s t} = \text{constant} \quad (C-4)$$

(b) For  $0 \leq r \leq D/2$ .

$$\frac{d}{dr} \left( r \frac{dT}{dr} \right) = - \frac{q_r r}{k_s t} \quad (C-5)$$

Integration of Eq. (C-4) twice yields the following equation for the temperature distribution in the cylindrical portion of the shield.

$$T = - (q_r/2k_s t) x^2 + C_1 x + C_2 \quad (C-6)$$

Integration of Eq. (C-5) twice yields the following expression for the temperature distribution in the end closure of the shield.

$$T = - (q_r/4k_s t) r^2 + C_3 \ln r + C_4 \quad (C-7)$$

The following boundary conditions were used to evaluate the constants of integration:

- (a) At  $x = 0$  ,  $T = T_o$
- (b) At  $x = L$  , or at  $r = D/2$  , the temperature given by Eqs. (C-6) and (C-7) must be the same.
- (c) At  $x = L$  or  $r = D/2$  , the heat transfer rate calculated from Eqs. (C-6) and (C-7) must be equal, or  $-(dT/dx) = (dT/dr)$  at this point.
- (d) At  $r = 0$  , the temperature must be finite.

Applying boundary condition (a) to Eq. (C-6), one finds that

$$C_2 = T_o \quad (C-8)$$

Applying boundary condition (d) to Eq. (C-7) results in

$$C_3 = 0 \quad (C-9)$$

Applying boundary condition (b), the following expression is obtained:

$$T_o + C_1 L - \frac{q_r L^2}{2 k_s t} = C_4 - \frac{q_r D^2}{16 k_s t} \quad (C-10)$$

Application of boundary condition (c) results in the following:

$$C_1 = \left[ \frac{q_r L}{k_s t} \right] \left[ 1 + \frac{1}{4} (D/L) \right] \quad (C-11)$$

Substitution of the value of the constant  $C_1$  from Eq. (C-11) into Eq. (C-10), yields the expression for the constant  $C_4$ .

$$C_4 = T_o + (q_r L^2 / 2 k_s t) \left[ 1 + \frac{1}{2} (D/L) + \frac{1}{8} (D/L)^2 \right] \quad (C-12)$$

From Eqs. (C-6) through (C-12), the following temperature distribution equations may be written:

(a) For  $0 \leq x \leq L$ .

$$T = T_o + (q_r L^2 / k_s t) (x/L) \left[ 1 + \frac{1}{2} (D/L) - \frac{1}{2} (x/L) \right] \quad (C-13)$$

(b) For  $0 \leq r \leq D/2$ .

$$T = T_o + \left( \frac{q_r L^2}{2 k_s t} \right) \left[ 1 + \frac{1}{2} (D/L) + \frac{1}{8} (D/L)^2 - \frac{1}{8} (2r/L)^2 \right] \quad (C-14)$$

The maximum temperature of the shield is found to be the temperature corresponding to  $r = 0$  or the temperature occurring at the center of the end closure disc. From Eq. (C-14) with  $r = 0$ , the maximum shield temperature is obtained.

$$T_{\max} = T_o + (q_r L^2 / 2k_s t) \left[ 1 + \frac{1}{2} (D/L) + \frac{1}{8} (D/L)^2 \right] \quad (C-15)$$

A numerical value for the maximum shield temperature may be calculated from Eq. (C-15), using the following values of the parameters:

Shield length,  $L = 15.25$  in.

Shield diameter,  $D = 10.75$  in.

Vacuum jacket temperature,  $T_a = 75^\circ\text{F} = 535^\circ\text{R}$

Shield thickness,  $t = 0.125$  in.

Shield thermal conductivity at liquid nitrogen temperature,

$k_s = 73$  Btu/hr-ft- $^\circ\text{F}$  for commercial copper

Emissivity of shield surface,  $e_1 = 0.05$  for copper with some oxide.

Emissivity of vacuum jacket,  $e_2 = 0.15$  for stainless steel.

The emissivity factor for this problem may be estimated from

$$F_e = \frac{1}{(1/e_1) + (A_1/A_2) [(1/e_2) - 1]} \quad (C-16)$$

where  $A_1$  = surface area of the shield =  $4.21 \text{ ft}^2$ ,  $A_2$  = surface area of the vacuum jacket =  $5.41 \text{ ft}^2$ . Substituting in the numerical values, the emissivity factor is:

$$F_e = 1/[20 + (0.778)(6.67 - 1)] = 0.0415$$

The radiant heat flux incident on the shield may be calculated, assuming an average temperature of the shield of  $143^\circ\text{R}$  ( $-317^\circ\text{F}$ ), from Eq. (C-3).

$$q_r = (0.173)(10^{-8})(0.0415) [(535)^4 - (143)^4] = 5.84 \text{ Btu/hr-ft}^2$$

The maximum temperature rise can then be determined from Eq. (C-15).

$$T_{\max} - T_o = \frac{(5.84)(1.271)^2}{(2)(73)(0.01042)} \left[ 1 + \frac{(10.75)}{(2)(15.25)} - \frac{(10.75)^2}{(8)(15.25)^2} \right]$$

$$T_{\max} - T_o = (6.21)(1.415) = 8.8^\circ\text{R}$$

The normal boiling point of liquid nitrogen is  $T_o = 139.2^\circ\text{R}$ ; therefore, the maximum shield temperature is:

$$T_{\max} = 139.2^\circ + 8.8^\circ = 148.0^\circ\text{R}$$

It may be concluded from the previous calculation that the error due to heat transfer between the shield and the inner vessel is quite small. At a pressure of 25 psia (the approximate operating pressure of the inner vessel during the experimental runs), the saturation temperature of liquid nitrogen is  $148.0^\circ\text{R}$ , which is the same as the maximum shield temperature found by the previous calculation. If a mean surface temperature of  $143^\circ\text{R}$  is assumed for the shield and guard vessel, and an emissivity factor of  $F_e = 0.07$  is used, the radiation heat transfer rate to the inner vessel for an inner vessel surface area of  $2.07 \text{ ft}^2$  may be estimated.

$$\dot{Q} = \sigma A F_e (T_i^4 - T_m^4) = (0.173)(10^{-8})(2.07)(0.07) [(148)^4 - (143)^4]$$

$$Q = 0.0153 \text{ Btu/hr}$$



Since heat transfer rates on the order of 500 Btu/hr were measured for the smaller plate, the heat exchange between the shield and the inner vessel introduced an error of  $(0.0153)(100)/(500) = 0.003\%$ , which was certainly negligible.

## APPENDIX D

### TIME RESPONSE FOR FREE CONVECTION

In the analysis of the present problem, the assumption that quasi-steady-state conditions prevailed, i.e., at any instant of time, the steady-state equations for heat and mass transfer applied. The purpose of this Appendix was to demonstrate that the time required to reach steady state was much shorter than the duration of a single measurement.

For unsteady-state conditions, the momentum, energy and diffusion equations, Eqs. (3-56), (3-57), and (3-58), may be written by including the change in momentum, energy, and mass stored within the elemental volume used for the original derivation. Excluding the effect of thermal diffusion, these equations are as follows:

(a) Momentum equation:

$$\begin{aligned} \frac{\partial}{\partial x} \left[ \int_0^\delta u^2 dy \right] + \frac{\partial}{\partial \tau} \left[ \int_0^\delta u dy \right] = g (T_\infty - T_w) \beta_t \int_0^\delta \theta dy - g \beta_m \int_0^\delta \phi dy - \\ - \mu \left( \frac{du}{dy} \right)_w \end{aligned} \quad (D-1)$$

(b) Energy equation:

$$\begin{aligned} \frac{\partial}{\partial x} \left[ \int_0^\delta \theta u dy \right] + \frac{\partial}{\partial \tau} \left[ \int_0^\delta \theta dy \right] = - \alpha \left( \frac{d\theta}{dy} \right)_w - \frac{D_{12}}{(1 - w_{1w})} \left( \frac{d\phi}{dy} \right)_w \end{aligned} \quad (D-2)$$

(c) Diffusion equation:

$$\frac{\partial}{\partial x} \left[ \int_0^\delta \phi u \, dy \right] + \frac{\partial}{\partial \tau} \left[ \int_0^\delta \phi \, dy \right] = - \left( \frac{1 - w_{1\infty}}{1 - w_{1W}} \right) D_{12} \left( \frac{d\phi}{dy} \right)_w \quad (D-3)$$

In the transient equations, the boundary layer thickness  $\delta$  and the parameter  $u_m$  in the velocity profile expression, Eq. (3-59) are functions of both the coordinate  $x$  and time; however, the same functions for  $u$ ,  $\theta$ , and  $\phi$  may be used to solve the transient problem as were used for the steady-state problem, if this additional fact is considered. If the velocity, temperature, and mass fraction profile equations, (Eqs. 3-59, 3-60, and 3-61), are substituted into the transient equations, Eqs. (D-1), (D-2), and (D-3), and the indicated integrations performed, the following expressions result:

(a) Momentum equation:

$$\frac{1}{105} \frac{\partial(u_m^2 \delta)}{\partial x} + \frac{1}{12} \frac{\partial(u_m \delta)}{\partial \tau} = \frac{1}{3} g [\beta_t (T_\infty - T_w) + \beta_m (w_{1\infty} - w_{1W})(\xi)] - (u_m v / \delta) \quad (D-4)$$

(b) Energy equation:

$$\frac{1}{30} \frac{\partial(u_m \delta)}{\partial x} + \frac{1}{3} \frac{\partial \delta}{\partial \tau} = \frac{2\alpha}{\delta} \left[ 1 + \left( \frac{\text{Pr}}{\text{Sc}} \right) \frac{(w_{1W} - w_{1\infty})}{(1 - w_{1W})(\xi)} \right] \quad (D-5)$$

(c) Diffusion equation:

$$\frac{(\xi)^2}{30} \frac{\partial(u_m \delta)}{\partial x} + \frac{(\xi)^2}{3} \frac{\partial \delta}{\partial \tau} = \frac{2 D_{12}}{\delta} \frac{(1 - w_{1\infty})}{(1 - w_{1w})} \quad (D-6)$$

The short-time solution to Eqs. (D-4), (D-5), and (D-6) was found by dropping the terms involving the partial derivative with respect to  $x$  (the first term in each equation) and making the following substitutions:

$$u_m = C_1 \tau \quad (D-7)$$

$$\delta = C_2 \tau^{1/2} \quad (D-8)$$

Upon solving for the parameters  $C_1$  and  $C_2$ , the following expressions are obtained:

$$C_1 = \frac{4 g [\beta_t (T_\infty - T_w) + \beta_m (w_{1\infty} - w_{1w})(\xi)] B_3}{(Pr + 1.50 B_3)} \quad (D-9)$$

$$C_2 = (12 \alpha B_3)^{1/2} \quad (D-10)$$

where,

$$B_3 = 1 - \left( \frac{Pr}{Sc} \right) \frac{(w_{1\infty} - w_{1w})}{(1 - w_{1w})(\xi)} \quad (D-11)$$

and the boundary layer thickness ratio is given by Eq. (3-95). From Eq. (3-88), the point value of the Nusselt number for short times is

$$Nu_x = \frac{2x}{\delta} = \frac{2}{\sqrt{12} (Fo_x B_3)^{1/2}} \quad (D-12)$$

where,  $Fo_x = \text{Fourier number} = \alpha\tau/x^2$  (D-13)

The heat transfer coefficient is a function of time alone for the short time solution.

$$h_c = \frac{2k}{\sqrt{12} (\alpha\tau)^{1/2}} \quad (D-14)$$

In order to determine the lower limit of time for which the steady state solution applies, the method of characteristics, as suggested by Siegel (40), was used. As developed by Siegel, the equation for the slope of the characteristic line (the line separating the regions for which the steady-state solution and the short-time solution are valid) is:

$$\frac{\delta}{12} \left( \frac{dx}{d\tau} \right)^2 - \frac{2\delta u_m}{105} \left( \frac{dx}{d\tau} \right) + \frac{\delta u_m^2}{1050} = 0 \quad (D-15)$$

Solving for the slope  $(dx/d\tau)$  from Eq. (D-15), there is obtained:

$$\frac{dx}{d\tau} = \frac{4}{35} u_m [1 \pm (\sqrt{2}/4)] \quad (D-16)$$

Since the lower limit on time for the steady-state solution to be valid is the desired result, the negative sign in Eq. (D-16) must be used, or

$$dx/d\tau = 0.0739 u_m \quad (D-17)$$

The equation for the characteristic line may be obtained by substituting the expression for  $u_m$  obtained in the steady-state analysis (see Eqs. 3-74 and 3-82) into Eq. (D-17) and integrating. The solution thus obtained yields the time required for the steady-state solution to become valid for a step change in both surface temperature and mass fraction at the surface for a vertical flat plate in free convection. In dimensionless form,

$$\frac{\alpha \tau_{ss}}{L^2} = Fo_{ss} = 5.24 \left[ \frac{(0.952 B_3 + Pr)(x/L)}{B_3 Gr_L Pr^2} \right]^{1/2} \quad (D-18)$$

An example of the time required to reach steady-state may be worked for the following typical values of the parameters:

$$T_\infty = 70^\circ\text{F}$$

$$w_{1\infty} = 0.10$$

$$T = -310^\circ\text{F}$$

$$w_{1w} = 0.000$$

$$L = 4 \text{ inches and } 10 \text{ inches}$$

$$Pr = 0.740$$

$$Pr/Sc = 1.422$$

With a boundary layer thickness ratio  $\xi = 1.193$ , the Grashof number is:

$$Gr_L = 2.48 \times 10^8 \quad \text{for the 4 in. plate}$$

$$Gr_L = 3.88 \times 10^9 \quad \text{for the 10 in. plate}$$

The parameter  $B_3 = 0.988$  for this example. Substitution of these values into Eq. (D-18) yields the following values for the Fourier number for steady-state.

$$Fo_{ss} = 5.86 \times 10^{-4} \quad \text{for the 4 in. plate}$$

$$Fo_{ss} = 1.48 \times 10^{-4} \quad \text{for the 10 in. plate}$$

For a thermal diffusivity of  $0.351 \text{ ft}^2/\text{hr}$ , the time required for steady state to be established may be calculated from the definition of the Fourier number.

$$\tau_{ss} = 1.85 \times 10^{-4} \text{ hr} = 0.67 \text{ sec. for the 4 in. plate}$$

$$\tau_{ss} = 2.92 \times 10^{-4} \text{ hr} = 1.03 \text{ sec. for the 10 in. plate}$$

Since these values of time were so much smaller than the duration of time required to make even a single measurement, it was concluded that the assumption of quasi-steady-state was a valid assumption in the present analysis.

## APPENDIX E

### APPLICATION OF RESULTS

In order to illustrate the manner in which the results of the present investigation may be applied in a typical frost formation problem, an example is worked out in this Appendix. Since no analytical expression was developed for the variation of frost thickness with time, the problem must be solved by a numerical technique.

#### E.1. Statement of the problem

A vertical flat plate having a height of 6 inches is placed in a room in which the dry bulb temperature is 80°F and the relative humidity is 80% for a barometric pressure of 14.7 psia. The plate is suddenly cooled to -300°F and maintained at this temperature. Determine the variation of the heat transfer rate, mass transfer rate, and frost thickness with time.

#### E.2. Procedure for solution

The following steps were used in the solution of the problem:

- (a) Assume a value for the interface temperature of the frost,  $T_w$ .
- (b) Calculate the convection, radiation, and latent heat components of the total heat transfer rate, the mass flux, and the total heat flux. Since the flow regime for the present problem is laminar, Eq. (6-1) was used to determine the average Nusselt number, and the convective component of heat flux was determined from



$$q_c = k (T_\infty - T_w) \overline{Nu}/L \quad (E-1)$$

The radiation component of heat flux was determined from Eq. (4-8) using a frost emissivity of 0.92.

$$q_r = \sigma e_f (T_\infty^4 - T_w^4) \quad (E-2)$$

The latent heat transport was calculated from Eq. (4-7), using the heat of sublimation at the frost surface temperature.

$$q_m = m_1 i_{sg} \quad (E-3)$$

The mass flux was determined by fitting the experimental points obtained in the present investigation to a power function of the product of Grashof and Prandtl numbers, or

$$\overline{Sh} = (4.95)(10^{-4})(Gr_L Pr)^{1/2} \quad (E-4)$$

The mass flux was then determined from

$$m_1 = \rho D_{12} (w_{1\infty} - w_{1w}) \overline{Sh}/L \quad (E-5)$$

The total heat flux was the sum of the three components, or

$$q_{total} = q_c + q_r + q_m \quad (E-6)$$

From the statement of the problem, one can determine the mass fraction of water vapor in the ambient air, which is required for the previously mentioned calculations, by first determining the specific humidity  $W_\infty$  from

$$W = \frac{0.622 p_1}{(p_b - p_1)} \quad (E-7)$$

From the steam tables, the saturation pressure of water at 80°F is 0.507 psia, so that the partial pressure of water vapor in air for a relative humidity of 80% is  $p_1 = (0.80)(0.507) = 0.407$  psia, and

$$W_\infty = (0.622)(0.407)/(14.7 - 0.407) = 0.01765$$

The mass fraction corresponding to this value of specific humidity is

$$w_{1\infty} = W_\infty/(1 + W_\infty) = (0.01765)/(1.01765) = 0.01735$$

(c) For the assumed frost surface temperature and plate surface temperature, the mean frost temperature may be determined from

$$T_f = 0.5 (T_w + T_s) \quad (E-8)$$

The frost thermal conductivity was then determined from Figure 14, and the frost density was determined from Figure 15.

(d) The frost thickness was determined from Eq. (5-18) and the calculated total heat flux.

$$t_f = k_f (T_w - T_s)/q_{\text{total}} \quad (E-9)$$

(e) The time interval required for the frost surface to change from one assumed temperature to the next was finally determined from

$$\Delta\tau = \rho_f \Delta t_f / m_1 \quad (E-10)$$

The results of the calculation are tabulated in Table 4. The frost thickness calculations were extended above the temperature

limits of the present investigation by the use of the data of Holten (11) up to  $-90^{\circ}\text{F}$ . The frost thickness calculations could not be extended above this temperature, since the data of Kamei et al. (2) at higher temperatures did not blend with the data of Holten et al.

TABLE 4

## SOLUTION TO EXAMPLE PROBLEM

Conditions of problem:

$T_{\infty} = 80^{\circ}\text{F}$

$T = -300^{\circ}\text{F}$

$w_{1\infty} = 0.01735$

$L = 6 \text{ inches}$

$P_b = 14.7 \text{ psia}$

$T_w$ $^{\circ}\text{F}$	$Gr_L$	$Pr$	$\overline{Nu}$	$q_c$ Btu/hr-ft <sup>2</sup>	$q_r$ Btu/hr-ft <sup>2</sup>	$q_m$ Btu/hr-ft <sup>2</sup>	$q_{total}$ Btu/hr-ft <sup>2</sup>
-300	$5.42 \times 10^8$		77.1	595	135	7.0	737
-270	4.11		72.0	533	134	8.0	675
-240	3.12		67.1	472	132	8.7	613
-210	2.32		62.3	412	130	9.1	551
-180	1.743		58.0	356	126	9.4	491
-150	1.301		53.9	302	121	9.4	432
-120	0.947		49.7	251	114	9.1	374
- 90	0.698		46.1	204	106	8.9	319
- 30	0.338		38.5	117.2	78.2	7.6	203.0
0	0.219		34.5	78.3	61.3	6.4	146.0
+ 32	$0.116 \times 10^8$		29.5	41.2	39.1	4.2	84.5

TABLE 4 (Contd.)

$T_w$ °F	$\overline{Sh}$	$m_1$ lb <sub>m</sub> /hr-ft <sup>2</sup>	$k_f$ Btu/hr-ft-°F	$\rho_f$ lb <sub>m</sub> /ft <sup>3</sup>	$t_f$ inches	$\Delta\tau$ hr.	time hr.
-300	11.53	$5.79 \times 10^{-3}$	- -	- -	0.0000	- -	0.000
-270	10.04	6.61	0.030	1.88	0.0160	0.433	0.433
-240	8.75	7.20	0.025	2.18	0.0294	0.368	0.801
-210	7.55	7.53	0.020	2.56	0.0392	0.285	1.086
-180	6.55	7.75	0.016	2.88	0.0468	0.242	1.328
-150	5.65	7.73	0.012	3.10	0.0505	0.123	1.451
-120	4.81	7.52	0.010	3.53	0.0583	0.297	1.748
- 90	4.14	7.29	0.0125	3.86	0.0986	0.550	2.298
- 60	3.47	6.83	0.0215	4.19	0.103	-(a)	- -
- 30	2.88	6.20	- -	- -	- -	- -	- -
0	2.32	5.28	- -	- -	- -	- -	- -
+ 32	1.69	$3.43 \times 10^{-3}$	- -	- -	- -	- -	- -

(a) The solution of the example problem was not carried out to longer times because of the lack of data on the thermal conductivity of frost formed between -90°F and 0°F. The frost thickness would approach a constant value after the frost-air interface temperature  $T_w$  reached 32°F.

APPENDIX F  
EXPERIMENTAL DATA

TABLE 5  
EXPERIMENTAL DATA FOR RUN NO. 1

Test conditions.

$$\begin{aligned} T_{\infty} &= 75.0^{\circ}\text{F} & T_s &= -310^{\circ}\text{F} \\ w_{1\infty} &= 0.01011 & L &= 4 \text{ inches} \\ p_b &= 14.30 \text{ psia} \end{aligned}$$

Time	$q_c$	$q_m$	$q_r$	$q_{\text{total}}$	$\rho_f$	$t_f$	$T_w$
min.	Btu/hr-ft <sup>2</sup>	Btu/hr-ft <sup>2</sup>	Btu/hr-ft <sup>2</sup>	Btu/hr-ft <sup>2</sup>	lb <sub>m</sub> /ft <sup>3</sup>	in.	°F
10	631	4.2	128	763	-	.019	-290
19	619	3.9	127	750	-	.034	-283
29	578	3.6	127	709	0.93	.041	-273
38	530	3.4	126	660	-	.046	-264
48	566	3.7	126	696	-	.050	-254
58	515	3.8	125	644	1.31	.056	-246
68	500	3.7	125	629	-	.061	-237
78	490	3.6	124	618	-	.068	-227
88	463	3.5	124	592	1.60	.073	-219

Note. Radiation heat flux was calculated using a frost emissivity of 0.92.

TABLE 6  
CALCULATED DATA FOR RUN NO. 1

Test conditions.

$$\begin{aligned} T_{\infty} &= 75.0^{\circ}\text{F} & T_s &= -310^{\circ}\text{F} \\ w_{1\infty} &= 0.01011 & L &= 4 \text{ inches} \\ p_b &= 14.30 \text{ psia} \end{aligned}$$

Time	$m_1$	$\bar{h}_c$	$\bar{h}_m$	$k_f$
min.	$\text{lb}_m/\text{hr-ft}^2$	$\text{Btu/hr-ft}^2\text{-}^{\circ}\text{F}$	$\text{ft/hr}$	$\text{Btu/hr-ft-}^{\circ}\text{F}$
10	$3.48 \times 10^{-3}$	1.729	3.14	0.0604
19	3.20	1.730	2.92	.0787
29	2.94	1.650	2.72	.0654
38	2.84	1.563	2.67	.0550
48	3.02	1.72	2.86	.0517
58	3.14	1.604	3.00	.0470
68	3.04	1.603	2.95	.0438
78	2.98	1.623	2.93	.0422
88	$2.88 \times 10^{-3}$	1.577	2.86	0.0396



TABLE 6 (Contd.)

Time min.	$Gr_L Pr$	$\overline{Nu}$	$\overline{Sh}$	$\overline{Nu} / \psi (Gr_L Pr)^{1/4}$
10	$1.498 \times 10^8$	56.3	7.34	0.623
19	1.390	55.7	6.35	.628
29	1.262	52.7	5.35	.608
38	1.175	49.2	4.77	.579
48	1.074	53.5	4.74	.643
58	0.998	49.3	4.63	.604
68	0.908	48.7	4.22	.611
78	0.826	48.7	3.88	.626
88	$0.766 \times 10^8$	46.8	3.53	.613

TABLE 7  
EXPERIMENTAL DATA FOR RUN NO. 2

Test conditions.

$$\begin{aligned} T_{\infty} &= 77.0^{\circ}\text{F} & T_s &= -310^{\circ}\text{F} \\ w_{1\infty} &= 0.01880 & L &= 4 \text{ inches} \\ p_b &= 14.28 \text{ psia} \end{aligned}$$

Time	$q_c$	$q_m$	$q_r$	$q_{\text{total}}$	$\rho_f$	$t_f$	$T_w$
min.	Btu/hr-ft <sup>2</sup>	Btu/hr-ft <sup>2</sup>	Btu/hr-ft <sup>2</sup>	Btu/hr-ft <sup>2</sup>	lb <sub>m</sub> /ft <sup>3</sup>	in.	°F
10	613	7.3	133	753	-	0.012	-280
20	552	7.2	132	691	-	.027	-257
30	517	6.9	131	655	1.75	.030	-238
40	463	6.4	130	599	-	.037	-223
50	463	7.6	129	600	-	.042	-212
60	434	9.3	128	571	2.20	.048	-203
70	433	11.2	127	571	-	.055	-195
80	415	13.1	126	554	-	.063	-188
90	398	14.3	125	537	2.48	0.072	-183

Note. Radiation heat flux  $q_r$  was calculated using a frost emissivity of 0.92.

TABLE 8  
CALCULATED DATA FOR RUN NO. 2

Test conditions.

$$T_{\infty} = 77.0^{\circ}\text{F}$$

$$T_s = -310^{\circ}\text{F}$$

$$w_{1\infty} = 0.01880$$

$$L = 4 \text{ inches}$$

$$p_b = 14.28 \text{ psia}$$

Time	$m_1$	$\bar{h}_c$	$\bar{h}_m$	$k_f$
min.	$\text{lb}_m/\text{hr-ft}^2$	$\text{Btu/hr-ft}^2\text{-}^{\circ}\text{F}$	$\text{ft/hr}$	$\text{Btu/hr-ft-}^{\circ}\text{F}$
10	$6.08 \times 10^{-3}$	1.717	2.75	0.0251
20	5.98	1.653	3.06	.0293
30	5.69	1.642	2.96	.0228
40	5.35	1.543	2.86	.0213
50	6.27	1.603	3.39	.0214
60	7.70	1.551	4.22	.0215
70	9.25	1.593	5.11	.0228
80	10.80	1.567	6.03	.0240
90	$11.80 \times 10^{-3}$	1.531	6.62	.0256

TABLE 8 (Contd.)

Time min.	$Gr_L Pr$	$\overline{Nu}$	$\overline{Sh}$	$\overline{Nu} / \psi (Gr_L Pr)^{1/4}$
10	$1.358 \times 10^8$	55.1	5.82	0.623
20	1.099	51.4	5.19	.612
30	0.911	49.8	4.27	.623
40	0.799	46.2	3.65	.597
50	0.723	47.2	4.00	.625
60	0.658	45.1	4.60	.611
70	0.608	46.1	5.34	.637
80	0.570	44.7	6.05	.628
90	$0.539 \times 10^8$	43.5	5.33	0.620

TABLE 9  
EXPERIMENTAL DATA FOR RUN NO. 3

Test conditions.

$$\begin{aligned} T_{\infty} &= 73.7^{\circ}\text{F} & T_s &= -310^{\circ}\text{F} \\ w_{1\infty} &= 0.01010 & L &= 10 \text{ inches} \\ p_b &= 14.30 \text{ psia} \end{aligned}$$

Time	$q_c$	$q_m$	$q_r$	$q_{\text{total}}$	$\rho_f$	$t_f$	$T_w$
min.	Btu/hr-ft <sup>2</sup>	Btu/hr-ft <sup>2</sup>	Btu/hr-ft <sup>2</sup>	Btu/hr-ft <sup>2</sup>	lb <sub>m</sub> /ft <sup>3</sup>	in.	°F
5	565	5.8	127	698	-	0.0055	-305
10	533	6.1	127	666	-	0.0130	-297
15	489	6.3	127	622	0.88	0.0190	-291
20	465	5.0	127	597	-	0.0235	-284
25	452	4.8	126	583	1.09	0.0290	-274

Note. Radiation heat flux  $q_r$  was calculated using a frost emissivity of 0.92.

TABLE 10  
CALCULATED DATA FOR RUN NO. 3

Test conditions.

$$\begin{aligned} T_{\infty} &= 73.7^{\circ}\text{F} & T_s &= -310^{\circ}\text{F} \\ w_{1\infty} &= 0.01010 & L &= 10 \text{ inches} \\ p_b &= 14.30 \text{ psia} \end{aligned}$$

Time	$m_1$	$\bar{h}_c$	$\bar{h}_m$	$k_f$
min.	lb <sub>m</sub> /hr-ft <sup>2</sup>	Btu/hr-ft <sup>2</sup> -°F	ft/hr	Btu/hr-ft-°F
5	$4.78 \times 10^{-3}$	1.467	4.23	0.0640
10	5.02	1.436	4.50	.0555
15	5.20	1.320	4.70	.0518
20	4.11	1.300	3.74	.0449
25	$3.94 \times 10^{-3}$	1.300	3.64	0.0508
=====				
Time	$Gr_L Pr$	$\overline{Nu}$	$\overline{Sh}$	$\overline{Nu}/\psi (Gr_L Pr)^{2/5}$
min.				
5	$2.80 \times 10^9$	121.6	28.2	0.0250
10	2.51	118.0	29.0	.0254
15	2.34	109.0	27.6	.0241
20	2.23	105.0	21.4	.0237
25	$2.00 \times 10^9$	103.6	18.8	0.0244

TABLE 11  
EXPERIMENTAL DATA FOR RUN NO. 4

Test conditions.

$$\begin{aligned} T_{\infty} &= 74.5^{\circ}\text{F} & T_s &= -310^{\circ}\text{F} \\ w_{1\infty} &= 0.01483 & L &= 10 \text{ inches} \\ p_b &= 14.35 \text{ psia} \end{aligned}$$

Time	$q_c$	$q_m$	$q_r$	$q_{\text{total}}$	$\rho_f$	$t_f$	$T_w$
min.	Btu/hr-ft <sup>2</sup>	Btu/hr-ft <sup>2</sup>	Btu/hr-ft <sup>2</sup>	Btu/hr-ft <sup>2</sup>	lb <sub>m</sub> /ft <sup>3</sup>	in.	°F
5	538	7.0	128	673	-	0.0100	-302
10	506	7.5	128	642	-	.0175	-288
15	485	8.5	127	620	0.96	.0260	-283
20	459	8.3	127	594	-	.0325	-276
25	441	8.6	127	577	-	.0380	-268
30	440	10.4	126	576	1.36	.0435	-262
35	436	8.1	126	570	-	.0495	-257
40	427	7.6	126	561	-	.0535	-252
45	412	7.2	126	545	1.66	0.0560	-248

Note. The radiation heat flux  $q_r$  was calculated using a frost emissivity of 0.92.

TABLE 12  
CALCULATED DATA FOR RUN NO. 4

Test conditions.

$$\begin{aligned} T_{\infty} &= 74.5^{\circ}\text{F} & T_s &= -310^{\circ}\text{F} \\ w_{1\infty} &= 0.01483 & L &= 10 \text{ inches} \\ p_b &= 14.35 \text{ psia} \end{aligned}$$

Time	$m_1$	$\bar{h}_c$	$\bar{h}_m$	$k_f$
min.	lb <sub>m</sub> /hr-ft <sup>2</sup>	Btu/hr-ft <sup>2</sup> -°F	ft/hr	Btu/hr-ft-°F
5	$5.83 \times 10^{-3}$	1.427	3.52	0.0700
10	6.23	1.397	3.84	.0426
15	7.01	1.252	4.36	.0496
20	6.90	1.308	4.32	.0473
25	7.13	1.286	4.51	.0435
30	8.56	1.307	5.45	.0435
35	6.72	1.312	4.31	.0444
40	6.24	1.306	4.04	.0431
45	$5.98 \times 10^{-3}$	1.276	3.90	0.0411



TABLE 12 (Contd.)

Time min.	$Gr_L Pr$	$\overline{Nu}$	$\overline{Sh}$	$\overline{Nu} \psi (Gr_L Pr)^n$
5	$2.65 \times 10^9$	118.3	23.4	0.0249
10	2.30	113.6	22.0	0.0253
15	2.20	109.2	23.7	.0248
20	2.02	104.3	21.9	.0245
25	1.908	101.8	21.1	0.597
30	1.810	102.7	24.2	.610
35	1.722	102.4	18.3	.618
40	1.637	101.2	16.5	.616
45	$1.577 \times 10^9$	98.3	15.3	0.603

## BIBLIOGRAPHY

1. K. O. Beatty, E. B. Finch, and E. M. Schoenborn, "Heat Transfer to Metal Under Frosting Conditions," Refrigeration Engineering, Vol. 59, Dec. 1951, pg. 1203.
2. S. Kamei, T. Mizushima, S. Kifune, and T. Koto, "Research on Frost Fromation in a Low Temperature Dehumidifier," Kyoto University, Chemical Engineering Japan, Vol. 14, 1950, pg. 53.
3. P. M. Chung and A. B. Algren, "Frost Formation and Heat Transfer on a Cylinder Surface in Humid Air Crossflow," ASHVAE Transactions, Vol. 65, Sept. 1958, pg. 213.
4. S. M. Andrichak, "Formation of a Layer of Frost on a Cylinder in Crossflow of Air," M. Sc. thesis, the Ohio State University, 1962.
5. S. Sugawara and Associates, "Research on the Heat Transfer During the Period of Frost Formation," Transactions of the Japanese Society of Mechanical Engineers, 1957.
6. R. J. Richards, K. Edmonds, and R. B. Jacobs, "Heat Transfer Between a Cryo-Surface and a Controlled Atmosphere," International Institute of Refrigeration Bulletin, 1962.
7. J. L. Loper, Trans. ASHRAE, Vol. 66, 1960.
8. R. V. Smith, D. K. Edmonds, E. G. F. Brentari, and R. J. Richards, "Analysis of the Frost Phenomena on a Cryo-Surface," Advances in Cryogenic Engineering, Vol. 9, Plenum Press, Inc., New York, 1964, pp. 88-97.

9. D. A. Van Gundy and J. R. Uglum, "Heat Transfer to an Uninsulated Surface at 20°K," Advances in Cryogenic Engineering, Vol. 7, Plenum Press, Inc., New York, 1962, pp. 377-384.
10. F. E. Ruccia and C. M. Mohr, "Atmospheric Heat Transfer to Vertical Tanks Filled with Liquid Oxygen," Advances in Cryogenic Engineering, Vol. 4, Plenum Press, Inc., New York, 1960, pp. 307-318.
11. D. C. Holten, "A Study of Heat and Mass Transfer to Uninsulated Liquid Oxygen Containers," Advances in Cryogenic Engineering, Vol. 6, Plenum Press, Inc., New York, 1961, pp. 499-508.
12. C. A. Whitehurst, "An Investigation of Heat and Mass Transfer by Free Convection From Humid Air to a Metal Plate Under Frosting Conditions," Ph.D. dissertation, Texas A. & M., 1962.
13. E. R. G. Eckert and R. M. Drake, Heat and Mass Transfer, McGraw-Hill Book Co., Inc., New York, 1959, pg. 457.
14. DeGroot, Thermodynamics of Irreversible Processes, Interscience Publishers, Inc., New York, 1952.
15. H. B. Callen, Thermodynamics, John Wiley and Sons, Inc., New York, 1960.
16. W. Jost, Diffusion in Solids, Liquids, Gases, Academic Press, Inc., New York, 1960.
17. S. Chapman and T. G. Cowling, The Mathematical Theory of Non-Uniform Gases, Cambridge University Press, London, 1952.
18. P. M. Chung and A. B. Algren, "Frost Formation and Heat Transfer on A Cylinder Surface in Humid Air Cross-Flow," Heating, Piping, and Air-Conditioning, Sept. - Oct., 1958.

19. W. Goodman, "Performance of Coils for Dehumidifying Air,"  
Heating, Piping, and Air Conditioning, Nov. 1938 - May 1939.
20. K. O. Beattie, E. B. Finch, and E. H. Schoenborn, "Heat Transfer  
From Humid Air to Metal Under Frosting Conditions," ASME - Inst.  
of Mech. Engrs., Sept. 1951.
21. E. R. G. Eckert and R. M. Drake, Heat and Mass Transfer, McGraw-  
Hill Book Co., Inc., New York, 1959, pg. 324.
22. E. R. G. Eckert and T. W. Jackson, Natl. Advisory Comm. Aeronaut.  
Report 1015, 1951.
23. A. I. Brown and S. M. Marco, Introduction to Heat Transfer, 3d  
Ed., McGraw-Hill Book Co., Inc., New York, 1958, pg. 164.
24. F. Kreith, Principles of Heat Transfer, International Textbook  
Co., Scranton, Pa., 1958, pg. 306.
25. R. B. Scott, Cryogenic Engineering, D. Van Nostrand Co., Inc.,  
Princeton, N. J., 1959, pg. 145.
26. Fluid Meters, Their Theory and Application, ASME Research Publi-  
cation, 5th edition, 1959.
27. N. E. Dorsey, Properties of Ordinary Water Substances, Reinhold  
Publishing Co., 1950, pg. 250.
28. E. Schmidt and W. Beckmann, Tech. Mech. Thermodynamics, Vol. 1,  
1930, pp. 1-24.
29. R. D. Present, Kinetic Theory of Gases, McGraw-Hill Book Co., Inc.,  
New York, 1958, pg. 149.
30. 1958 Heating Ventilating and Air Conditioning Guide, Vol. 36, pg.  
153.

31. L. A. Bromley, "Heat Transfer in Stable Film Boiling," Chem. Eng. Prog., Vol. 46, 1950, pp 221-227.
32. H. Merte and J. A. Clark, "Boiling Heat Transfer Data for Liquid Nitrogen at Standard and Near-Zero Gravity," Advances in Cryogenic Engineering, Vol. 7, Plenum Press, Inc., New York, 1962, pp. 546-550.
33. R. W. Vance, Cryogenic Technology, John Wiley and Sons, Inc., New York, 1963, pg. 149.
34. C. R. Wilke, J. Chem. Physics, Vol. 18, 1950, pg. 517.
35. A. L. Lindsay and L. A. Bromley, Ind. Engr. Chem., Vol. 42, 1950, pg. 508.
36. S. Chapman, Proc. Royal Society, London, Vol. 177A, 1940, pg. 38.
37. J. F. Lee, F. W. Sears, and D. L. Turcotte, Statistical Thermodynamics, Addison-Wesley Pub. Co., Inc., Reading, Mass., 1963, pg. 81-82.
38. W. Jost, Diffusion in Solids, Liquids, and Gases, Academic Press, Inc., New York, 1960, pg. 515.
39. K. E. Drew and T. L. Ibbs, Thermal Diffusion in Gases, Cambridge University Press, London, 1952, pg. 27-28.
40. R. Siegel, "Transient Free Convection from a Vertical Flat Plate," Trans. ASME, Vol. 80, 1958, pp. 347-359.